Chowdhuri, Pritindra “Power System Transients”
The Electric Power Engineering Handbook
Ed. L.L. Grigsby
Boca Raton: CRC Press LLC, 2001

10

Power System Transients

Pritindra Chowdhuri
Tennessee Technological University

10

Power System Transients

Francisco de la Rosa
DLR Electric Power Reliability

Pritindra Chowdhuri
Tennessee Technological University

Stephen R. Lambert
Shawnee Power Consulting, LLC

Juan A. Martinez-Velasco
Universitat Politecnica de Catalunya

Robert C. Degeneff
Rensselaer Polytechnic Institute

William Chisholm
Ontario Hydro Technologies

10.1 Characteristics of Lightning Strokes

Francisco de la Rosa

Lightning, one of Mother Nature's most spectacular events, started to appear significantly demystified after Franklin showed its electric nature with his famous electrical kite experiment in 1752. Although a great deal of research on lightning has been conducted since then, lightning stands nowadays as a topic of considerable interest for investigation (Uman, 1969, 1987). This is particularly true for the improved design of electric power systems, since lightning-caused interruptions and equipment damage during thunderstorms stand as the leading causes of failures in the electric utility industry.

Lightning Generation Mechanism

First Strokes

The wind updrafts and downdrafts that take place in the atmosphere, create a charging mechanism that separates electric charges, leaving negative charge at the bottom and positive charge at the top of the cloud. As charge at the bottom of the cloud keeps growing, the potential difference between cloud and ground, which is positively charged, grows as well. This process will continue until air breakdown occurs. See Fig. 10.1.

The way in which a cloud-to-ground flash develops involves a stepped leader that starts traveling downwards following a preliminary breakdown at the bottom of the cloud. This involves a positive pocket of charge, as illustrated in Fig. 10.1. The stepped leader travels downwards in steps several tens of meters in length and pulse currents of at least 1 kA in amplitude (Uman, 1969). When this leader is near ground, the potential to ground can reach values as large as 100 MV before the attachment process with one of the upward streamers is completed. Figure 10.2 illustrates a case when the downward leader is intercepted by the upward streamer developing from a tree.

It is important to highlight that the terminating point on the ground is not decided until the downward leader is some tens of meters above the ground plane and that it will be attached to one of the growing upward streamers from elevated objects such as trees, chimneys, power lines, and communication facilities. It is actually under this principle that lightning protection rods work, i.e., they have to be strategically located so as to insure the formation of an upward streamer with a high probability of intercepting

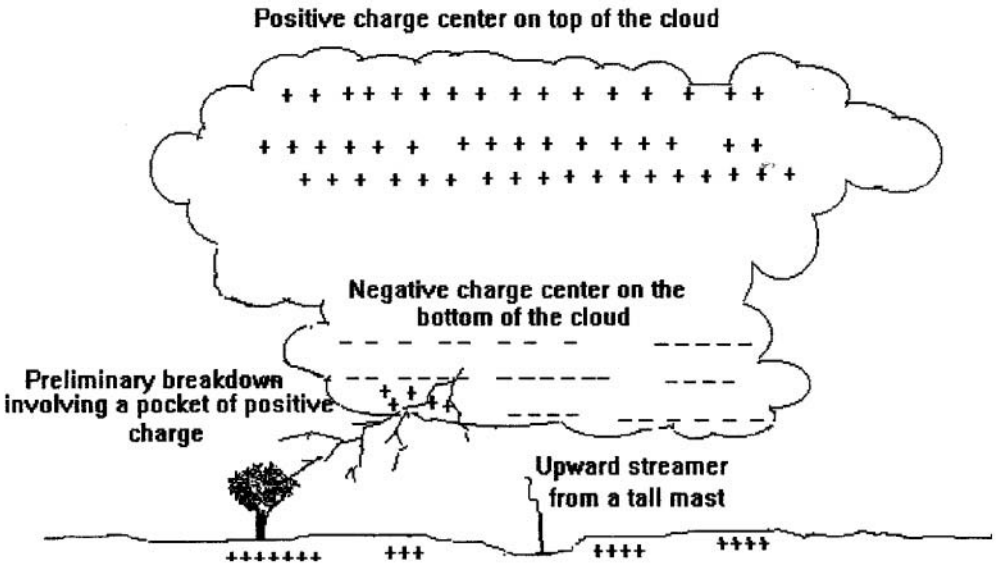

FIGURE 10.1 Separation of electric charge within a thundercloud.

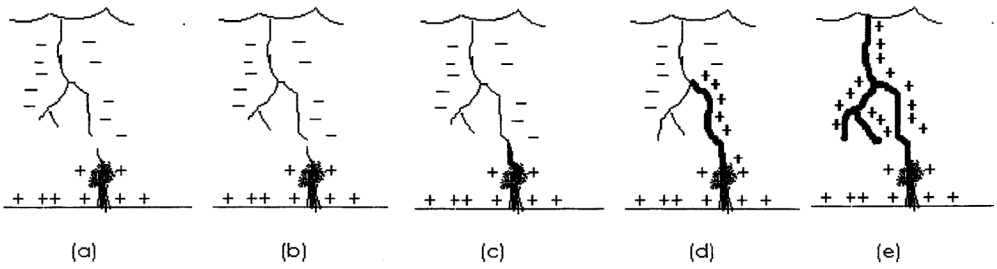

FIGURE 10.2 Attachment between downward and upward leaders in a cloud-to-ground flash.

downward leaders approaching the protected area. For this to happen, upward streamers developing from protected objects within the shielded area have to compete unfavorably with those developing from the tip of the lightning rods.

Just after the attachment process takes place, the charge that is lowered from the cloud base through the leader channel is conducted to ground while a breakdown current pulse, known as the return stroke, travels upward along the channel. The return stroke velocity is around one third the speed of light. The median peak current value associated with the return stroke is reported to be on the order of 30 kA, with rise time and time to half values around 5 and 75 μs, respectively. See Table 10.1 adapted from (Berger et al., 1975).

Associated with this charge transfer mechanism (an estimated 5 C charge is lowered to ground through the stepped leader) are the electric and magnetic field changes that can be registered at close distances

TABLE 10.1 Lightning Current Parameters for Negative Flashes[a]

Parameters	Units	Sample Size	Value Exceeding in 50% of the Cases
Peak current (minimum 2 kA)	kA	101	30
First strokes		135	12
Subsequent strokes			
Charge (total charge)	C		
First strokes		93	5.2
Subsequent strokes		122	1.4
Complete flash		94	7.5
Impulse charge	C		
(excluding continuing current)		90	4.5
First strokes		117	0.95
Subsequent strokes			
Front duration (2 kA to peak)	μs		
First strokes		89	5.5
Subsequent strokes		118	1.1
Maximum di/dt	kA/μs		
First strokes		92	12
Subsequent strokes		122	40
Stroke duration	μs		
(2 kA to half peak value on the tail)		90	75
First strokes		115	32
Subsequent strokes			
Action integral ($\grave{o}i^2dt$)	A^2s		
First strokes		91	5.5×10^4
Subsequent strokes		88	6.0×10^3
Time interval between strokes	ms	133	33
Flash duration	ms		
All flashes		94	13
Excluding single-stroke flashes		39	180

[a] Adapted from Berger et al., Parameters of lightning flashes, *Electra No. 41*, 23–37, July 1975.

from the channel and that can last several milliseconds. Sensitive equipment connected to power or telecommunication lines can get damaged when large overvoltages created via electromagnetic field coupling are developed.

Subsequent Strokes

After the negative charge from the cloud base has been transferred to ground, additional charge can be made available on the top of the channel when discharges known as J and K processes take place within the cloud (Uman, 1969). This can lead to some three to five strokes of lightning following the first stroke. A so-called dart leader develops from the top of the channel lowering charges, typically of 1 C, until recently believed to follow the same channel of the first stroke. Studies conducted in the past few years, however, indicate that around half of all lightning discharges to earth, both single- and multiple-stroke flashes, strike ground at more than one point, with the spatial separation between the channel terminations varying from 0.3 to 7.3 km, with a geometric mean of 1.3 km (Thottappillil et al., 1992).

Generally, dart leaders develop no branching and travel downward at velocities of around 3×10^6 m/s. Subsequent return strokes have peak currents usually smaller than first strokes but faster zero-to-peak rise times. The mean inter-stroke interval is about 60 ms, although intervals as large as a few tenths of a second can be involved when a so-called continuing current flows between strokes (this happens in 25–50% of all cloud-to-ground flashes). This current, which is on the order of 100 A, is associated with charges of around 10 C and constitutes a direct transfer of charge from cloud to ground (Uman, 1969).

The percentage of single-stroke flashes presently suggested by CIGRE of 45% (Anderson and Eriksson, 1980), is considerably higher than the following figures recently obtained form experimental results: 17% in Florida (Rakov et al., 1994), 14% in New Mexico (Rakov et al., 1994), 21% in Sri Lanka (Cooray and Jayaratne, 1994) and 18% in Sweden (Cooray and Perez, 1994).

Parameters of Importance for Electric Power Engineering

Ground Flash Density

Ground flash density, frequently referred as GFD or Ng, is defined as the number of lightning flashes striking ground per unit area and per year. Usually it is a long-term average value and ideally it should take into account the yearly variations that take place within a solar cycle — believed to be the period within which all climatic variations that produce different GFD levels occur.

A 10-year average GFD map of the continental U.S. obtained by and reproduced here with permission from Global Atmospherics, Inc. of Tucson, AZ, is presented in Fig. 10.3. Note the considerably large GFD levels affecting the state of Florida, as well as all the southern states along the Gulf of Mexico (Alabama, Mississippi, Louisiana, and Texas). High GFD levels are also observed in the southeastern states of Georgia and South Carolina. To the west, Arizona is the only state with GFD levels as high as 8 flashes/km^2/year. The lowest GFD levels (<0.5 flashes/km^2/year) are observed in the western states, notably in California, Oregon, and Washington on the Pacific Ocean, in a spot area of Colorado, and in the northeastern state of Maine on the Atlantic Ocean.

It is interesting to mention that a previous (five-year average) version of this map showed levels of around 6 flashes/km^2/year also in some areas of Illinois, Iowa, Missouri, and Indiana, not seen in the present version. This is often the result of short-term observations, that do not reflect all climatic variations that take place in a longer time frame.

The low incidence of lightning does not necessarily mean an absence of lightning-related problems. Power lines, for example, are prone to failures even if GFD levels are low when they are installed in terrain with high-resistivity soils, like deserts or when lines span across hills or mountains where ground wire or lightning arrester earthing becomes difficult.

The GFD level is an important parameter to consider for the design of electric power and telecommunication facilities. This is due to the fact that power line performance and damage to power and telecommunication equipment are considerably affected by lightning. Worldwide, lightning accounts for most of the power supply interruptions in distribution lines and it is a leading cause of failures in

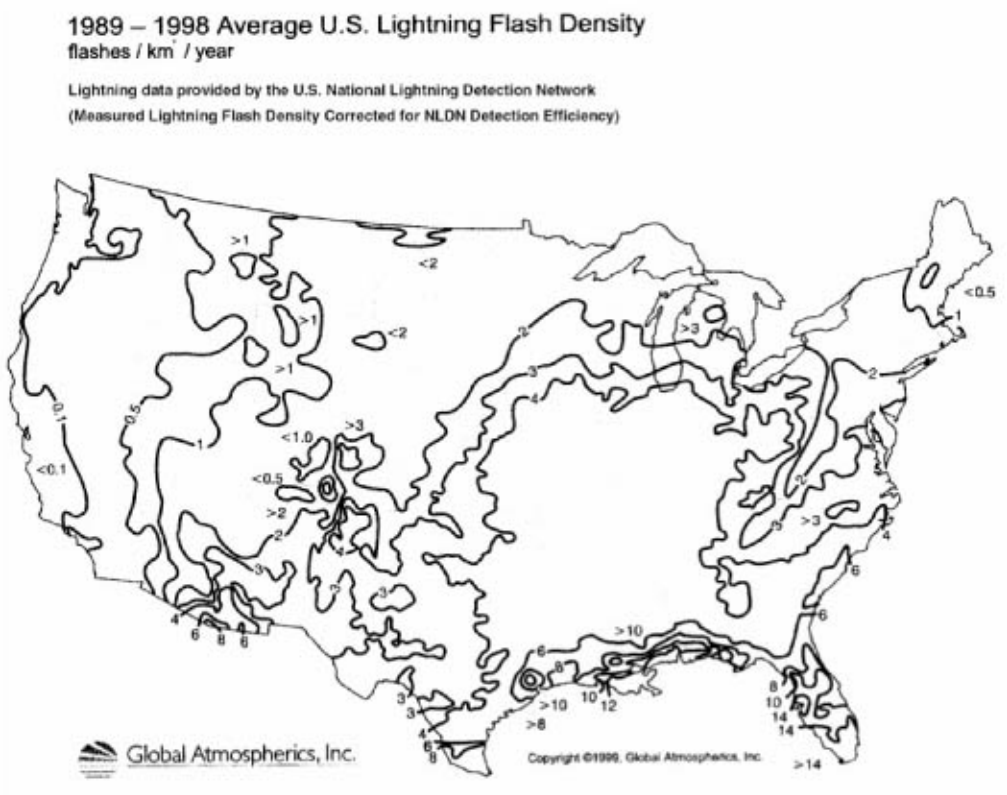

FIGURE 10.3 10-year average GFD map of the U.S. (Reproduced with permission from Global Atmospherics, Inc. of Tucson, AZ.)

transmission systems. In the U.S. alone, an estimated 30% of all power outages are lightning-related on annual average, with total costs approaching one billion dollars (Kithil, 1998).

In De la Rosa et al. (1998), it is discussed how to determine GFD as a function of TD (Thunder Days or Keraunic Level) or TH (Thunder-Hours). This is important where GFD data from lightning location systems are not available. Basically, any of these parameters can be used to get a *rough* approximation of Ground Flash Density. Using the expressions described in Anderson et al. and MacGorman et al. (1984, 1984), respectively:

$$\mathrm{Ng} = 0.04\ \mathrm{TD}^{1.25}\ \ \mathrm{flashes}/\mathrm{km}^2/\mathrm{year} \tag{10.1}$$

$$\mathrm{Ng} = 0.054\ \mathrm{TD}^{1.1}\ \ \mathrm{flashes}/\mathrm{km}^2/\mathrm{year} \tag{10.2}$$

Current Peak Value

Finally, regarding current peak values, first strokes are associated with peak currents around two to three times larger than subsequent strokes. According to De la Rosa et al. (1998), electric field records, however, suggest that subsequent strokes with higher electric field peak values may be present in one out of three cloud-to-ground flashes. These may be associated with current peak values greater than the first stroke peak.

Tables 10.1 and 10.2 are summarized and adapted from (Berger et al., 1975) for negative and positive flashes, respectively. They present statistical data for 127 cloud-to-ground flashes, 26 of them positive, measured in Switzerland. These are the type of lightning flashes known to hit flat terrain and structures of moderate height. This summary, for simplicity, shows only the 50% or statistical value, based on the

TABLE 10.2 Lightning Current Parameters for Positive Flashes[a]

Parameters	Units	Sample Size	Value Exceeding in 50% of the Cases
Peak current (minimum 2 kA)	kA	26	35
Charge (total charge)	C	26	80
Impulse charge (excluding continuing current)	C	25	16
Front duration (2 kA to peak)	μs	19	22
Maximum di/dt	kA/μs	21	2.4
Stroke duration (2 kA to half peak value on the tail)	μs	16	230
Action integral ($\grave{o}i^2dt$)	A^2s	26	6.5×10^5
Flash duration	ms	24	85

[a] Adapted from Berger et al., Parameters of lightning flashes, *Electra No. 41,* 23–37, July 1975.

log-normal approximations to the respective statistical distributions. These data are amply used as primary reference in the literature on both lightning protection and lightning research.

The action integral is an interesting concept (i.e., the energy that would be dissipated in a 1-Ω resistor if the lightning current were to flow through it). This is a parameter that can provide some insight on the understanding of forest fires and on damage to power equipment, including surge arresters, in power line installations. All the parameters presented in Tables 10.1 and 10.2 are estimated from current oscillograms with the shortest measurable time being 0.5 μs (Berger and Garbagnati, 1984). It is thought that the distribution of front duration might be biased toward larger values and the distribution of di/dt toward smaller values (De la Rosa et al., 1998).

Incidence of Lightning to Power Lines

One of the most accepted expressions to determine the number of direct strikes to an overhead line in an open ground with no nearby trees or buildings, is that described by Eriksson (1987):

$$N = Ng\left(\frac{28h^{0.6} + b}{10}\right) \tag{10.3}$$

where

- h is the pole or tower height (m) — negligible for distribution lines
- b is the structure width (m)
- Ng is the Ground Flash Density (flashes/km²/year)
- N is the number of flashes striking the line/100 km/year. For unshielded distribution lines, this is comparable to the fault index due to direct lightning hits. For transmission lines, this is an indicator of the exposure of the line to direct strikes. (The response of the line being a function of overhead ground wire shielding angle on one hand and on conductor-tower surge impedance and footing resistance on the other hand).

Note the dependence of the incidence of strikes to the line with height of the structure. This is important since transmission lines are several times taller than distribution lines, depending on their operating voltage level.

Also important is that in the real world, power lines are to different extents shielded by nearby trees or other objects along their corridors. This will decrease the number of direct strikes estimated by Eq. (10.3) to a degree determined by the distance and height of the objects. In IEEE Std. 1410-1997, a shielding factor is proposed to estimate the shielding effect of nearby objects to the line. An important aspect of this reference work is that objects within 40 m from the line, particularly if equal or higher that 20 m, can attract most of the lightning strikes that would otherwise hit the line. Likewise, the same

objects would produce insignificant shielding effects if located beyond 100 m from the line. On the other hand, sectors of lines extending over hills or mountain ridges may increase the number of strikes to the line.

The above-mentioned effects may, in some cases, cancel each other so that the estimation obtained form Eq. (10.3) can still be valid. However, it is recommended that any assessment of the incidence of lightning strikes to a power line be performed by taking into account natural shielding and orographic conditions along the line route. This also applies when identifying troubled sectors of the line for installation of metal oxide surge arresters to improve its lightning performance.

Finally, although meaningful only for distribution lines, the inducing effects of lightning, also described in De la Rosa et al. (1998) and Anderson et al. (1984), have to be considered to properly understand their lightning performance or when dimensioning the outage rate improvement after application of any mitigation action. Under certain conditions, like in circuits without grounded neutral, with low critical flashover voltages, high GFD levels, or located on high resistivity terrain, the number of outages produced by close lightning can considerably surpass those due to direct strikes to the line.

Conclusions

We have tried to present a brief overview of lightning and its effects in electric power lines. It is important to mention that a design and/or assessment of power lines considering the influence of lightning overvoltages has to undergo a more comprehensive manipulation, outside the scope of this limited discussion.

Aspects like the different methods available to calculate shielding failures and backflashovers in transmission lines, or the efficacy of remedial measures are not covered here. Among these, overhead ground wires, metal oxide surge arresters, increased insulation, or use of wood as an arc quenching device, can only be mentioned. The reader is encouraged to look further at the references or to get experienced advice for a more comprehensive understanding of the subject.

References

Anderson, R. B. and Eriksson, A. J., Lightning parameters for engineering applications, *Electra No. 69*, 65–102, March 1980.

Anderson, R. B., Eriksson, A. J., Kroninger, H., Meal, D. V., and Smith, M. A., Lightning and thunderstorm parameters, in *IEE Lightning and Power Systems Conf. Publ. No. 236*, London, 1984.

Berger, K., Anderson, R. B., and Kroninger, H., Parameters of lightning flashes, *Electra No. 41*, 23–37, July 1975.

Berger, K. and Garbagnati, E., Lightning current parameters, results obtained in Switzerland and in Italy, in *Proc. URSI Conf.*, Florence, Italy, 1984.

Cooray, V. and Jayaratne, K. P. S., Characteristics of lightning flashes observed in Sri Lanka in the tropics, *J. Geophys. Res. 99,* 21,051–21,056, 1994.

Cooray, V. and Perez, H., Some features of lightning flashes observed in Sweden, *J. Geophys. Res. 99,* 10,683–10,688, 1994.

Eriksson, A. J., The incidence of lighting strikes to power lines, in *IEEE Trans. on Power Delivery*, PWRD-2(2), 859–870, July 1987.

IEEE Std. 1410-1997, IEEE Guide for Improving the Lightning Performance of Electric Power Distribution Lines, *IEEE PES*, December, 1997, Section 5.

Kithil, R., Lightning protection codes: Confusion and costs in the USA, in *Proc. of the 24th Int'l Lightning Protection Conference*, Birmingham, U.K., Sept 16, 1998.

MacGorman, D. R., Maier, M. W., and Rust, W. D., Lightning strike density for the contiguous United States from thunderstorm duration records, in *NUREG/CR-3759, Office of Nuclear Regulatory Research, U.S. Nuclear Regulatory Commission,* Washington, D.C., 44, 1984.

Rakov, M. A., Uman, M. A., and Thottappillil, R., Review of lightning properties from electric field and TV observations, *J. Geophys. Res. 99,* 10,745–10,750, 1994.

De la Rosa, F., Nucci, C. A., and Rakov, V. A., Lightning and its impact on power systems, in *Proc. Int'l Conf. on Insulation Coordination for Electricity Development in Central European Countries*, Zagreb, Croatia, 1998.

Thottappillil, R., Rakov, V. A., Uman, M. A., Beasley, W. H., Master, M. J., and Shelukhin, D. V., Lightning subsequent stroke electric field peak greater than the first stroke and multiple ground terminations, *J. Geophys. Res.*, 97, 7,503–7,509, 1992.

Uman, M. A. *Lightning*, Dover, New York, 1969, Appendix E.

Uman, M. A., *The Lightning Discharge*, International Geophysics Series, Vol. 39, Academic Press, Orlando, FL, Chapter 1, 1987.

10.2 Overvoltages Caused by Direct Lightning Strokes

Pritindra Chowdhuri

A lightning stroke is defined as a direct stroke if it hits either the tower or the shield wire or the phase conductor. This is illustrated in Fig. 10.4. When the insulator string at a tower flashes over by direct hit either to the tower or to the shield wire along the span, it is called a backflash; if the insulator string flashes over by a strike to the phase conductor, it is called a shielding failure for a line shielded by shield wires. Of course, for an unshielded line, insulator flashover is caused by backflash when the stroke hits the tower or by direct contact with the phase conductor. In the analysis of performance and protection of power systems, the most important parameter which must be known is the insulation strength of the system. It is not a unique number. It varies according to the type of the applied voltage, e.g., DC, AC, lightning, or switching surges. For the purpose of lightning performance, the insulation strength has been defined in two ways: basic impulse insulation level (BIL) and critical flashover voltage (CFO or V_{50}). BIL has been defined in two ways. The statistical BIL is the crest value of a standard (1.2/50-μs) lightning impulse voltage that the insulation will withstand with a probability of 90% under specified conditions. The conventional BIL is the crest value of a standard lightning impulse voltage that the insulation will withstand for a specific number of applications under specified conditions. CFO or V_{50} is the crest value of a standard lightning impulse voltage that the insulation will withstand during 50% of the applications. In this section, the conventional BIL will be used as the insulation strength under lightning impulse voltages. Analysis of direct strokes to overhead lines can be divided into two classes: unshielded lines and shielded lines. The first discussion involves the unshielded lines.

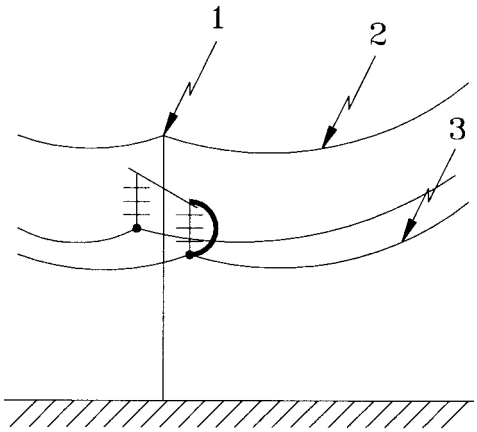

FIGURE 10.4 Illustration of direct lightning strokes to line. (1) backflash caused by direct stroke to tower; (2) backflash caused by direct stroke to shield wire; (3) insulator flashover by direct stroke to phase conductor (shielding failure).

Direct Strokes to Unshielded Lines

If lightning hits one of the phase conductors, the return-stroke current splits into two equal halves, each half traveling in either direction of the line. The traveling current waves produce traveling voltage waves that are given by:

$$V = \frac{Z_o I}{2} \tag{10.4}$$

where I is the return-stroke current and Z_o is the surge impedance of the line, given by $Z_o = (L/C)^{1/2}$, and L and C are the series inductance and capacitance to ground per meter length of the line. These traveling voltage waves stress the insulator strings from which the line is suspended as these voltages arrive at the succeeding towers. The traveling voltages are attenuated as they travel along the line by ground resistance and mostly by the ensuing corona enveloping the struck line. Therefore, the insulators of the towers adjacent to the struck point are most vulnerable. If the peak value of the voltage, given by Eq. (10.4), exceeds the BIL of the insulator, then it might flash over causing an outage. The minimum return-stroke current that causes an insulator flashover is called the critical current, I_c, of the line for the specified BIL. Thus, following Eq. (10.4):

$$I_c = \frac{2\,BIL}{Z_o} \tag{10.5}$$

Lightning may hit one of the towers. The return-stroke current then flows along the struck tower and over the tower-footing resistance before being dissipated in the earth. The estimation of the insulator voltage in that case is not simple, especially because there has been no concensus about the modeling of the tower in estimating the insulator voltage. In the simplest assumption, the tower is neglected. Then, the tower voltage, including the voltage of the cross arm from which the insulator is suspended, is the voltage drop across the tower-footing resistance, given by $V_{tf} = IR_{tf}$, where R_{tf} is the tower-footing resistance. Neglecting the power-frequency voltage of the phase conductor, this is then the voltage across the insulator. It should be noted that this voltage will be of opposite polarity to that for stroke to the phase conductor for the same polarity of the return-stroke current.

Neglecting the tower may be justified for short towers. The effect of the tower for transmission lines must be included in the estimation of the insulator voltage. For these cases, the tower has also been represented as an inductance. Then the insulator voltage is given by $V_{ins} = V_{tf} + L(dI/dt)$, where L is the inductance of the tower.

However, it is known that voltages and currents do travel along the tower. Therefore, the tower should be modeled as a vertical transmission line with a surge impedance, Z_t, where the voltage and current waves travel with a velocity, v_t. The tower is terminated at the lower end by the tower-footing resistance, R_{tf}, and at the upper end by the lightning channel, which can be assumed to be another transmission line of surge impedance, Z_{ch}. Therefore, the traveling voltage and current waves will be repeatedly reflected at either end of the tower while producing voltage at the cross arm, V_{ca}. The insulator from which the phase conductor is suspended will then be stressed at one end by V_{ca} (to ground) and at the other end by the power-frequency phase-to-ground voltage of the phase conductor. Neglecting the power- frequency voltage, the insulator voltage, V_{ins} will be equal to the cross-arm voltage, V_{ca}. This is schematically shown in Fig. 10.5a. The initial voltage traveling down the tower, V_{to}, is $V_{to}(t) = Z_t I(t)$, where I(t) is the initial tower current which is a function of time, t. The voltage reflection coefficients at the two ends of the tower are given by:

$$a_{r1} = \frac{R_{tf} - Z_t}{R_{tf} + Z_t} \quad \text{and} \quad a_{r2} = \frac{Z_{ch} - Z_t}{Z_{ch} + Z_t}. \tag{10.6}$$

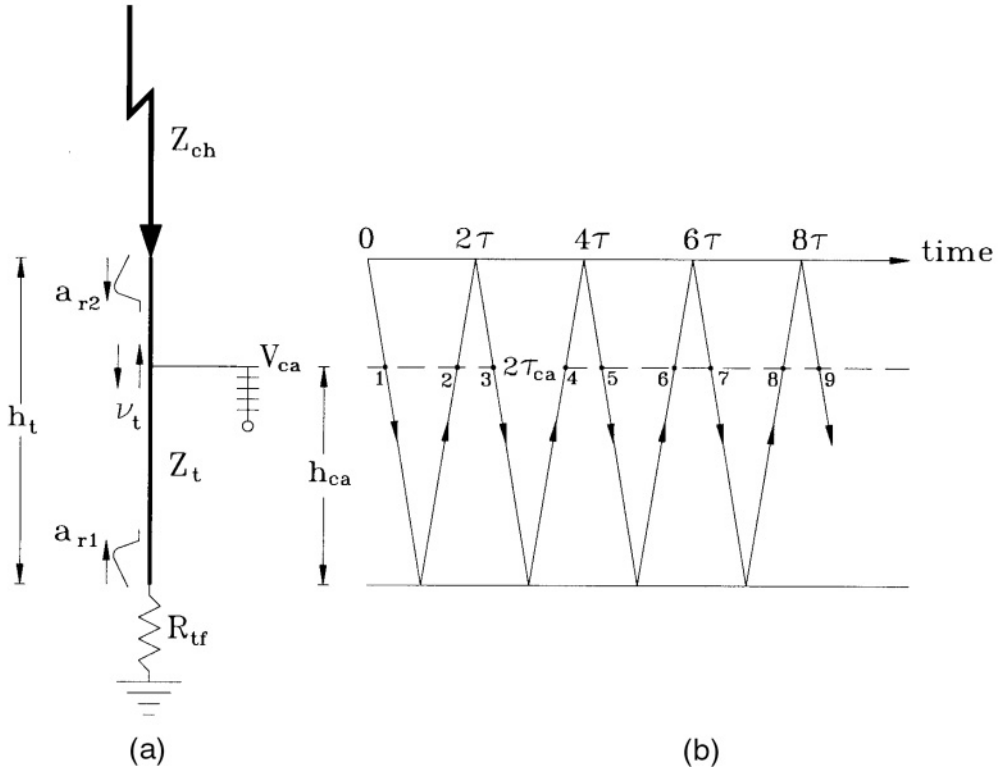

FIGURE 10.5 Lightning channel striking tower top: (a) schematic of struck tower; (b) voltage lattice diagram.

Figure 10.5b shows the lattice diagram of the progress of the multiple reflected voltage waves along the tower. The lattice diagram, first proposed by Bewley (1951), is the space-time diagram that shows the position and direction of motion of every incident, reflected, and transmitted wave on the system at every instant of time. In Fig. 10.5, if the heights of the tower and the cross arm are h_t and h_{ca}, respectively, and the velocity of the traveling wave along the tower is ν_t, then the time of travel from the tower top to its foot is $\tau_1 = h_t/\nu_t$, and the time of travel from the cross arm to the tower foot is $\tau_{ca} = h_{ca}/\nu_t$. In Fig. 10.5b, the two solid horizontal lines represent the positions of the tower top and the tower foot, respectively. The broken horizontal line represents the cross-arm position. It takes $(\tau_t - \tau_{ca})$ seconds for the traveling wave to reach the cross arm after lightning hits the tower top at $t = 0$. This is shown by point 1 on Fig. 10.5b. Similarly, the first reflected wave from the tower foot (point 2 in Fig. 10.5b) reaches the cross arm at $t = (\tau_t + \tau_{ca})$. The first reflected wave from the tower top (point 3 in Fig. 10.5b) reaches the cross arm at $t = (3\tau_t - \tau_{ca})$. The downward-moving voltage waves will reach the cross arm at $t = (2n-1)\tau_t - \tau_{ca}$, and the upward-moving voltage waves will reach the cross arm at $t = (2n-1)\tau_t + \tau_{ca}$, where $n = 1, 2, \cdots, n$. The cross-arm voltage, $V_{ca}(t)$ is then given by:

$$V_{ca}(t) = \sum_{n=1}^{n} (a_{r1}a_{r2})^{n-1} V_{to}\left(t-(2n-1)\tau_t+\tau_{ca}\right)u\left(t-(2n-1)\tau_t+\tau_{ca}\right)+$$
$$a_{r1}\sum_{n=1}^{n} (a_{r1}a_{r2})^{n-1} V_{to}\left(t-(2n-1)\tau_t-\tau_{ca}\right)u\left(t-(2n-1)\tau_t-\tau_{ca}\right) \quad (10.7)$$

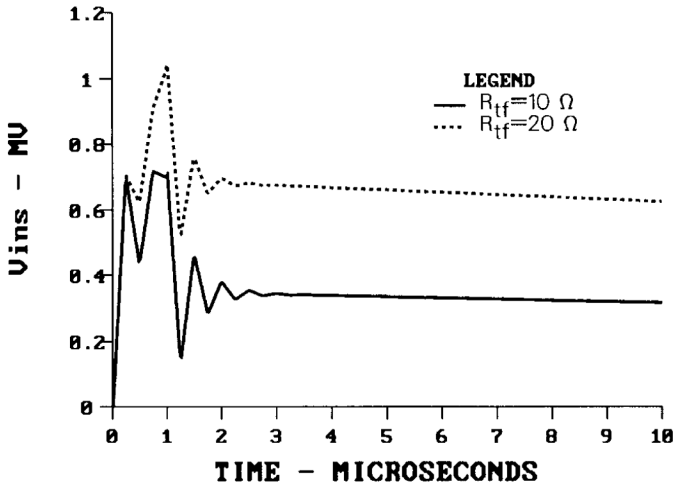

FIGURE 10.6 Profiles of insulator voltage for an unshielded line for a lightning stroke to tower. Tower height = 30 m; cross-arm height = 27.0 m; phase-conductor height = 25.0 m cross-arm width = 2.0 m; return-stroke current = 30 kA @1/50-μs; Z_t = 100 Ω; Z_{ch} = 500 Ω.

The voltage profiles of the insulator voltage, $V_{ins}(= V_{ca})$ for two values of tower-footing resistances, R_{tf}, are shown in Fig. 10.6. It should be noticed that the V_{ins} is higher for higher R_{tf} and that it approaches the voltage drop across the tower-footing resistance (IR_{tf}) with time. However, the peak of V_{ins} is significantly higher than the voltage drop across R_{tf}. Higher peak of V_{ins} will occur for (i) taller tower and (ii) shorter front time of the stroke current (Chowdhuri, 1996).

Direct Strokes to Shielded Lines

One or more conductors are strung above and parallel to the phase conductors of single- and double-circuit overhead power lines to shield the phase conductors from direct lightning strikes. These shield wires are generally directly attached to the towers so that the return-stroke currents are safely led to ground through the tower-footing resistances. Sometimes, the shield wires are insulated from the towers by short insulators to prevent power-frequency circulating currents from flowing in the closed-circuit loop formed by the shield wires, towers, and the earth return. When lightning strikes the shield wire, the short insulator flashes over, connecting the shield wire directly to the grounded towers.

For a shielded line, lightning may strike a phase conductor, the shield wire, or the tower. If it strikes a phase conductor but the magnitude of the current is below the critical current level, then no outage occurs. However, if the lightning current is higher than the critical current of the line, then it will precipitate an outage that is called the shielding failure. In fact, sometimes, shielding is so designed that a few outages are allowed, with the objective of reducing the excessive cost of shielding. However, the critical current for a shielded line is higher than that for an unshielded line because the presence of the grounded shield wire reduces the effective surge impedance of the line. The effective surge impedance of a line shielded by one shield wire is given by (Chowdhuri, 1996):

$$Z_{eq} = Z_{11} - \frac{Z_{12}^2}{Z_{22}} \tag{10.8}$$

$$\text{where } Z_{11} = 60\,\ell n\frac{2h_p}{r_p};\ Z_{22} = 60\,\ell n\frac{2h_s}{r_s};\ Z_{12} = 60\,\ell n\frac{d_{p's}}{d_{ps}} \tag{10.9}$$

Here, h_p and r_p are the height and radius of the phase conductor, h_s and r_s are the height and radius of the shield wire, $d_{p's}$ is the distance from the shield wire to the image of the phase conductor in the ground, and d_{ps} is the distance from the shield wire to the phase conductor. Z_{11} is the surge impedance of the phase conductor in the absence of the shield wire, Z_{22} is the surge impedance of the shield wire, and Z_{12} is the mutual surge impedance between the phase conductor and the shield wire.

It can be shown that either for strokes to tower or for strokes to shield wire, the insulator voltage will be the same if the attenuation caused by impulse corona on the shield wire is neglected (Chowdhuri, 1996). For a stroke to tower, the return-stroke current will be divided into three parts: two parts going to the shield wire in either direction from the tower, and the third part to the tower. Thus, lower voltage will be developed along the tower of a shielded line than that for an unshielded line for the same return-stroke current, because lower current will penetrate the tower. This is another advantage of a shield wire. The computation of the cross-arm voltage, V_{ca}, is similar to that for the unshielded line, except for the following modifications in Eqs. (10.6) and (10.7):

1. The initial tower voltage is equal to IZ_{eq}, instead of IZ_t as for the unshielded line, where Z_{eq} is the impedance as seen from the striking point, i.e.,

$$Z_{eq} = \frac{0.5 Z_s Z_t}{0.5 Z_s + Z_t}, \tag{10.10}$$

   where $Z_s = 60\ell n(2h_s/r_s)$ is the surge impedance of the shield wire.
2. The traveling voltage wave moving upward along the tower, after being reflected at the tower foot, encounters three parallel branches of impedances, the lightning-channel surge impedance, and the surge impedances of the two halves of the shield wire on either side of the struck tower. Therefore, Z_{ch} in Eq. (10.6) should be replaced by $0.5Z_sZ_{ch}/(0.5Z_s + Z_{ch})$.

The insulator voltage, V_{ins}, for a shielded line is not equal to V_{ca}, as for the unshielded line. The shield-wire voltage, which is the same as the tower-top voltage, V_{tt}, induces a voltage on the phase conductor by electromagnetic coupling. The insulator voltage is, then, the difference between V_{ca} and this coupled voltage:

$$V_{ins} = V_{ca} - k_{sp} V_{tt}, \tag{10.11}$$

where $k_{sp} = Z_{12}/Z_{22}$. It can be seen that the electromagnetic coupling with the shield wire reduces the insulator voltage. This is another advantage of the shield wire. To compute V_{tt}, we go back to Fig. 10.5. As the cross arm is moved toward the tower top, τ_{ca} approaches τ_t, and naturally, at tower top $\tau_{ca} = \tau_t$. Then, except the wave 1, the pairs of upward-moving and downward-moving voltages (e.g., 2 and 3, 4 and 5, etc.) arrive at the tower top at the same time. Putting $\tau_{ca} = \tau_t$ in Eq. (10.7), and writing $a_{t2} = 1 + a_{r2}$, we get V_{tt}:

$$V_{tt}(t) = V_{to}u(t) + a_{t2}a_{r1}\sum_{n=1}^{n}(a_{r1}a_{r2})^{n-1}V_{to}(t-2n\tau_t)u(t-2n\tau_t). \tag{10.12}$$

$$\text{From Eq. (10.6)},\ a_{t2} = 1 + a_{r2} = \frac{2Z_{ch}}{Z_{ch} + Z_t}. \tag{10.13}$$

The coefficient, a_{t2}, is called the coefficient of voltage transmission.

When lightning strikes the tower, equal voltages (IZ_{eq}) travel along the tower as well as along the shield wire in both directions. The voltages on the shield wire are reflected at the subsequent towers and arrive

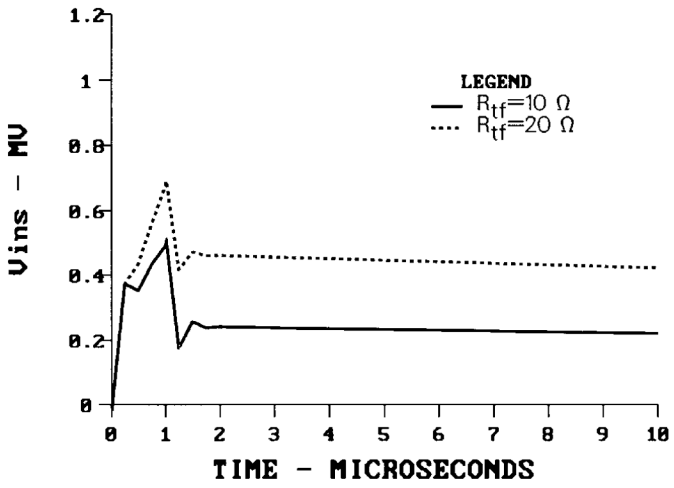

FIGURE 10.7 Profiles of insulator voltage for a shielded line for lightning stroke to tower.Tower height = 30 m; cross-arm height = 27.0 m; phase-conductor height = 25.0 m cross-arm width = 2.0 m; return-stroke current = 30 kA @1/50-μs; Z_t = 100 Ω; Z_{ch} = 500 Ω.

back at the struck tower at different intervals as voltages of opposite polarity (Chowdhuri, 1996). Generally, the reflections from the nearest towers are of any consequence. These reflected voltage waves lower the tower-top voltage. The tower-top voltage remains unaltered until the first reflected waves arrive from the nearest towers. The profiles of the insulator voltage for the same line as in Fig. 10.6 but with a shield wire are shown in Fig. 10.7. Comparing Figs. 10.6 and 10.7, it should be noticed that the insulator voltage is significantly reduced for a shielded line for a stroke to tower. This reduction is possible because (i) a part of the stroke current is diverted to the shield wire, thus reducing the initial tower-top voltage ($V_{to} = I_t Z_t$, $I_t < I$), and (ii) the electromagnetic coupling between the shield wire and the phase conductor induces a voltage on the phase conductor, thus lowering the voltage difference across the insulator ($V_{ins} = V_{ca} - k_{sp} V_{tt}$).

Shielding Design

Striking distance of the lightning stroke plays a crucial role in the design of shielding. Striking distance is defined as the distance through which a descending stepped leader will strike a grounded object. Whitehead and his associates (1968; 1969) proposed a simple relation between the striking distance, r_s, and the return-stroke current, I, (in kA) of the form:

$$r_s = aI^b \left(m\right) \tag{10.14}$$

where a and b are constants. The most frequently used value of a is 8 or 10, and that of b is 0.65. Let us suppose that a stepped leader with prospective return-stroke current of I_s, is descending near a horizontal conductor, P, (Fig. 10.8a). Its striking distance, r_s, will be given by Eq. (10.14). It will hit the surface of the earth when it penetrates a plane which is r_s meters above the earth. The horizontal conductor will be struck if the leader touches the surface of an imaginary cylinder of radius, r_s, with its center at the center of the conductor. The attractive width of the horizontal conductor will be ab in Fig. 10.8a. It is given by:

$$ab = 2\omega_p = 2\sqrt{r_s^2 - \left(r_s - h_p\right)^2} = 2\sqrt{h_p\left(2r_s - h_p\right)} \quad \text{for } r_s > h_p \text{ and} \tag{10.15a}$$

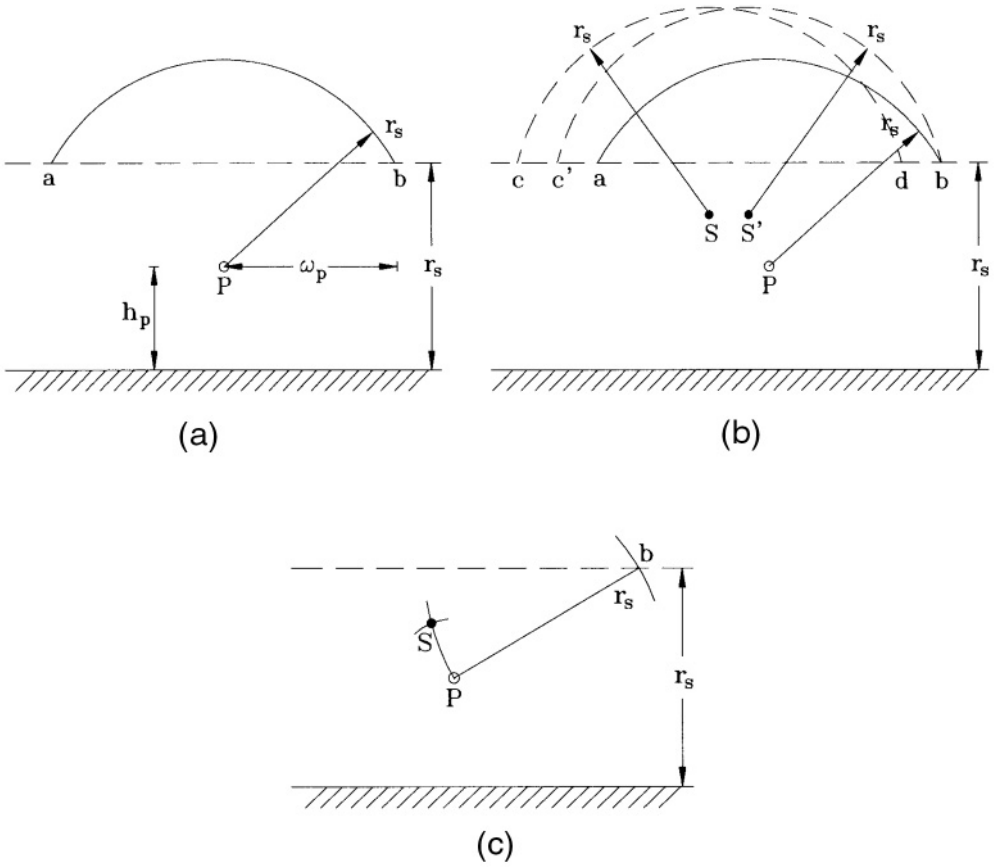

FIGURE 10.8 Principle of shielding: (a) electrogeometric model; (b) shielding principle; (c) placement of shield wire for perfect shielding.

$$ab = 2\omega_p = 2r_s \quad \text{for } r_s \le h_p, \tag{10.15b}$$

where h_p is the height of the conductor. For a multiconductor line with a separation distance, d_p, between the outermost conductors, the attractive width will be $2\omega_p + d_p$.

Now, if a second horizontal conductor, S, is placed near P, the attractive width of S will be cd (Fig. 10.8b). If S is intended to completely shield P, then the cylinder around S and the r_s-plane above the earth's surface must completely surround the attractive cylinder around P. However, as Fig. 10.8b shows, an unprotected width, db remains. Stepped leaders falling through db will strike P. If S is repositioned to S′ so that the point d coincides with b, then P is completely shielded by S.

The procedure to place the conductor, S, for perfect shielding of P is shown in Fig. 10.8c. Knowing the critical current, I_c, from Eq. (10.5), the corresponding striking distance, r_s, is computed from Eq. (10.14). A horizontal straight line is drawn at a distance r_s above the earth's surface. An arc of radius, r_s, is drawn with P as center, which intersects the r_s-line above earth at b. Then, an arc of radius, r_s, is drawn with b as center. This arc will go through P. Now, with P as radius, another arc is drawn of radius r_{sp}, where r_{sp} is the minimum required distance between the phase conductor and a grounded object. This arc will intersect the first arc at S, which is the position of the shield wire for perfect shielding of P.

Figure 10.9 shows the placement of a single shield wire above a three-phase horizontally configured line for shielding. In Fig. 10.9a, the attractive cylinders of all three phase conductors are contained within the attractive cylinder of the shield wire and the r_s-plane above the earth. However, in Fig. 10.9b where

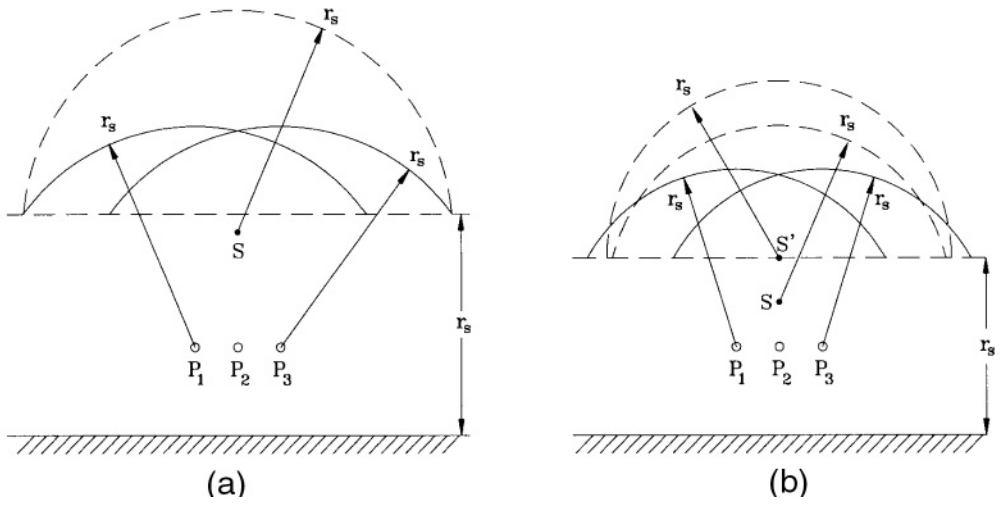

FIGURE 10.9 Shielding of three-phase horizontally configured line by single shield wire: (a) perfect shielding; (b) imperfect shielding.

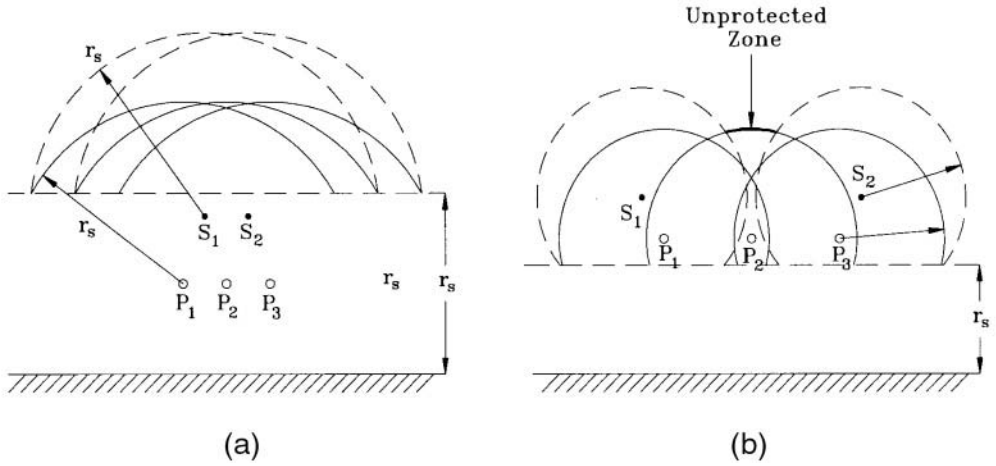

FIGURE 10.10 Shielding of three-phase horizontally configured line by two shield wires: (a) perfect shielding; (b) imperfect shielding.

the critical current is lower, the single shield wire at S cannot perfectly shield the two outer phase conductors. Raising the shield wire helps in reducing the unprotected width, but, in this case, it cannot completely eliminate shielding failure. As the shield wire is raised, its attractive width increases until the shield-wire height reaches the r_s-plane above earth, where the attractive width is the largest, equal to the diameter of the r_s-cylinder of the shield wire. Raising the shield-wire height further will then be actually detrimental. In this case, either the insulation strength of the line should be increased (i.e., the critical current increased) or two shield wires should be used.

Figure 10.10 shows the use of two shield wires. In Fig. 10.10a, all three phase conductors are completely shielded by the two shield wires. However, for smaller I_c (i.e., smaller r_s), part of the attractive cylinder of the middle phase conductor is left exposed (Fig. 10.10b). This shows that the middle phase conductor may experience shielding failure even when the outer phase conductors are perfectly shielded. In that case, either the insulation strength of the line should be increased or the height of the shield wires raised, or both.

Significant Parameters

The most significant parameter in estimating the insulator voltage is the return-stroke current, i.e., its peak value, waveshape, and statistical distributions of the amplitude and waveshape. The waveshape of the return-stroke current is generally assumed to be double exponential where the current rapidly rises to its peak exponentially, and subsequently decays exponentially:

$$I(t) = I_o\left(e^{-a_1 t} - e^{-a_2 t}\right). \tag{10.16}$$

The parameters, I_o, a_1, and a_2 are determined from the given peak, I_p, the front time, t_f, and the time to half value, t_h, during its subsequent decay. However, the return-stroke current can also be simulated as a linearly rising and linearly falling wave:

$$I(t) = \alpha_1 t u(t) - \alpha_2 (t - t_f) u(t - t_f), \tag{10.17}$$

$$\text{where,}\quad \alpha_1 = \frac{I_p}{t_f},\ \text{and}\ \alpha_2 = \frac{2t_h - t_f}{2t_f(t_h - t_f)} I_p. \tag{10.18}$$

I_o, a_1, and a_2 of the double exponential function in Eq. (10.16) are not very easy to evaluate. In contrast, α_1 and α_2 of the linear function in Eq. (10.17) are easy to evaluate as given in Eq. (10.18). The results from the two waveshapes are not significantly different, particularly for lightning currents where t_f is on the order of a few microseconds and t_h is several tens of microseconds. As t_h is very long compared to t_f, the influence of t_h on the insulator voltage is not significant. Therefore, any convenient number can be assumed for t_h (e.g., 50 μs) without loss of accuracy.

The statistical variations of the peak return-stroke curent, I_p, fits the log-normal distribution (Popolansky, 1972). The probability density function, $p(I_p)$, of I_p can then be expressed as:

$$p(I_p) = \frac{1}{\sqrt{2\pi}\, I_p\, \sigma_{\ell n I_p}} e^{-0.5\left(\frac{\ell n I_p - \ell n I_{pm}}{\sigma_{\ell n I_p}}\right)^2}, \tag{10.19}$$

where $\sigma_{\ell nIp}$ is the standard deviation of ℓnI_p, and I_{pm} is the median value of the return-stroke current, I_p. The cumulative probability, P_c, that the peak current in any lightning flash will exceed I_p kA can be determined by integrating Eq. (10.19) as follows:

$$\text{Putting}\ u = \frac{\ell n I_p - \ell n I_{pm}}{\sqrt{2}\,\sigma_{\ell n I_p}} \tag{10.20}$$

$$P_c(I_p) = \frac{1}{\sqrt{\pi}} \int_u^\infty e^{-u^2}\, du = 0.5\,\text{erfc}(u). \tag{10.21}$$

The probability density function, $p(t_f)$, of the front time, t_f, can be similarly determined by replacing I_{pm} and $\sigma_{\ell nIp}$ by the corresponding t_{fm} and $\sigma_{\ell ntf}$ in Eqs. (10.20) and (10.21). Assuming no correlation between I_p and t_f, the joint probability density function of I_p and t_f is $p(I_p, t_f) = p(I_p)p(t_f)$. The equation for $p(I_p, t_f)$ becomes more complex if there is a correlation between I_p and t_f (Chowdhuri, 1996). The

statistical parameters (I_{pm}, $\sigma_{\ell nIp}$, t_{fm} and $\sigma_{\ell ntf}$) have been analyzed in (Anderson and Eriksson, 1980; Eriksson, 1986) and are given in (Chowdhuri, 1996):

$$t_{fm} = 3.83\ \mu s;\ \sigma_{\ell ntf} = 0.553$$

$$\text{For } I_p \le 20\ \text{kA: } I_{pm} = 61.1\ \text{kA};\ \sigma_{\ell nIp} = 1.33$$

$$\text{For } I_p > 20\ \text{kA: } I_{pm} = 33.3\ \text{kA};\ \sigma_{\ell nIp} = 0.605$$

Besides I_p anf t_f, the ground flash density, n_g, is the third significant parameter in estimating the lightning performance of power systems. The ground flash density is defined as the average number of lightning strokes per square kilometer per year in a geographic region. It should be borne in mind that the lightning activity in a particular geographic region varies by a large margin from year to year. Generally, the ground flash density is averaged over ten years. In the past, the index of lightning severity was the keraunic level (i.e., the number of thunder days in a region) because that was the only parameter available. Several empirical equations have been used to relate keraunic level with n_g. However, there has been a concerted effort in many parts of the world to measure n_g directly, and the measurement accuracy has also been improved in recent years.

Outage Rates by Direct Strokes

The outage rate is the ultimate gauge of lightning performance of a transmission line. It is defined as the number of outages caused by lightning per 100 km of line length per year. One needs to know the attractive area of the line in order to estimate the outage rate. The line is assumed to be struck by lightning if the stroke falls within the attractive area. The electrical shadow method has been used to estimate the attractive area. According to the electrical shadow method, a line of height, h_ℓ m, will attract lightning from a distance of $2h_\ell$ m from either side. Therefore, for a 100-km length, the attractive area will be $0.4h_\ell$ km^2. This area is then a constant for a specific overhead line of given height, and is independent of the severity of the lightning stroke (i.e., I_p). The electrical shadow method has been found to be unsatisfactory in estimating the lightning performance of an overhead power line. Now, the electrogeometric model is used in estimating the attractive area of an overhead line. The attractive area is estimated from the striking distance, which is a function of the return-stroke current, I_p, as given by Eq. (10.14). Although it has been suggested that the striking distance should also be a function of other variables (Chowdhuri and Kotapalli, 1989), the striking distance as given by Eq. (10.14) is being universally used.

The first step in the estimation of outage rate is the determination of the critical current. If the return-stroke current is less than the critical current, then the insulator will not flash over if the line is hit by the stepped leader. If one of the phase conductors is struck, such as for an unshielded line, then the critical current is given by Eq. (10.5). However, for strikes either to the tower or to the shield wire of a shielded line, the critical current is not that simple to compute if the multiple reflections along the tower are considered as in Eqs. (10.7) or (10.12). For these cases, it is best to compute the insulator voltage first by Eqs. (10.7) or by (10.12) for a return-stroke current of 1 kA, then estimate the critical current by taking the ratio between the insulation strength and the insulator voltage caused by 1 kA of return-stroke current of the specified front time, t_f, bearing in mind that the insulator voltage is a function of t_f.

Methods of estimation of the outage rate for unshielded and shielded lines will be somewhat different. Therefore, they are discussed separately.

Unshielded Lines

The vertical towers and the horizontal phase conductors coexist for an overhead power line. In that case, there is a race between the towers and the phase conductors to catch the lightning stroke. Some lightning strokes will hit the towers and some will hit the phase conductors. Figure 10.11 illustrates how to estimate the attractive areas of the towers and the phase conductors.

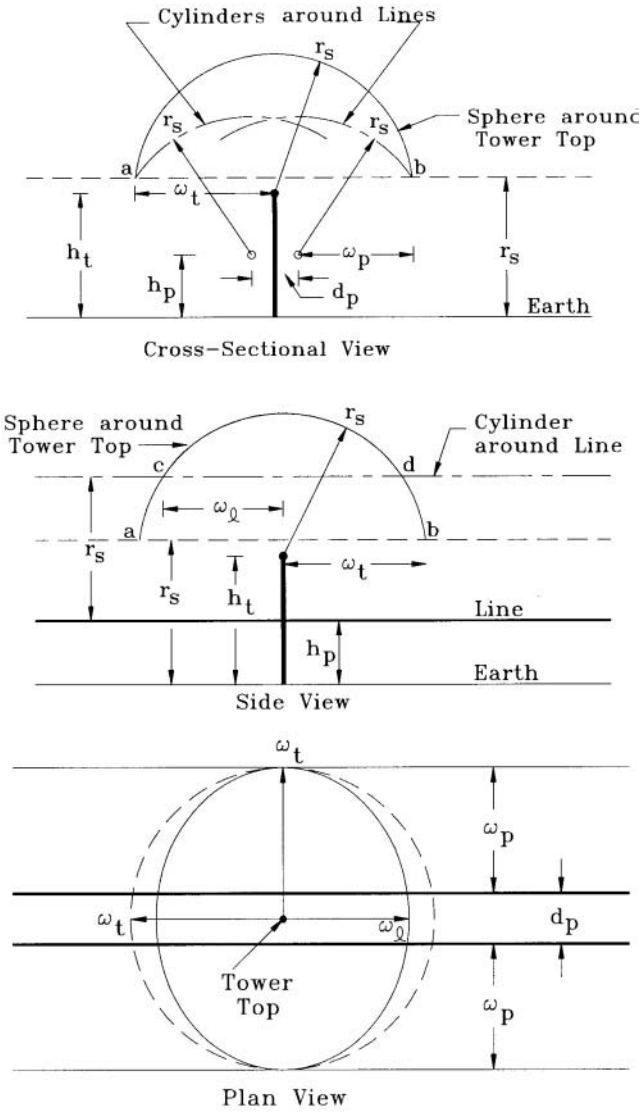

FIGURE 10.11 Attractive areas of tower and horizontal conductors.

The tower and the two outermost phase conductors are shown in Fig. 10.11. In the cross-sectional view, a horizontal line is drawn at a distance r_s from the earth's surface, where r_s is the striking distance corresponding to the return-stroke current, I_s. A circle (cross-sectional view of a sphere) is drawn with radius, r_s, and center at the tip of the tower, cutting the line above the earth at a and b. Two circles (representing cylinders) are drawn with radius, r_s, and centers at the outermost phase conductors, cutting the line above the earth again at a and b. The horizontal distance between the tower tip and either a or b is ω_t. The side view of Fig. 10.11 shows where the sphere around the tower top penetrates both the r_s-plane (a and b) above ground and the cylinders around the outermost phase conductors (c and d). The projection of the sphere around the tower top on the r_s-plane is a circle of radius, ω_t, given by:

$$\omega_t = \sqrt{r_s^2 - \left(r_s - h_t\right)^2} = \sqrt{h_t\left(2r_s - h_t\right)}. \tag{10.22}$$

The projection of the sphere on the upper surface of the two cylinders around the outer phase conductors will be an ellipse with its minor axis, $2\omega_\ell$, along a line midway between the two outer phase conductors and parallel to their axes; the major axis of the ellipse will be 2_ω, as shown in the plan view of Fig. 10.11. ω_ℓ is given by:

$$\omega_\ell = \sqrt{r_s^2 - \left(r_s - h_t + h_p\right)^2}. \tag{10.23}$$

If a lightning stroke with return-stroke current I_s or greater, falls within the ellipse, then it will hit the tower. It will hit one of the phase conductors if it falls outside the ellipse but within the width $(2\omega_p + d_p)$; it will hit the ground if it falls outside the width $(2\omega_p + d_p)$. Therefore, for each span length, ℓ_s, the attractive areas for the tower (A_t) and for the phase conductors (A_p) will be:

$$A_t = \pi\omega_t\omega_\ell \quad \text{and} \tag{10.24a}$$

$$A_p = \left(2\omega_p + d_p\right)\ell_s - A_t. \tag{10.24b}$$

The above analysis was performed for the shielding current of the overhead line when the sphere around the tower top and the cylinders around the outer phase conductors intersect the r_s-plane above ground at the same points (points a and b in Fig. 10.11). In this case, $2\omega_t = 2\omega_p + d_p$. The sphere and the cylinders will intersect the r_s-plane at different points for different return-stroke currents; their horizontal segments (widths) can be similarly computed. The equation for ω_t was given above. The equation for ω_p was given in Eq. (10.15). Due to conductor sag, the effective height of a conductor is lower than that at the tower. The effective height is generally assumed as:

$$h_p = h_{pt} - \frac{2}{3}\left(\text{midspan sag}\right), \tag{10.25}$$

where h_{pt} is the height of the conductor at the tower.

The critical current, i_{cp}, for stroke to a phase conductor is computed from Eq. (10.5). It should be noted that i_{cp} is independent of the front time, t_f, of the return-stroke current. The critical current, i_{ct}, for stroke to tower is a function of t_f. Therefore, starting with a short t_f, such as 0.5 μs, the insulator voltage is determined with 1 kA of tower injected current; then, the critical tower current for the selected t_f is determined by the ratio of the insulation strength (e.g., BIL) to the insulator voltage determined with 1 kA of tower injected current. The procedure for estimating the outage rate is started with the lower of the two critical currents (i_{cp} or i_{ct}). If i_{cp} is the lower one, which is usually the case, the attractive areas, A_p and A_t, are computed for that current. If $i_{cp} < i_{ct}$, then this will not cause any flashover if it falls within A_t. In other words, the towers act like partial shields to the phase conductors. However, all strokes with i_{cp} and higher currents falling within A_p will cause flashover. The cumulative probability, $P_c(i_{cp})$, for strokes with currents i_{cp} and higher is given by Eq. (10.21). If there are n_{sp} spans per 100 km of the line, then the number of outages for lightning strokes falling within A_p along the 100-km stretch of the line will be:

$$nfp_o = n_g P_c\left(i_{cp}\right) p\left(t_f\right) \Delta t_f n_{sp} A_p \tag{10.26}$$

where $p(t_f)$ is the probability density function of t_f, and Δt_f is the front step size. The stroke current is increased by a small step (e.g., 500 A), Δi, $(i = i_{cp} + \Delta i)$, and the enlarged attractive area, A_{p1}, is calculated. All strokes with currents i and higher falling within A_{p1} will cause outages. However, the outage rate for

strokes falling within A_p for strokes i_{cp} and greater has already been computed in Eq. (10.26). Therefore, only the additional outage rate, Δnfp, should be added to Eq. (10.26):

$$\Delta nfp = n_g P_c(i) p(t_f) \Delta t_f n_{sp} \Delta A_p, \tag{10.27}$$

where $\Delta A_p = A_{p1} - A_p$. The stroke current is increased in steps of Δi and the incremental outages are added until the stroke current is very high (e.g., 200 kA) when the probability of occurrence becomes acceptably low. Then, the front time, t_f is increased by a small step, Δt_f, and the computations are repeated until the probabilty of occurrence of higher t_f is low (e.g., $t_f = 10.5$ μs). In the mean time, if the stroke current becomes equal to i_{ct}, then the outages due to strokes to the tower should be added to the outages caused by strokes to the phase conductors. The total outage rate is then given by:

$$nft = nfp + nft \tag{10.28a}$$

$$nfp = nfpo + n_g n_{sp} \sum P_c(i) p(t_f) \Delta t_f \, \Delta A_p, \quad \text{and} \tag{10.28b}$$

$$nft = nfto + n_g n_t \sum_{t_f} \sum_{i} P_c(i) p(t_f) \Delta t_f \, \Delta A_t. \tag{10.28c}$$

With digital computers, the total outage rates can be computed within a few seconds.

Shielded Lines

For strokes to the shield wire, the voltage at the adjacent towers will be the same as that for stroke to the tower for the same stroke current. Therefore, there will be only one critical current for strokes to shielded lines, unlike the unshielded lines. The critical current for shielded lines can be computed similar to that for the unshielded lines, except Eq. (10.11) is now used instead of Eq. (10.7).

Otherwise, the computation for shielded lines is similar to that for unshielded lines. The variables h_p and d_p for the phase conductors are replaced by h_s and d_s, which are the shield-wire height and the separation distance between the shield wires, respectively. For a line with a single shield wire, $d_s = 0$. Generally, shield wires are attached to the tower at its top. However, the effective height of the shield wire is lower than that of the tower due to sag. The effective height of the shield wire, h_s, can be computed from Eq. (10.25) by replacing h_{pt} by h_{st}, the shield-wire height at tower.

References

Anderson, R. B. and Eriksson, A. J., Lightning parameters for engineering applications, *Electra*, 69, 65–102, 1980.

Armstrong, H. R. and Whitehead, E. R., Field and analytical studies of transmission line shielding, *IEEE Trans. on Power Appar. and Syst.*, PAS-87, 270-281, 1968.

Bewley, L. V., *Traveling Waves on Transmission Systems*, 2nd ed., John Wiley, New York, 1951.

Brown, G. W. and Whitehead, E. R., Field and analytical studies of transmission line shielding: Part II, *IEEE Trans. on Power Appar. and Syst.*, PAS-88, 617-626, 1969.

Chowdhuri, P., *Electromagnetic Transients in Power Systems*, Research Studies Press, Taunton, U.K. and Taylor and Francis, Philadelphia, PA, 1996.

Chowdhuri, P. and Kotapalli, A. K., Significant parameters in estimating the striking distance of lightning strokes to overhead lines, *IEEE Trans. on Power Delivery* 4, 1970–1981, 1989.

Eriksson, A. J., Notes on lightning parameters, CIGRE Note 33-86 (WG33-01) IWD, 15 July 1986.

Popolansky, F., Frequency distribution of amplitudes of lightning currents, *Electra*, 22, 139–147, 1972.

10.3 Overvoltages Caused by Indirect Lightning Strokes

Pritindra Chowdhuri

A direct stroke is defined as a lightning stroke when it hits either a shield wire, tower, or a phase conductor. An insulator string is stressed by very high voltages caused by a direct stroke. An insulator string can also be stressed by high transient voltages when a lightning stroke hits the nearby ground. An indirect stroke is illustrated in Fig. 10.12.

The voltage induced on a line by an indirect lightning stroke has four components:

1. The charged cloud above the line induces bound charges on the line while the line itself is held electrostatically at ground potential by the neutrals of connected transformers and by leakage over the insulators. When the cloud is partially or fully discharged, these bound charges are released and travel in both directions on the line giving rise to the traveling voltage and current waves.
2. The charges lowered by the stepped leader further induce charges on the line. When the stepped leader is neutralized by the return stroke, the bound charges on the line are released and thus produce traveling waves similar to that caused by the cloud discharge.
3. The residual charges in the return stroke induce an electrostatic field in the vicinity of the line and hence an induced voltage on it.
4. The rate of change of current in the return stroke produces a magnetically induced voltage on the line.

If the lightning has subsequent strokes, then the subsequent components of the induced voltage will be similar to one or the other of the four components discussed above.

The magnitudes of the voltages induced by the release of the charges bound either by the cloud or by the stepped leader are small compared with the voltages induced by the return stroke. Therefore, only the electrostatic and the magnetic components induced by the return stroke are considered in the following analysis. The initial computations are performed with the assumption that the charge distribution along the leader stroke is uniform, and that the return-stroke current is rectangular. However, the result with the rectangular current wave can be transformed to that with currents of any other waveshape by the convolution integral (Duhamel's theorem). It was also assumed that the stroke is vertical and that the overhead line is lossfree and the earth is perfectly conducting. The vertical channel of the return stroke is shown in Fig. 10.13, where the upper part consists of a column of residual charge which is neutralized by the rapid upward movement of the return-stroke current in the lower part of the channel.

Figure 10.14 shows a rectangular system of coordinates where the origin of the system is the point where lightning strikes the surface of the earth. The line conductor is located at a distance y_o meters from the origin, having a mean height of h_p meters above ground and running along the x-direction. The origin of time ($t = 0$) is assumed to be the instant when the return stroke starts at the earth level.

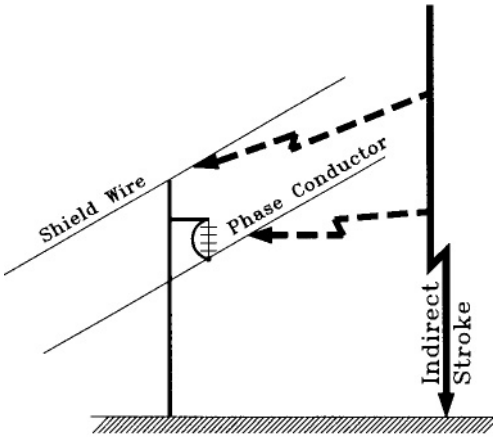

FIGURE 10.12 Illustration of direct and indirect lightning strokes.

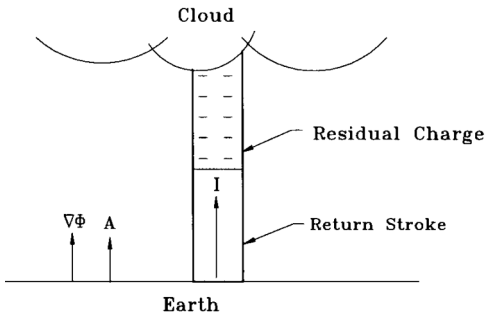

FIGURE 10.13 Return stroke with the residual charge column.

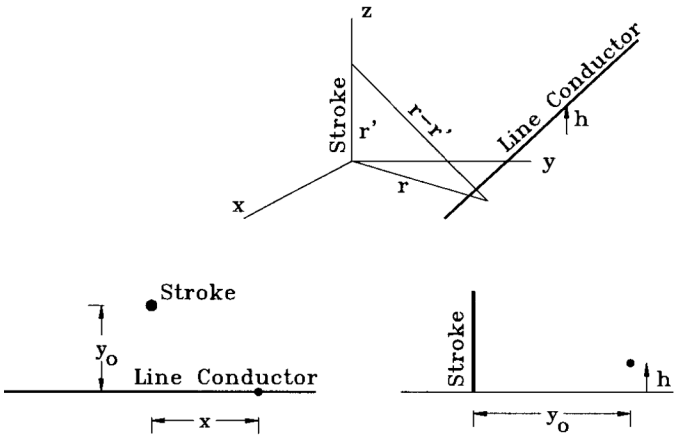

FIGURE 10.14 Coordinate system of line conductor and lightning stroke.

Inducing Voltage

The total electric field created by the charge and the current in the lightning stroke at any point in space is

$$E_i = E_{ei} + E_{mi} = -\nabla\phi - \frac{\partial A}{\partial t}, \tag{10.29}$$

where ϕ is the *inducing* scalar potential created by the residual charge at the upper part of the return stroke and A is the *inducing* vector potential created by the upward-moving return-stroke current (Fig. 10.13). ϕ and A are called the retarded potentials, because these potentials at a given point in space and time are determined by the charge and current at the source (i.e., the lightning channel) at an earlier time; the difference in time (i.e., the retardation) is the time required to travel the distance between the source and the field point in space with a finite velocity, which in air is $c = 3 \times 10^8$ m/s. These electromagnetic potentials can be deduced from the distribution of the charge and the current in the return-stroke channel. The next step is to find the inducing electric field [Eq. (10.29)]. The *inducing* voltage, V_i, is the line integral of E_i:

$$V_i = -\int_0^{h_p} E_i \cdot dz = -\int_0^{h_p} E_{ei} \cdot dz - \int_0^{h_p} E_{mi} \cdot dz = V_{ei} + V_{mi}. \tag{10.30}$$

As the height, h_p, of the line conductor is small compared with the length of the lightning channel, the inducing electric field below the line conductor can be assumed to be constant, and equal to that on the ground surface:

$$V_i = \left(\nabla\phi + \frac{\partial A}{\partial t}\right) \cdot h_p. \tag{10.31}$$

The inducing voltage will act on each point along the length of the overhead line. However, because of the retardation effect, the earliest time, t_o, the disturbance from the lightning channel will reach a point on the line conductor would be:

$$t_o = \frac{\sqrt{x^2 + y_o^2}}{c}. \tag{10.32}$$

Therefore, the inducing voltage at a point on the line remains zero until $t = t_o$. Hence,

$$V_i = \psi(x,t)u(t - t_o), \tag{10.33}$$

where $u(t - t_o)$ is the shifted unit step function. The continuous function, $\psi(x,t)$, is the same as Eq. (10.31), and is given, for a negative stroke with uniform charge density along its length, by (Rusck, 1958):

$$\psi(x,t) = -\frac{60 I_o h_p}{\beta}\left[\frac{1-\beta^2}{\sqrt{\beta^2 c^2 (t - t_o)^2 + (1-\beta^2) r^2}} - \frac{1}{\sqrt{h_c^2 + r^2}}\right], \tag{10.34}$$

where

I_o = step-function return-stroke current, A
h_p = height of line above ground, m
β = v/c
v = velocity of return stroke
r = distance of point x on line from point of strike, m
h_c = height of cloud charge center above ground, m

The inducing voltage is the voltage at a field point in space with the same coordinates as a corresponding point on the line conductor, but without the presence of the line conductor. The inducing voltage at different points along the length of the line conductor will be different. The overhead line being a good conductor of electricity, these differences will tend to be equalized by the flow of current. Therefore, the actual voltage between a point on the line and the ground below it will be different from the inducing voltage at that point. This voltage, which can actually be measured on the line conductor, is defined as the *induced* voltage. The calculation of the induced voltage is the primary objective.

Induced Voltage

Neglecting losses, an overhead line may be represented as consisting of distributed series inductance L (H/m), and distributed shunt capacitance C (F/m). The effect of the inducing voltage will then be equivalent to connecting a voltage source along each point of the line (Fig. 10.15). The partial differential equation for such a configuration will be:

$$-\frac{\partial V}{\partial x}\Delta x = L\Delta x \frac{\partial I}{\partial t} \text{ and} \tag{10.35}$$

$$-\frac{\partial I}{\partial x}\Delta x = C\Delta x \frac{\partial}{\partial t}(V - V_i). \tag{10.36}$$

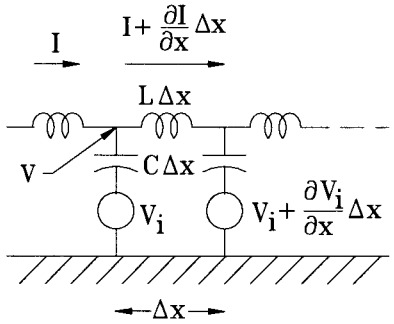

FIGURE 10.15 Equivalent circuit of transmission line with inducing voltage.

Differentiating Eq. (10.35) with respect to x, and eliminating I, the equation for the induced voltage can be written as:

$$\frac{\partial^2 V}{\partial x^2}-\frac{1}{c^2}\frac{\partial^2 V}{\partial t^2}=-\frac{1}{c^2}\frac{\partial^2 V_i}{\partial t^2}=F(x,t), \tag{10.37}$$

$$\text{where } c=\frac{1}{\sqrt{LC}}=\frac{1}{\sqrt{\epsilon_o\mu_o}}=3\times 10^8 \text{ m s}. \tag{10.38}$$

$$\text{In Laplace transform, } \frac{\partial^2 V(x,s)}{\partial x^2}-\frac{s^2}{c^2}V(x,s)=-\frac{s^2}{c^2}V_i(x,s)=F(x,s). \tag{10.39}$$

Equation (10.39) is an inhomogeneous wave equation for the induced voltage along the overhead line. It is valid for any charge distribution along the leader channel and any waveshape of the return-stroke current. Its solution can be obtained by assuming F(x,t) to be the superposition of impulses which involves the definition of Green's function (Morse and Feshbach, 1950).

Green's Function

To obtain the voltage caused by a distributed source, F(x), the effects of each elementary portion of the source are calculated and then integrated for the whole source. If G(x;x′) is the voltage at a point x along the line caused by a unit impulse source at a source point x′, the voltage at x caused by a source distribution F(x′) is the integral of G(x;x′)F(x′) over the whole domain (a,b) of x′ occupied by the source, provided that F(x′) is a piecewise continuous function in the domain $a \le x' \le b$,

$$V(x)=\int_a^b G(x;x')F(x')dx'. \tag{10.40}$$

The function G(x;x′), called the Green's function, is, therefore, a solution for a case which is homogeneous everywhere except at one point. Green's function, G(x;x′), has the following properties:

$$(a)\quad G(x;x'+0)-G(x;x'-0)=0 \tag{10.41}$$

$$(b)\quad \left(\frac{dG}{dx}\right)_{x'+0}-\left(\frac{dG}{dx}\right)_{x'-0}=1 \tag{10.42}$$

(c) G(x;x′) satisfies the homogeneous equation everywhere in the domain, except at the point x = x′, and (d) G(x;x′) satisfies the prescribed homogeneous boundary conditions.

Green's function can be found by converting Eq. (10.39) to a homogeneous equation and replacing V(x,s) by G(x;x′,s):

$$\frac{\partial^2 G(x;x',s)}{\partial x^2} - \frac{s^2}{c^2} G(x;x',s) = 0. \tag{10.43}$$

The general solution of Eq. (10.43) is given by:

$$G(x;x',s) = A e^{\frac{sx}{c}} + B e^{-\frac{sx}{c}}. \tag{10.44}$$

The constants A and B are found from the boundary conditions and from the properties of Green's function.

Induced Voltage of a Doubly Infinite Single-Conductor Line

The induced voltage at any point, x, on the line can be determined by invoking Eq. (10.40), where $G(x;x') \cdot F(x')$ is the integrand. $F(x')$ is a function of the amplitude and waveshape of the inducing voltage, V_i [Eq. (10.33)], whereas the Green's function, $G(x;x')$ is dependent on the boundary conditions of the line and the properties of Green's function. In other words, it is a function of the line configuration and is independent of the lightning characteristics. Therefore it is appropriate to determine the Green's function first.

Evaluation of Green's Function

As Green's function is finite for $x \to -\infty$ and $x \to +\infty$,

$$G_1 = A e^{\frac{sx}{c}} \text{ for } x < x'; \; G_2 = B e^{-\frac{sx}{c}} \text{ for } x > x'.$$

From Eq. (10.41): $$A e^{\frac{sx'}{c}} = B e^{-\frac{sx'}{c}}, \text{ i.e., } B = A e^{\frac{2sx'}{c}}.$$

From Eq. (10.42): $$A = -\frac{c}{2s} e^{-\frac{sx}{c}}; \text{ hence, } B = -\frac{c}{2s} e^{\frac{sx}{c}}.$$

$$G_1(x;x',s) = -\frac{c}{2s} \exp\left(-\frac{s(x'-x)}{c}\right) \text{ for } x < x' \text{ and} \tag{10.45}$$

$$G_2(x;x',s) = -\frac{c}{2s} \exp\left(\frac{s(x-x')}{c}\right) \text{ for } x > x'. \tag{10.46}$$

By applying Eq. (10.40):

$$V(x,s) = -\frac{c}{2s} \int_{-\infty}^{x} e^{\frac{s}{c}(x'-x)} F(x',s)\,dx' - \frac{c}{2s} \int_{x}^{\infty} e^{-\frac{s}{c}(x'-x)} F(x',s)\,dx' = V_1(x,s) + V_2(x,s). \tag{10.47}$$

Induced Voltage Caused by Return-Stroke Current of Arbitrary Waveshape

The induced voltage caused by return-stroke current, I(t), of arbitrary waveshape can be computed from Eq. (10.39) by several methods. In method I, the inducing voltage, V_i, due to I(t) is found by applying Duhamel's integral (Haldar and Liew, 1988):

$$V_i = \frac{d}{dt}\int_0^t I(t-\tau)\,V_{istep}(x',\tau)\,d\tau, \tag{10.48}$$

where V_{istep} is the inducing voltage caused by a unit step-function current. In other words,

$$V_{istep}(x',\tau) = \psi_o(x',\tau)\,u(\tau - t_o), \tag{10.49}$$

where $\psi_o(x',\tau) = \psi(x',\tau)/I_o$, and $\psi(x',\tau)$ is given in Eq. (10.34). Inserting Eq. (10.49) in Eq. (10.48), and taking Laplace transform of V_i in Eq. (10.48):

$$V_i(x',s) = sI(s)\,\psi_o(x',s)\,e^{-st_o} \quad \text{and} \tag{10.50}$$

$$F(x',s) = -\frac{s^2}{c^2}V_i(x',s) = -\frac{s^3}{c^2}I(s)\,\psi_o(x',s)\,e^{-st_o}. \tag{10.51}$$

Replacing F(x′,s) in Eq. (10.47) by Eq. (10.51), the induced voltage, V(x,s) is:

$$V(x,s) = \frac{1}{2c}\left[sI(s)\left\{s\int_{-\infty}^{x}\psi_o(x',s)\,e^{-s\left(t_o-\frac{x'-x}{c}\right)}dx' + s\int_{x}^{\infty}\psi_o(x',s)\,e^{-s\left(t_o+\frac{x'-x}{c}\right)}dx'\right\}\right]. \tag{10.52}$$

Inverting to time domain by convolution integral:

$$\begin{aligned} V(x,t) = {} & \frac{1}{2c}\int_0^t \frac{d}{dt}I(t-\tau)\left[\frac{d}{d\tau}\int_{-\infty}^{x}\psi_o\left(x',\tau+\frac{x'-x}{c}\right)u\left(\tau - t_o + \frac{x'-x}{c}\right)dx'\right]d\tau + \\ & \frac{1}{2c}\int_0^t \frac{d}{dt}I(t-\tau)\left[\frac{d}{d\tau}\int_{x}^{\infty}\psi_o\left(x',\tau-\frac{x'-x}{c}\right)u\left(\tau - t_o - \frac{x'-x}{c}\right)dx'\right]d\tau = V_1(x,t) + V_2(x,t) \end{aligned} \tag{10.53}$$

Because of the shifted unit step function in $V_1(x,t)$:

$$\tau \geq t_o - \frac{x'-x}{c}.$$

$$\begin{aligned} &\text{In the limit, } \tau = t_o - \frac{x_{o1}-x}{c} = \frac{\sqrt{x_{o1}^2+y_o^2}}{c} - \frac{x_{o1}-x}{c} \\ &\text{or, } x_{o1} = \frac{y_o^2 - (c\tau - x)^2}{2(c\tau - x)}. \end{aligned} \tag{10.54}$$

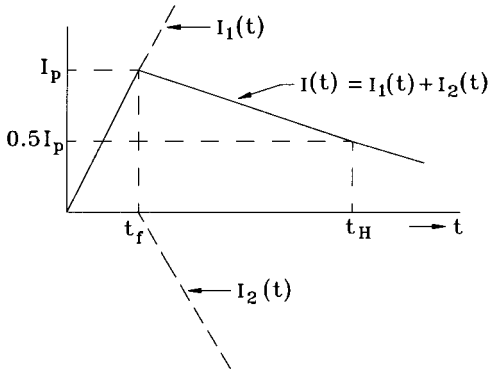

FIGURE 10.16 A linearly rising and falling lightning return-stroke current.

$$\text{Similarly, for } V_2(x,t):\ x_{o2} = \frac{(c\tau + x)^2 - y_o^2}{2(c\tau + x)}. \tag{10.55}$$

Replacing $-\infty$ by x_{o1} in $V_1(x,t)$, and ∞ by x_{o2} in $V_2(x,t)$ in Eq. (10.53):

$$V_1(x,t) = \frac{1}{2c}\int_0^t \frac{d}{dt}I(t-\tau)\cdot\frac{d}{d\tau}\left\{\int_{x_{o1}}^{x}\Psi_o\left(x,\tau+\frac{x'-x}{c}\right)dx'\right\}u(\tau-t_o)\,d\tau \text{ and} \tag{10.56}$$

$$V_2(x,t) = \frac{1}{2c}\int_0^t \frac{d}{dt}I(t-\tau)\cdot\frac{d}{d\tau}\left\{\int_{x}^{x_{o2}}\psi_o\left(x,\tau-\frac{x'-x}{c}\right)dx'\right\}u(\tau-t_o)\,d\tau. \tag{10.57}$$

A lightning return-stroke current can be represented by a linearly rising and linearly falling wave with sufficient accuracy (Fig. 10.16) (Chowdhuri, 1996):

$$I(t) = \alpha_1 tu(t) - \alpha_2(t-t_f)u(t-t_f) = I_1(t) + I_2(t), \tag{10.58}$$

$$\text{where } \alpha_1 = \frac{I_p}{t_f} \text{ and } \alpha_2 = \frac{2t_H - t_f}{2t_f(t_H - t_f)}I_p. \tag{10.59}$$

It will be evident from Eq. (10.58) that $V_1(x,t)$ in Eq. (10.56) will have two components: one component, $V_{11}(x,t)$, will be a function of $I_1(t)$, and the other component, $V_{21}(x,t)$, will be a function of $I_2(t)$, i.e., $V_1(x,t) = V_{11}(x,t) + V_{21}(x,t)$. Similarly, $V_2(x,t) = V_{12}(x,t) + V_{22}(x,t)$. After integration and simplifying Eq. (10.56), $V_{11}(x,t)$ can be written as:

$$V_{11}(x,t) = -\frac{\alpha_1 h_p}{\beta}\times 10^{-7}\,u(t-t_o)\left[(1-\beta^2)\ell n\frac{f_{11}(\tau=t)\cdot f_{21}(\tau=t_o)}{f_{11}(\tau=t_o)\cdot f_{21}(\tau=t)} + \ell n\frac{f_{31}(\tau=t)}{f_{31}(\tau=t_o)}\right] \tag{10.60}$$

where

$$f_{11}(\tau) = m_{11} + \sqrt{m_{11}^2 + a_{11}^2};\ f_{21}(\tau) = m_{21} + \sqrt{m_{21}^2 + a_{11}^2};\ f_{31}(\tau) = x_{o1} + \sqrt{x_{01}^2 + y_o^2 + h_c^2};$$

$$m_{11} = x + \beta^2(c\tau - x);\ m_{21} = x_{o1} + \beta^2(c\tau - x);\ a_{11}^2 = (1-\beta^2)\left[y_o^2 + \beta^2(c\tau - x)^2\right].$$

The expression for $V_{21}(x,t)$ is similar to Eq. (10.60), except that α_1 is replaced by $(-\alpha_2)$, and t is replaced by $(t - t_f)$. The computation of $V_2(x,t)$ is similar; namely,

$$V_{12}(x,t) = -\frac{\alpha_1 h_p}{\beta} \times 10^{-7}\, u(t - t_o)\left[(1-\beta^2)\ell n \frac{f_{12}(\tau = t)\cdot f_{22}(\tau = t_o)}{f_{12}(\tau = t_o)\cdot f_{22}(\tau = t)} - \ell n \frac{f_{32}(\tau = t)}{f_{32}(\tau = t_o)}\right], \quad (10.61)$$

where

$$f_{12}(\tau) = m_{12} + \sqrt{m_{12}^2 + a_{12}^2};\ f_{22}(\tau) = m_{22} + \sqrt{m_{22}^2 + a_{12}^2};\ f_{32}(\tau) = x_{o2} + \sqrt{x_{o2}^2 + y_o^2 + h_o^2};$$

$$m_{12} = x_{o2} - \beta^2(c\tau + x);\ m_{22} = x - \beta^2(c\tau + x);\ a_{12}^2 = (1-\beta^2)\left[y_o^2 + \beta^2(c\tau + x)^2\right].$$

$V_{22}(x,t)$ can similarly determined by replacing α_1 in Eq. (10.61) by $(-\alpha_2)$, and replacing t by $(t - t_f)$.

The second method of determining the induced voltage, V(x,t), is to solve Eq. (10.47), for a unit step-function return-stroke current, then find the induced voltage for the given return-stroke current wave-shape by applying Duhamel's integral (Chowdhuri and Gross, 1967; Chowdhuri, 1989). The solution of Eq. (10.47) for a unit step-function return-stroke current is given by (Chowdhuri, 1989):

$$V_{step}(x,t) = (V_{11} + V_{12} + V_{21} + V_{22})\, u(t - t_o), \quad (10.62)$$

where

$$V_{11} = \frac{30 h_p (1-\beta^2)}{\beta^2 (ct - x)^2 + y_o^2}\left[\beta(ct - x) + \frac{(ct - x)x - y_o^2}{\sqrt{c^2t^2 + \frac{1-\beta^2}{\beta^2}(x^2 + y_o^2)}}\right], \quad (10.63)$$

$$V_{12} = \frac{-30 h_p}{\beta}\left[1 - \frac{1}{\sqrt{k_1^2 + 1}} - \beta^2\right]\frac{1}{ct - x}, \quad (10.64)$$

$$V_{21} = \frac{30 h_p (1-\beta^2)}{\beta^2 (ct + x)^2 + y_o^2}\left[\beta(ct + x) - \frac{(ct + x)x + y_o^2}{\sqrt{c^2t^2 + \frac{1-\beta^2}{\beta^2}(x^2 + y_o^2)}}\right], \quad (10.65)$$

$$V_{22} = \frac{-30 h_p}{\beta}\left[1 - \frac{1}{\sqrt{k_2^2 + 1}} - \beta^2\right]\frac{1}{ct + x}, \quad (10.66)$$

$$k_1 = \frac{2h_c(ct - x)}{y_o^2 + (ct - x)^2}, \tag{10.67}$$

$$k_2 = \frac{2h_c(ct + x)}{y_o^2 + (ct + x)^2}. \tag{10.68}$$

The expressions for the induced voltage, caused by a linearly rising and falling return-stroke current, are given in Appendix I.

The advantage of method II is that once the induced voltage caused by a step-function return-stroke current is computed, then it can be used as the reference in computing the induced voltage caused by currents of any given waveshape by applying Duhamel's integral, thus avoiding the mathematical manipulations for every given waveshape. However, the mathematical procedures are simpler for method I than for method II.

A third method to solve Eq. (10.37) is to apply numerical method which bypasses all mathematical complexities (Agrawal et al., 1980). However, the accuracy of the numerical method strongly depends upon the step size of computation. Therefore, the computation of the induced voltage of long lines, greater than 1 km, becomes impractical.

Induced Voltages on Multiconductor Lines

Overhead power lines are usually three-phase lines. Sometimes several three-phase circuits are strung from the same tower. Shield wires and neutral conductors are part of the multiconductor system. The various conductors in a multiconductor system interact with each other in the induction process for lightning strokes to nearby ground. The equivalent circuit of a two-conductor system is shown in Fig. 10.17. Extending to an n-conductor system, the partial differential equation for the induced voltage, in matrix form, is (Chowdhuri, 1996; Chowdhuri and Gross, 1969; Cinieri and Fumi, 1979; Chowdhuri, 1990):

$$\frac{\partial^2[V]}{\partial x^2} - \frac{1}{c^2}\frac{\partial^2[V]}{\partial t^2} = -[L][C_g]\frac{\partial^2[V_i]}{\partial t^2} = -[M]\frac{\partial^2[V_i]}{\partial t^2}, \tag{10.69}$$

where [L] is an $n \times n$ matrix whose elements are:

$$L_{rr} = 2 \times 10^{-7}\,\ell n\frac{2h_r}{r_r};\; L_{rs} = 2 \times 10^{-7}\,\ell n\frac{d_{r's}}{d_{rs}}.$$

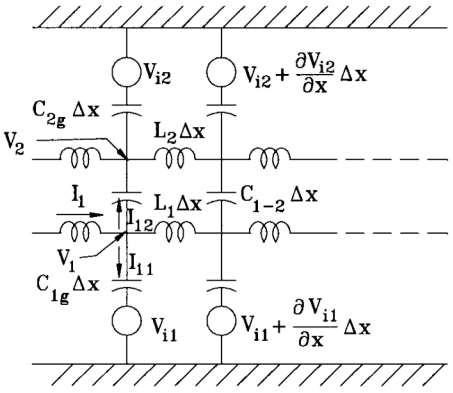

FIGURE 10.17 Equivalent circuit of a two-conductor system.

$[C_g]$ is an n × n diagonal matrix whose elements are, $C_{jg} = C_{j1} + C_{j2} + \cdots + C_{jn}$, where C_{jr} is an element of an n × n matrix, $[C] = [p]^{-1}$ and:

$$P_{rr} = 18 \times 10^9 \ell n \frac{2h_r}{r_r}; \; p_{rs} = 18 \times 10^9 \ell n \frac{d_{r's}}{d_{rs}},$$

h_r and r_r are the height above ground and radius of the r-th conductor, $d_{r's}$ is the distance between the image of the r-th conductor below earth and the s-th conductor, d_{rs} is the distance between the r-th and s-th conductors. From Eq. (10.69), for the j-th conductor:

$$\frac{\partial^2 V_j}{\partial x^2} - \frac{1}{c^2}\frac{\partial^2 V_j}{\partial t^2} = -\left(M_{j1}\frac{\partial^2 V_{i1}}{\partial t^2} + \cdots + M_{jj}\frac{\partial^2 V_{ij}}{\partial t^2} + \cdots + M_{jn}\frac{\partial^2 V_{in}}{\partial t^2} \right). \tag{10.70}$$

If the ratio of the inducing voltage of the m-th conductor to that of the j-th conductor is k_{mj} (m = 1,2,…n), then

$$\frac{\partial^2 V_j}{\partial x^2} - \frac{1}{c^2}\frac{\partial^2 V_j}{\partial t^2} = -c^2\left(M_{j1}k_{1j} + \cdots + M_{jj} + \cdots + M_{jn}k_{nj}\right)\frac{1}{c^2}\frac{\partial^2 V_{ij}}{\partial t^2} = \left(M_j c^2\right)F_j(x,t), \tag{10.71}$$

$$\text{where } M_j = M_{j1}k_{1j} + \cdots + M_{jj} + \cdots + M_{jn}k_{nj} \text{ and } F_j(x,t) = \frac{1}{c^2}\frac{\partial^2 V_{ij}}{\partial t^2}. \tag{10.72}$$

If the j-th conductor in its present position existed alone, the partial differential equation of its induced voltage, V_{js}, would have been the same as Eq. (10.37), i.e.,

$$\frac{\partial^2 V_{js}}{\partial x^2} - \frac{1}{c^2}\frac{\partial^2 V_{js}}{\partial t^2} = F_j(x,t). \tag{10.73}$$

Therefore, the ratio of the induced voltage of the j-th conductor in an n-conductor system to that of a single conductor at the same position would be:

$$\frac{V_j}{V_{js}} = M_j c^2. \tag{10.74}$$

The inducing voltage being nearly proportional to the conductor height, and the lateral distance of the stroke point being significantly larger than the separation distance between phase conductors, the presence of other conductors in a horizontally configured line will be minimal. On the other hand, for a vertically configured line, the induced voltage of the highest conductor will be lower than that for the same conductor without any neighboring conductors. Similarly, the lowest conductor voltage will be pulled up by the presence of the neighboring conductors of higher elevation, and the middle conductor will be the least affected by the presence of the other conductors (Chowdhuri, 1996).

Effects of Shield Wires on Induced Voltages

If there are (n + r) conductors, of which r conductors are grounded (r shield wires), then the partial differential equation for the induced voltages of the n number of phase conductors is given by (Chowdhuri, 1996; Chowdhuri and Gross, 1969; Cinieri and Fumi, 1979; Chowdhuri, 1990):

$$\frac{\partial^2[V_n]}{\partial x^2}-\frac{1}{c^2}\frac{\partial^2[V_n]}{\partial t^2}=-[L'][C_{gn}]\frac{\partial^2[V_{in}]}{\partial t^2}=-[M_g]\frac{\partial^2[V_{in}]}{\partial t^2}. \tag{10.75}$$

The matrix [L′] is obtained by partitioning the (n+r)x(n+r) inductance matrix of the (n + r) conductors, and putting $[L'] = [L_{nn}] - [L_{nr}][L_{rr}]^{-1}[L_{rn}]$, where:

$$[L]_{(n+r),(n+r)}=\begin{bmatrix}L_{nn} & L_{nr}\\ L_{rn} & L_{rr}\end{bmatrix}. \tag{10.76}$$

$[C_{gn}]$ is an n × n diagonal matrix each element of which is the sum of the elements of the corresponding row, up to the n-th row, of the original (n + r) × (n + r) capacitance matrix of the (n + r) conductors, $[C] = [p]^{-1}$, where [p] is the matrix of the potential coefficients of the (n + r) conductors. The j-th element of $[C_{gn}]$ is given by:

$$C_{jgn}(j\le n)=\sum_{k=1}^{n+r}C_{jk}. \tag{10.77}$$

From Eq. (10.75), the induced voltage of the j-th conductor is:

$$\frac{\partial^2 V_j}{\partial x^2}-\frac{1}{c^2}\frac{\partial^2 V_j}{\partial t^2}=-c^2\left(M_{gj1}k_{1j}+\cdots+M_{gij}+\cdots+M_{gjn}k_{nj}\right)\frac{1}{c^2}\frac{\partial^2 V_{ij}}{\partial t^2}=\left(M_{gj}c^2\right)F_j(x,t). \tag{10.78}$$

Defining the protective ratio as the ratio of the induced voltages on the j-th conductor with and without the shield wires in place:

$$\text{Protective Ratio}=\frac{M_{gj}}{M_j}, \tag{10.79}$$

where M_j is given by Eq. (10.72).

Estimation of Outage Rates Caused by Nearby Lightning Strokes

The knowledge of the following two parameters are essential for estimating the outage rate of an overhead power line: (i) basic insulation level of the line, BIL, and (ii) ground flash density of the region, n_g (number of strokes per km² per year). With this knowledge, the electrogeometric model is constructed to estimate the attractive area (Fig. 10.18). According to the electrogeometric model, the striking distance

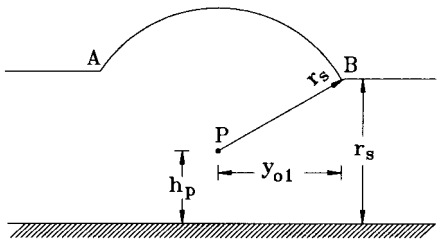

FIGURE 10.18 Electrogeometric model for estimating the least distance of ground strike.

of a lightning stroke is proportional to the return-stroke current. The following relation is used to estimate this striking distance, r_s:

$$r_s = 8I_p^{0.65}(\text{m}), \tag{10.80}$$

where I_p is the peak of the return-stroke current. In the cross-sectional view of Fig. 10.18, a horizontal line (representing a plane) is drawn at a distance of r_s meters from the ground plane corresponding to the return-stroke current, I_p. A circular arc is drawn with its center on the conductor, P, and r_s as radius. This represents a cylinder of attraction above the line conductor. The circular arc and the horizontal line intersect at points A and B. The strokes falling between A and B will strike the conductor resulting in direct strokes; those falling outside AB will hit the ground, inducing voltages on the line. The horizontal projection of A or B is y_{o1}, which is given by:

$$y_{o1} = \sqrt{r_s^2 - (r_s - h_p)^2}, \quad \text{for } r_s > h_p \text{ and} \tag{10.81a}$$

$$y_{o1} = r_s, \quad \text{for } r_s \le h_p. \tag{10.81b}$$

y_{o1} is the shortest distance of a lightning stroke of given return-stroke current from the overhead line which will result in a flash to ground.

Analysis of field data shows that the statistical variation of the peak, I_p, and the time to crest, t_f, of the return-stroke current fit lognormal distribution (Anderson and Eriksson, 1980). The probability density function, $p(I_p)$ of I_p then can be expressed as:

$$p(I_p) = \frac{e^{-0.5f_1}}{I_p \cdot \sigma(\ell n I_p) \cdot \sqrt{2\pi}}, \tag{10.82}$$

$$\text{where} \quad f_1 = \left(\frac{\ell n I_p - \ell n I_{pm}}{\sigma(\ell n I_p)} \right)^2 \quad \text{and} \tag{10.83}$$

$\sigma(\ell n I_p)$ = standard deviation of $\ell n I_p$, and I_{pm} = median value of I_p. Similarly, the probability density function of t_f can be expressed as:

$$p(t_f) = \frac{e^{-0.5f_2}}{t_f \cdot \sigma(\ell n t_f) \cdot \sqrt{2\pi}}, \tag{10.84}$$

$$\text{where} \quad f_2 = \left(\frac{\ell n t_f - \ell n t_{fm}}{\sigma(\ell n t_f)} \right)^2. \tag{10.85}$$

The joint probability density function, $p(I_p, t_f)$, is given by:

$$p(I_p, t_f) = \frac{e^{-\frac{0.5}{1-\rho^2}\left(f_1 - 2\rho\sqrt{f_1 \cdot f_2} + f_2\right)}}{(2\pi)(I_p \cdot t_f)\left(\sigma(\ell n I_p) \cdot \sigma(\ell n t_f)\right)\sqrt{1-\rho^2}}, \tag{10.86}$$

where ρ = coefficient of correlation. The statistical parameters of return-stroke current are as follows (Anderson and Eriksson, 1980; Eriksson, 1986):

For $I_p \le 20$ kA: Median peak current, $I_{pm1} = 61.1$ kA
Log (to base e) of standard deviation, $\sigma(\ell n I_{p1}) = 1.33$
Median time to crest, $t_{fm1} = 3.83$ μs
Log (to base e) of standard deviation, $\sigma(\ell n t_{f1}) = 0.553$

For $I_p > 20$ kA: Median peak current, $I_{pm2} = 33.3$ kA
Log (to base e) of standard deviation, $\sigma(\ell n I_{p2}) = 0.605$
Median time to crest, $t_{fm2} = 3.83$ μs
Log (to base e) of standard deviation, $\sigma(\ell n t_{f2}) = 0.553$

Correlation coefficient, $\rho = 0.47$

To compute the outage rate, the return-stroke current, I_p, is varied from 1 kA to 200 kA in steps of 0.5 kA (Chowdhuri, 1989). The current front time, t_f, is varied from 0.5 μs to 10.5 μs in steps of 0.5 μs. At each current level, the shortest possible distance of the stroke, y_{o1}, is computed from Eq. (10.81). Starting at $t_f = 0.5$ μs, the induced voltage is calculated as a function of time and compared with the given BIL of the line. If the BIL is not exceeded, then the next higher level of current is chosen. If the BIL is exceeded, then the lateral distance of the stroke from the line, y, is increased by Δy (e.g., 1 m), the induced voltage is recalculated and compared with the BIL of the line. The lateral distance, y, is progressively increased until the induced voltage does not exceed BIL. This distance is called y_{o2}. For the selected I_p and t_f, the induced voltage will then exceed the BIL of the line and cause line flashover, if the lightning stroke hit the ground between y_{o1} and y_{o2} along the length of the line. For a 100-km sector of the line, the attractive area, A, will be (Fig. 10.19):

$$A = 0.2\left(y_{o2} - y_{o1}\right) \text{km}^2. \tag{10.87}$$

The joint probability density function, $p(I_p,t_f)$, is then computed from Eq. (10.86) for the selected $I_p - t_f$ combination. If n_g is the ground flash density of the region, the expected number of flashovers per 100 km per year for that particular $I_p - t_f$ combination will be:

$$\text{nfo} = p\left(I_p, t_f\right) \cdot \Delta I_p \cdot \Delta t_f \cdot n_g \cdot A, \tag{10.88}$$

where Δi_p = current step, and Δt_f = front-time step.

The front time, t_f, is then increased by $t_f = 0.5$ μs to the next step, and nfo for the same current but with the new t_f is computed and added to the previous nfo. Once $t_f = 10.5$ μs is reached, the return-stroke current is increased by $\Delta i_p = 0.5$ kA, and the whole procedure repeated until the limits $I_p = 200$ kA and $t_f = 10.5$ μs are reached. The cumulative nfo will then give the total number of expected line flashovers per 100 km per year for the selected BIL.

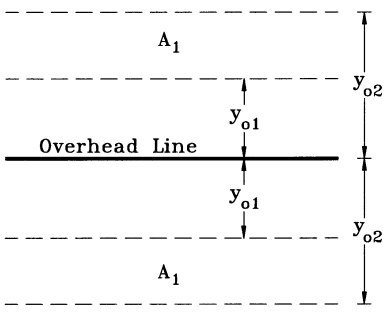

FIGURE 10.19 Attractive area of lightning ground flash to cause line flashover. $A = 2A_1 = 0.2(y_{o2} - y_{o1})$ km^2.

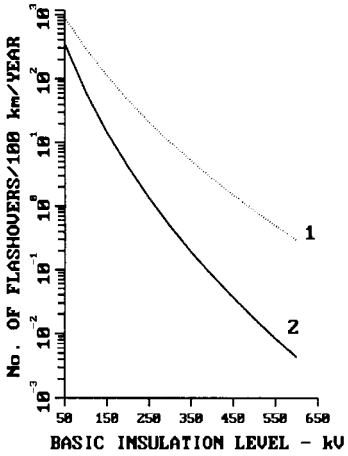

FIGURE 10.20 Flashover rate of overhead line *vs.* BIL. Curve 1: no shield wire: Curve 2: one shield wire. Line height, h_p = 10 m; Shield-wire height, h_{sh} = 11 m; ground flash density, n_g = 10/km^2/year.

The lightning-induced outage rates of a 10-m high single conductor are plotted in Fig. 10.20. The effectiveness of the shield wire, as shown in the figure, is optimistic, bearing in mind that the shield wire was assumed to be held at ground potential. The shield wire will not be held at ground potential under transient conditions. Therefore, the effectiveness of the shield wire will be less than the idealized case shown in Fig. 10.20.

References

Agrawal, A. K., Price, H. J., and Gurbaxani, S. H., Transient response of multiconductor transmission lines excited by a nonuniform electromagnetic field, *IEEE Trans. on Electromagnetic Compatibility*, EMC-22, 119, 1980.

Anderson, R. B. and Eriksson, A. J., Lightning parameters for engineering applications, *Electra* 69, 65, 1980.

Chowdhuri, P., Analysis of lightning-induced voltages on overhead lines, *IEEE Trans. on Power Delivery,* 4, 479, 1989.

Chowdhuri, P., *Electromagnetic Transients in Power Systems*, Research Studies Press/John Wiley & Sons, Taunton, U.K./New York, 1996, Chap. 1.

Chowdhuri, P., Estimation of flashover rates of overhead power distribution lines by lightning strokes to nearby ground, *IEEE Trans. on Power Delivery,* 4, 1982–1989.

Chowdhuri, P., Lightning-induced voltages on multiconductor overhead lines, *IEEE Trans. on Power Delivery*, 5, 658, 1990.

Chowdhuri, P. and Gross, E. T. B., Voltage surges induced on overhead lines by lightning strokes, *Proc. IEE* (U.K.), 114, 1899, 1967.

Chowdhuri, P. and Gross, E. T. B., Voltages induced on overhead multiconductor lines by lightning strokes, *Proc. IEE* (U.K.), 116, 561, 1969.

Cinieri, E. and Fumi, A., The effect of the presence of multiconductors and ground wires on the atmospheric high voltages induced on electrical lines, (in Italian), *L'Energia Elettrica*, 56, 595, 1979.

Eriksson, A. J., Notes on lightning parameters for system performance estimation, CIGRE Note 33-86 (WG33- 01) IWD, 15 July 1986.

Haldar, M. K. and Liew, A. C., Alternative solution for the Chowdhuri-Gross model of lightning-induced voltages on power lines, *Proc. IEE* (U.K.), 135, 324, 1988.

Morse, P. M. and Feshbach, H., *Methods of Theoretical Physics*, Vol. 1, McGraw-Hill, New York, 1950, Chap. 7.

Rusck, S., Induced lightning over-voltages on power-transmission lines with special reference to the over-voltage protection of low-voltage networks, *Trans. Royal Inst. of Tech.,* 120, 1, 1958.

Appendix I: Voltage Induced by Linearly Rising and Falling Return-Stroke Current

$$V(x,t) = V_1(x,t)u(t-t_o) + V_2(x,t)u(t-t_{of})$$

where

$$V_1(x,t) = \frac{30\,\alpha_1 h_p}{\beta c}\left[b_o \cdot \ell n\frac{f_{12}}{f_{11}} + 0.5\,\ell n(f_{13})\right];\; V_2(x,t) = -\frac{30\alpha_2 h_p}{\beta c}\left[b_o \cdot \ell n\frac{f_{12a}}{f_{11a}} + 0.5\,\ell n(f_{13a})\right]$$

$$b_o = 1-\beta^2;\; t_{of} = t_o + t_f;\; t_{tf} = t - t_f$$

$$f_1 = m_1 + (ct-x)^2 - y_o^2;\; f_2 = m_1 - (ct-x)^2 + y_o^2$$

$$f_3 = m_0 - (ct_o - x)^2 + y_o^2;\; f_4 = m_o + (ct_o - x)^2 - y_o^2$$

$$f_s = n_1 + (ct+x)^2 - y_o^2;\; f_6 = n_1 - (ct+x)^2 + y_o^2$$

$$f_7 = n_o - (ct_o + x)^2 + y_o^2;\; f_8 = n_o + (ct_o + x)^2 - y_o^2$$

$$f_9 = b_o(\beta^2 x^2 + y_o^2) + \beta^2 c^2 t^2(1+\beta^2);\; f_{10} = 2\beta^2 ct\sqrt{\beta^2 c^2 t^2 + b_o(x^2 + y_o^2)}$$

$$f_{11} = \frac{c^2t^2 - x^2}{y_o^2};\; f_{12} = \frac{f_9 - f_{10}}{b_o^2 y_o^2};\; f_{13} = \frac{f_1 \cdot f_3 \cdot f_5 \cdot f_7}{f_2 \cdot f_4 \cdot f_6 \cdot f_8}$$

$$f_{1a} = m_{1a} + (ct_{tf} - x)^2 - y_o^2;\; f_{2a} = m_{1a} - (ct_{tf} - x)^2 + y_0^2$$

$$f_{3a} = f_3;\; f_{4a} = f_4;\; f_{7a} = f_7;\; f_{8a} = f_8$$

$$f_{5a} = n_{1a} + (ct_{tf} + x)^2 - y_o^2;\; f_{6a} = n_{1a} - (ct_{tf} + x)^2 + y_o^2$$

$$f_{9a} = b_o(\beta^2 x^2 + y_o^2) + \beta^2 c^2 t_{tf}^2(1+\beta^2);\; f_{10a} = 2\beta^2 ct_{tf}\sqrt{\beta^2 c^2 t_{tf}^2 + b_o(x^2 + y_o^2)}$$

$$f_{11a} = \frac{c^2 t_{tf}^2 - x^2}{y_o^2};\; f_{12a} = \frac{f_{9a} - f_{10a}}{b_o^2 y_o^2};\; f_{13a} = \frac{f_{1a} \cdot f_{3a} \cdot f_{5a} \cdot f_{7a}}{f_{2a} \cdot f_{4a} \cdot f_{6a} \cdot f_{8a}}$$

$$m_o = \sqrt{\left[(ct_o - x)^2 + y_o^2\right]^2 + 4h_c^2(ct_o - x)^2};\; m_1 = \sqrt{\left[(ct-x)^2 + y_o^2\right]^2 + 4h_c^2(ct-x)^2}$$

$$n_o = \sqrt{\left[\left(ct_o + x\right)^2 + y_o^2\right]^2 + 4h_c^2\left(ct_o + x\right)^2}\;;\; n_1 = \sqrt{\left[\left(ct + x\right)^2 + y_o^2\right]^2 + 4h_c^2\left(ct + x\right)^2}$$

$$m_{1a} = \sqrt{\left[\left(ct_{tf} - x\right)^2 + y_o^2\right]^2 + 4h_c^2\left(ct_{tf} - x\right)^2}\;;\; n_{1a} = \sqrt{\left[\left(ct_{tf} + x\right)^2 + y_o^2\right]^2 + 4h_c^2\left(ct_{tf} + x\right)^2}$$

10.4 Switching Surges

Stephen R. Lambert

Switching surges occur on power systems as a result of instantaneous changes in the electrical configuration of the system, and such changes are mainly associated with switching operations and fault events. These overvoltages generally have crest magnitudes which range from about 1 per unit to 3 pu for phase-to-ground surges and from about 2.0 to 4 pu for phase-to-phase surges (in pu on the phase to ground crest voltage base) with higher values sometimes encountered as a result of a system resonant condition. Waveshapes vary considerably with rise times ranging from 50 μs to thousands of μs and times to half-value in the range of hundreds of μs to thousands of μs. For insulation testing purposes, a waveshape having a time to crest of 250 μs with a time to half-value of 2000 μs is often used.

The following addresses the overvoltages associated with switching various power system devices. Possible switching surge magnitudes are indicated, and operations and areas of interest that might warrant investigation when applying such equipment are discussed.

Transmission Line Switching Operations

Surges associated with switching transmission lines (overhead, SF_6, or cable) include those that are generated by line energizing, reclosing (three phase and single phase operations), fault initiation, line dropping (deenergizing), fault clearing, etc. During an energizing operation, for example, closing a circuit breaker at the instant of crest system voltage results in a 1 pu surge traveling down the transmission line and being reflected at the remote, open terminal. The reflection interacts with the incoming wave on the phase under consideration as well as with the traveling waves on adjacent phases. At the same time, the waves are being attenuated and modified by losses. Consequently, it is difficult to accurately predict the resultant waveshapes without employing sophisticated simulation tools such as a transient network analyzer (TNA) or digital programs such as the Electromagnetic Transients Program (EMTP).

Transmission line overvoltages can also be influenced by the presence of other equipment connected to the transmission line — shunt reactors, series or shunt capacitors, static var systems, surge arresters, etc. These devices interact with the traveling waves on the line in ways that can either reduce or increase the severity of the overvoltages being generated.

When considering transmission line switching operations, it can be important to distinguish between "energizing" and "reclosing" operations, and the distinction is made on the basis of whether the line's inherent capacitance retains a trapped charge at the time of line closing (reclosing operation) or whether no trapped charge exists (an energizing operation). The distinction is important as the magnitude of the switching surge overvoltage can be considerably higher when a trapped charge is present; with higher magnitudes, insulation is exposed to increased stress, and devices such as surge arresters will, by necessity, absorb more energy when limiting the higher magnitudes. Two forms of trapped charges can exist — DC and oscillating. A trapped charge on a line with no other equipment attached to the line exists as a DC trapped charge, and the charge can persist for some minutes before dissipating (Beehler, 1964). However, if a transformer (power or wound potential transformer) is connected to the line, the charge will decay rapidly (usually in less than 0.5 sec) by discharging through the saturating branch of the transformer (Marks, 1969). If a shunt reactor is connected to the line, the trapped charge takes on an

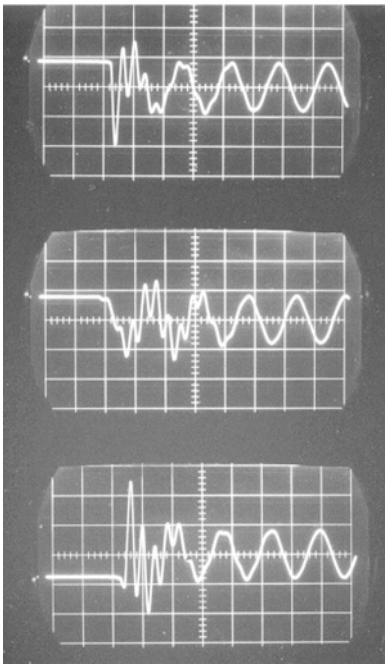

(10 μs/div)

FIGURE 10.21 DC trapped charge.

oscillatory waveshape due to the interaction between the line capacitance and the reactor inductance. This form of trapped charge decays relatively rapidly depending on the Q of the reactor, with the charge being reduced by as much as 50% within 0.5 seconds.

Figures 10.21 and 10.22 show the switching surges associated with reclosing a transmission line. In Fig. 10.21 note the DC trapped charge (approximately 1.0 pu) that exists prior to the reclosing operation (at 20 μs). Figure 10.22 shows the same case with an oscillating trapped charge (a shunt reactor was present on the line) prior to reclosing. Maximum surges were 3.0 for the DC trapped charge case and 2.75 pu for the oscillating trapped charge case (both occurred on phase c).

The power system configuration behind the switch or circuit breaker used to energize or reclose the transmission line also affects the overvoltage characteristics (shape and magnitude) as the traveling wave interactions occurring at the junction of the transmission line and the system (i.e., at the circuit breaker) as well as reflections and interactions with equipment out in the system are important. In general, a stronger system (higher short circuit level) results in somewhat lower surge magnitudes than a weaker system, although there are exceptions. Consequently, when performing simulations to predict overvoltages, it is usually important to examine a variety of system configurations (e.g., a line out of service or contingencies) that might be possible and credible.

Single phase switching as well as three phase switching operations may also need to be considered. On EHV transmission lines, for example, most faults (approximately 90%) are single phase in nature, and opening and reclosing only the faulted phase rather than all three phases, reduces system stresses. Typically, the overvoltages associated with single phase switching have a lower magnitude than those that occur with three phase switching (Koschik et al., 1978).

Switching surge overvoltages produced by line switching are statistical in nature — that is, due to the way that circuit breaker poles randomly close (excluding specially modified switchgear designed to close on or near voltage zero), the instant of electrical closing may occur at the crest of the system voltage, at voltage zero, or somewhere in between. Consequently, the magnitude of the switching surge varies with each switching event. For a given system configuration and switching operation, the surge voltage

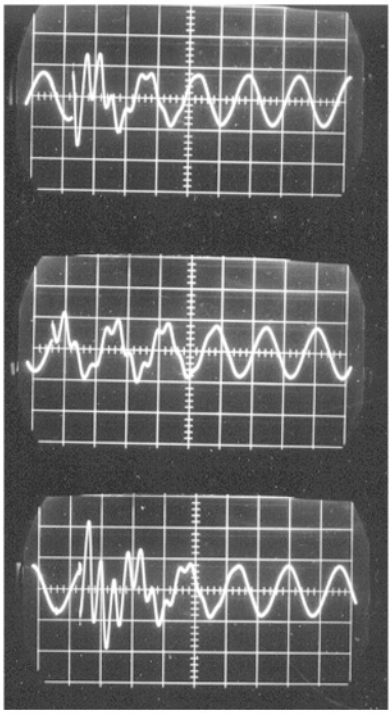

(10 μs/div)

FIGURE 10.22 Oscillating trapped charge.

magnitude at the open end of the transmission line might be 1.2 pu for one closing event and 2.8 pu for the next (Johnson et al., 1964; Hedman et al., 1964), and this statistical variation can have a significantly impact on insulation design (see Section 10.8 on insulation coordination).

Typical switching surge overvoltage statistical distributions (160 km line, 100 random closings) are shown in Figs. 10.23 and 10.24 for phase-to-ground and phase-to-phase voltages (Lambert, 1988), and

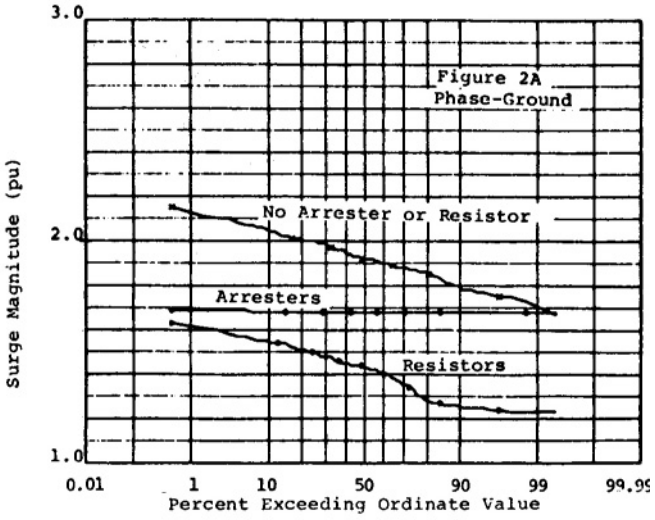

FIGURE 10.23 Phase-to-ground overvoltage distribution.

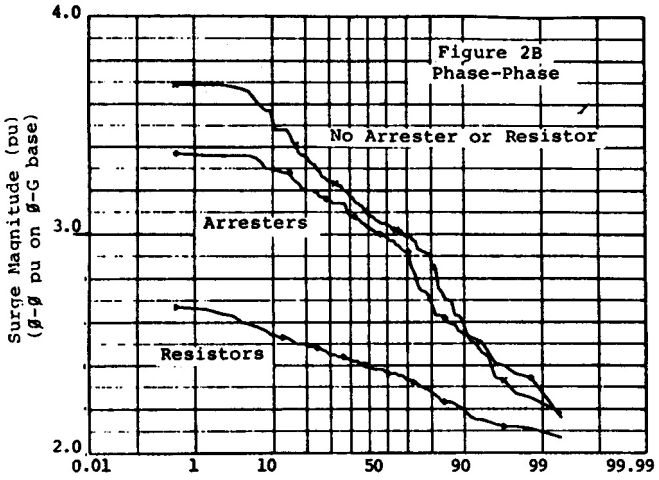

FIGURE 10.24 Phase-to-phase overvoltage distribution.

the surge magnitudes indicated are for the highest that occurred on any phase during each closing. With no surge limiting action (by arresters or circuit breaker preinsertion resistors), phase-to-ground surges varied from 1.7 to 2.15 pu with phase-to-phase surges ranging from 2.2 to 3.7 pu. Phase-to-phase surges can be important to line-connected transformers and reactors as well as to transmission line phase-to-phase conductor separation distances when line uprating or compact line designs are being considered.

Figure 10.23 also demonstrates the effect of the application of surge arresters on phase-to-ground surges, and shows the application of resistors preinserted in the closing sequence of the circuit breaker (400 Ω for 5.56 ms) is even more effective than arresters in reducing surge magnitude. The results shown on Fig. 10.24, however, indicate that while resistors are effective in limiting phase-to-phase surges, arresters applied line to ground are generally not very effective at limiting phase-to-phase overvoltages.

Line dropping (deenergizing) and fault clearing operations also generate surges on the system, although these typically result in phase-to-ground overvoltages having a maximum value of 2 to 2.2 pu. Usually the concern with these operations is not with the phase-to-ground or phase-to-phase system voltages, but rather with the recovery voltage experienced by the switching device. The recovery voltage is the voltage which appears across the interrupting contacts of the switching device (a circuit breaker for example) following current extinction, and if this voltage has too high a magnitude, or in some instances rises to its maximum too quickly, the switching device may not be capable of successfully interrupting.

The occurrence of a fault on a transmission line also can result in switching surge type overvoltages, especially on parallel lines. These voltages usually have magnitudes on the order of 1.8–2.2 pu and are usually not a problem (Kimbark and Legate, 1968; Madzarevic et al., 1977).

Series Capacitor Bank Applications

Installation of a series capacitor bank in a transmission line (standard or thyristor controlled) has the potential for increasing the magnitude of phase-to-ground and phase-to-phase switching surge overvoltages due to the trapped charges that can be present on the bank at the instant of line reclosing. In general, surge arresters limit the phase-to-ground and phase-to-phase overvoltages to acceptable levels; however, one problem that can be serious is the recovery voltage experienced by circuit breakers when clearing faults on a series compensated line. Depending the bank's characteristics and on fault location with respect to the bank's location, a charge can be trapped on the bank, and this trapped charge can add to the surges already being generated during the fault clearing operation (Wilson, 1972). The first circuit breaker to clear is sometimes exposed to excessive recovery voltages under such conditions.

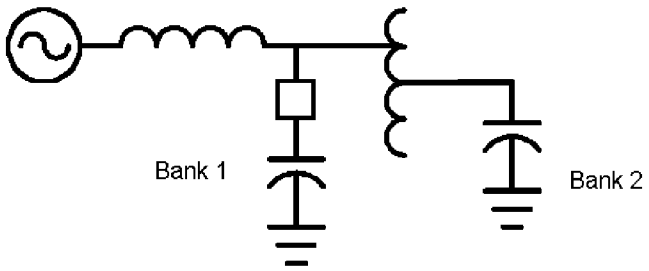

FIGURE 10.25 Voltage magnification circuit.

Shunt Capacitor Bank Applications

Energizing a shunt capacitor bank typically results in maximum overvoltages of about 2 pu or less. However, there are two conditions where significant overvoltages can be generated. One involves a configuration (shown on Fig. 10.25) where two banks are separated by a significant inductance (e.g., a transformer) (Schultz et al., 1959). When one bank is switched, if the system inductance and bank 1 capacitance has the same natural frequency as that of the transformer leakage inductance and the bank 2 capacitance, then a voltage magnification can take place.

Another configuration that can result in damaging overvoltages involves energizing a capacitor bank with a transformer terminated transmission line radially fed from the substation at which the capacitor bank is located (Jones and Fortson, 1985). During bank switching, phase-to-phase surges are imposed on the transformer, and because these are not very well suppressed by the usual phase-to-ground application of surge arresters, transformer failures have been known to result. Various methods to reduce the surge magnitude have included the application of controlled circuit breaker closing techniques (closing near voltage zero), and resistors or reactors preinserted in the closing sequence of the switching devices.

Restriking of the switching device during bank deenergizing can result in severe line-to-ground overvoltages of 3 pu to 5 pu or more (rarely) (Johnson et al., 1955; Greenwood, 1971). Surge arresters are used to limit the voltages to acceptable levels, but at higher system voltages, the energy discharged from the bank into the arrester can exceed the arrester's capability.

Shunt Reactor Applications

Switching of shunt reactors (and other devices characterized as having small inductive currents such as transformer magnetizing currents, motor starting currents, etc.) can generate high phase-to-ground overvoltages as well as severe recovery voltages (Greenwood, 1971), especially on lower voltage equipment such as reactors applied on the tertiary of transformers. Energizing the devices seldom generates high overvoltages, but overvoltages generated during deenergizing, as a result of current chopping by the switching device when interrupting the small inductive currents, can be significant. Neglecting damping, the phase-to-ground overvoltage magnitude can be estimated by:

$$V = i\sqrt{\frac{L}{C}} \tag{10.89}$$

where i is the magnitude of the chopped current (0 to perhaps as high as 10 A or more), L is the reactor's inductance, and C is the capacitance of the reactor (on the order of a few thousand picofarads). When C is small, especially likely with dry-type reactors often used on transformer tertiaries, the surge impedance term can be large, and hence the overvoltage can be excessive.

To mitigate the overvoltages, surge arresters are sometimes useful, but the application of a capacitor on the terminals of the reactor (or other equipment) have a capacitance on the order of 0.25–0.5 μF is very helpful. In the equation above, note that if C is increased from pF to μF, the surge impedance term is dramatically reduced, and hence the voltage is reduced.

References

Beehler, J. E., Weather, corona, and the decay of trapped energy on transmission lines, *IEEE Trans. on Power Appar. and Syst.* 83, 512, 1964.

Greenwood, A., *Electrical Transients in Power Systems*, John Wiley & Sons, New York, 1971.

Hedman, D. E., Johnson, I. B., Titus, C. H., and Wilson, D. D., Switching of extra-high-voltage circuits, II — surge reduction with circuit breaker resistors, *IEEE Trans. on Power Appar. and Syst.* 83, 1196, 1964.

Johnson, I. B., Phillips, V. E., and Simmons, Jr., H. O., Switching of extra-high-voltage circuits, I — system requirements for circuit breakers, *IEEE Trans. on Power Appar. and Syst.* 83, 1187, 1964.

Johnson, I. B., Schultz, A. J., Schultz, N. R., and Shores, R. R., Some fundamentals on capacitance switching, *AIEE Trans. on Power Appar. and Syst.* PAS-74, 727, 1955.

Jones, R. A. and Fortson, Jr., H. S., Considerations of phase-to-phase surges in the application of capacitor banks, IEEE PES Summer Meeting, 1985, 85 SM 400-7.

Kimbark, E. W. and Legate, A. C., Fault surge versus switching surge: A study of transient overvoltages caused by line-to-ground faults, *IEEE Trans. on Power Appar. and Syst.* PAS-87, 1762, 1968.

Koschik, V., Lambert, S. R., Rocamora, R. G., Wood, C. E., and Worner, G., Long line single-phase switching transients and their effect on station equipment, *IEEE Trans. on Power Appar. and Syst.* PAS-97, 857, 1978.

Lambert, S. R., Effectiveness of zinc oxide surge arresters on substation equipment probabilities of flashover, *IEEE Trans. on Power Delivery* 3(4), 1928, 1988.

Madzarevic, V., Tseng, F. K., Woo, D. H., Niebuhr, W. D., and Rocamora, R. G., Overvoltages on ehv transmission lines due to fault and subsequent bypassing of series capacitors, IEEE PES Winter Meeting, January 1977, F77 237-1.

Marks, L. W., Line discharge by potential transformers, *IEEE Trans. on Power Appar. and Syst.* PAS-88, 293, 1969.

Schultz, A. J., Johnson, J. B., and Schultz, N. R., Magnification of switching surges, *AIEE Trans. on Power Appar. and Syst.* 77, 1418, 1959.

Wilson, D. D., Series compensated lines — voltages across circuit breakers and terminals caused by switching, *IEEE PES Summer Meeting,* 1972, T72 565-0.

10.5 Very Fast Transients

Juan A. Martinez-Velasco

Transient phenomena in power systems are caused by switching operations, faults, and other disturbances, such as lightning strokes. They may appear with a wide range of frequencies that vary from DC to several MHz. A distinction is usually made between slow electromechanical transients and faster electromagnetic transients. The latter type of transients can occur on a time scale that goes from microseconds to several cycles. Due to frequency-dependent behavior of power components and difficulties for developing models accurate enough for a wide frequency range, the frequency ranges are classified into groups, with overlapping between them. An accurate mathematical representation of each power component can generally be developed for a specific frequency range (CIGRE, 1990).

Very Fast Transients (VFT), also known as Very Fast Front Transients, belong to the highest frequency range of transients in power systems. According to the classification proposed by the CIGRE Working Group 33-02, VFT may vary from 100 kHz up to 50 MHz (1990). According to IEC 71-1, the shape of a very fast front overvoltage is "usually unidirectional with time to peak < 0.1 μs, total duration < 3 ms, and with superimposed oscillations at frequency 30 kHz $< f <$ 100 MHz" (1993). In practice, the term VFT is restricted to transients with frequencies above 1 MHz. Several causes can originate these transients in power systems: disconnector operations and faults within gas insulated substations (GIS), switching of motors and transformers with short connections to the switchgear, certain lightning conditions (IEC 71-2, 1996).

This section is exclusively dedicated to explaining the origin, and to analyze the propagation and the effects of VFT in GIS. These transients have a rise time in the range of 4 to 100 ns, and are normally followed by oscillations ranging from 1 to 50 MHz. Their magnitude is in the range of 1.5 to 2 per unit of the line-to-neutral voltage crest, but they can also reach values higher than 2.5 per unit. These values are generally below the BIL of the GIS and connected equipment of lower voltage classes. VFT in GIS are of greater concern at the highest voltages, for which the ratio of the BIL to the system voltage is lower (Yamagata et al., 1996). External VFT can be dangerous for secondary and adjacent equipment.

Origin of VFT in GIS

VFT within a gas-insulated substation (GIS) are usually generated by disconnect switch operations, although other events, such as the closing of a grounding switch or a fault, can also cause VFT.

A large number of pre- or restrikes can occur during a disconnector operation due to the relatively slow speed of the moving contact (Ecklin et al., 1980). Figure 10.26 shows a very simple configuration used to explain the general switching behavior and the pattern of voltages on opening and closing of a disconnector at a capacitive load (Boggs et al., 1982). During an opening operation, sparking occurs as soon as the voltage between the source and the load exceeds the dielectric strength across contacts. After

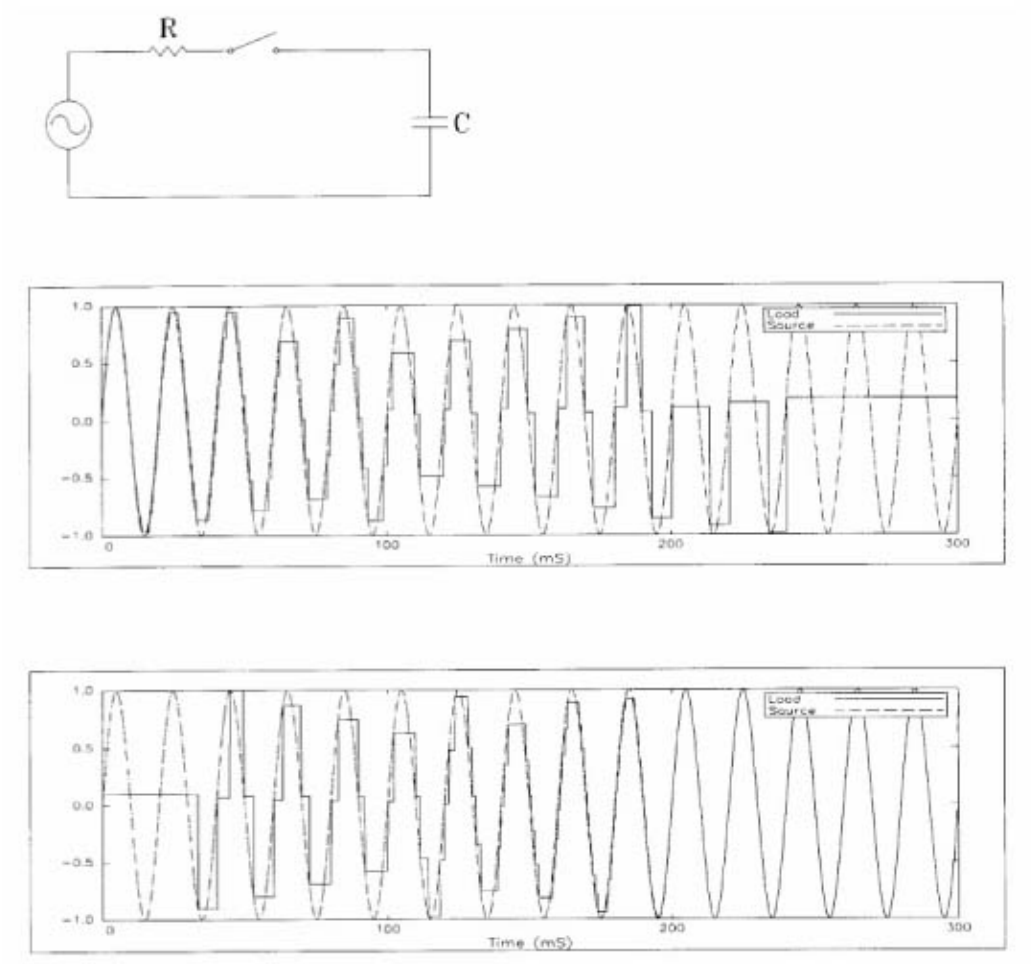

FIGURE 10.26 Variation of load and source side voltages during disconnector switching: (a) scheme of the circuit, (b) opening operation; (c) closing operation.

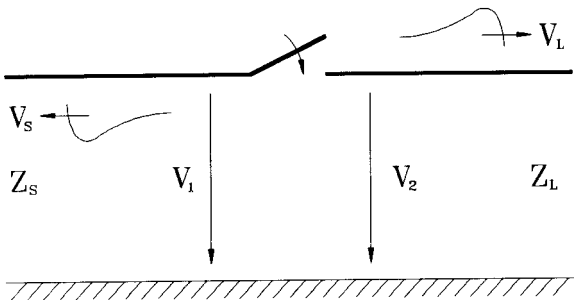

FIGURE 10.27 Generation of very fast transients.

a restrike, a high-frequency current will flow through the spark and equalize the capacitive load voltage to the source voltage. The potential difference across the contacts will fall and the spark will extinguish. The subsequent restrike occurs when the voltage between contacts reaches the new dielectric strength level that is determined by the speed of the moving contact and other disconnector characteristics. The behavior during a closing operation is very similar, and the load side voltage will follow the supply voltage until the contact-make. For a discussion of the physics involved in the restrikes and prestrikes of a disconnect switch operation see (Boggs et al., 1982).

The scheme shown in Fig. 10.27 will be very useful to illustrate the generation of VFT due to a disconnector operation. The breakdown of a disconnector when it is closing originates two surges V_L and V_S which travel outward in the bus duct and back into the source side respectively. The magnitude of both traveling surges is given by

$$V_L = \frac{Z_L}{Z_S + Z_L}\left(V_1 - V_2\right) \qquad V_S = -V_L \tag{10.90}$$

where Z_S and Z_L are the surge impedances on the source and on the load side respectively. V_1 is the intercontact spark voltage, while V_2 is the trapped charge voltage at the load side.

Steep fronted traveling surges can also be generated in case of a line-to-ground fault, as the voltage collapse at the fault location occurs in a similar way as in the disconnector gap during striking.

Propagation of VFT in GIS

VFT in GIS can be divided into internal and external. Internal transients can produce overvoltages between the inner conductor and the enclosure, while external transients can cause stress on secondary and adjacent equipment. A summary about the propagation and main characteristics of both types of phenomena follows.

Internal Transients

Breakdown phenomena across the contacts of a disconnector during a switch operation or a line-to-ground fault generate very short rise time traveling waves which propagate in either direction from the breakdown location. As a result of the fast rise time of the wave front, the propagation throughout a substation must be analyzed by representing GIS sections as low-loss distributed parameter transmission lines, each section being characterized by a surge impedance and a transit time. Traveling waves are reflected and refracted at every point where they encounter a change in the surge impedance. The generated transients depend on the GIS configuration and on the superposition of the surges reflected and refracted on line discontinuities like breakers, "T" junctions, or bushings. As a consequence of multiple reflections and refractions, traveling voltages can increase above the original values and very high-frequency oscillations occur.

The internal damping of the VFT influencing the highest frequency components is determined by the spark resistance. Skin effects due to the aluminum enclosure can be generally neglected. The main portion of the damping of the VFT occurs by outcoupling at the transition to the overhead line. Due to the traveling wave behavior of the VFT, the overvoltages caused by disconnector switches show a spatial distribution. Normally the highest overvoltage stress is reached at the open end of the load side.

Overvoltages are dependent on the voltage drop at the disconnector just before striking, and on the trapped charge that remains on the load side of the disconnector. For a normal disconnector with a slow speed, the maximum trapped charge reaches 0.5 pu resulting in a most unfavorable voltage collapse of 1.5 pu. For these cases, the resulting overvoltages are in the range of 1.7 pu and reach 2 pu for very specific cases. For a high-speed disconnector, the maximum trapped charge could be 1 pu and the highest overvoltages reach values up to 2.5 pu. Although values larger than 3 pu have been reported, they have been derived by calculation using unrealistic simplified simulation models. The main frequencies depend on the length of the GIS sections affected by the disconnector operation and are in the range of 1 to 50 MHz.

The following examples will be useful to illustrate the influence of some parameters on the frequency and magnitude of VFT in GIS. Figure 10.28 shows two very simple cases, a single bus duct and a "T" junction in which GIS components are modeled as lossless distributed parameter transmission lines. The source side is represented as a step-shaped source in series with a resistance. This is a simplified modeling of an infinite length bus duct. The surge impedance of all bus sections is 50 **Ω**. For the simplest configuration, the reflections of the traveling waves at both terminals of the duct will produce, when the source resistance is neglected, a pulse-shaped transient of constant magnitude — 2 pu — and constant frequency at the open terminal. The frequency of this pulse can be calculated from the following expression

$$f = \frac{1}{4\,\tau} \tag{10.91}$$

where τ is the transit time of the line. If the propagation velocity is close to that of light, the frequency, in MHz, of the voltage generated at the open terminal will be

$$f \approx \frac{75}{d} \tag{10.92}$$

where d is the duct length, in meters. When a more realistic representation of the source is used, R = 40 **Ω**, the maximum overvoltage at the open terminal will depend on the voltage at the disconnector just before striking, and on the trapped charge which remains on the load side.

Overvoltages can reach higher values in more complex GIS configurations. The simulations performed for the "T" configuration shown in Fig. 10.28 gave in all cases higher values than in the previous case, where node 4 is the location where the highest overvoltages were originated.

External Transients

Internally generated VFT propagate throughout the GIS and reach bushings where they cause transient enclosure voltages and traveling waves that propagate along the overhead transmission line. An explanation about the generation of external transients and some comments on their main characteristics follow.

Transient Enclosure Voltages

Transient enclosure voltages (TEV), also known as transient ground potential rises (TGPR), are short-duration high-voltage transients that appear on the enclosure of the GIS through the coupling of internal transients to enclosure at enclosure discontinuities. The simplified circuit shown in Fig. 10.29 is used to explain the generation of TEV (Meppelink et al., 1989). At the GIS-air interface, three transmission lines can be distinguished: the coaxial GIS transmission line, the transmission line formed by the bushing conductor and the overhead line, and the GIS enclosure-to-ground transmission line. When an internal wave propagates to the gas-to-air bushing, a portion of the transient is coupled onto the overhead

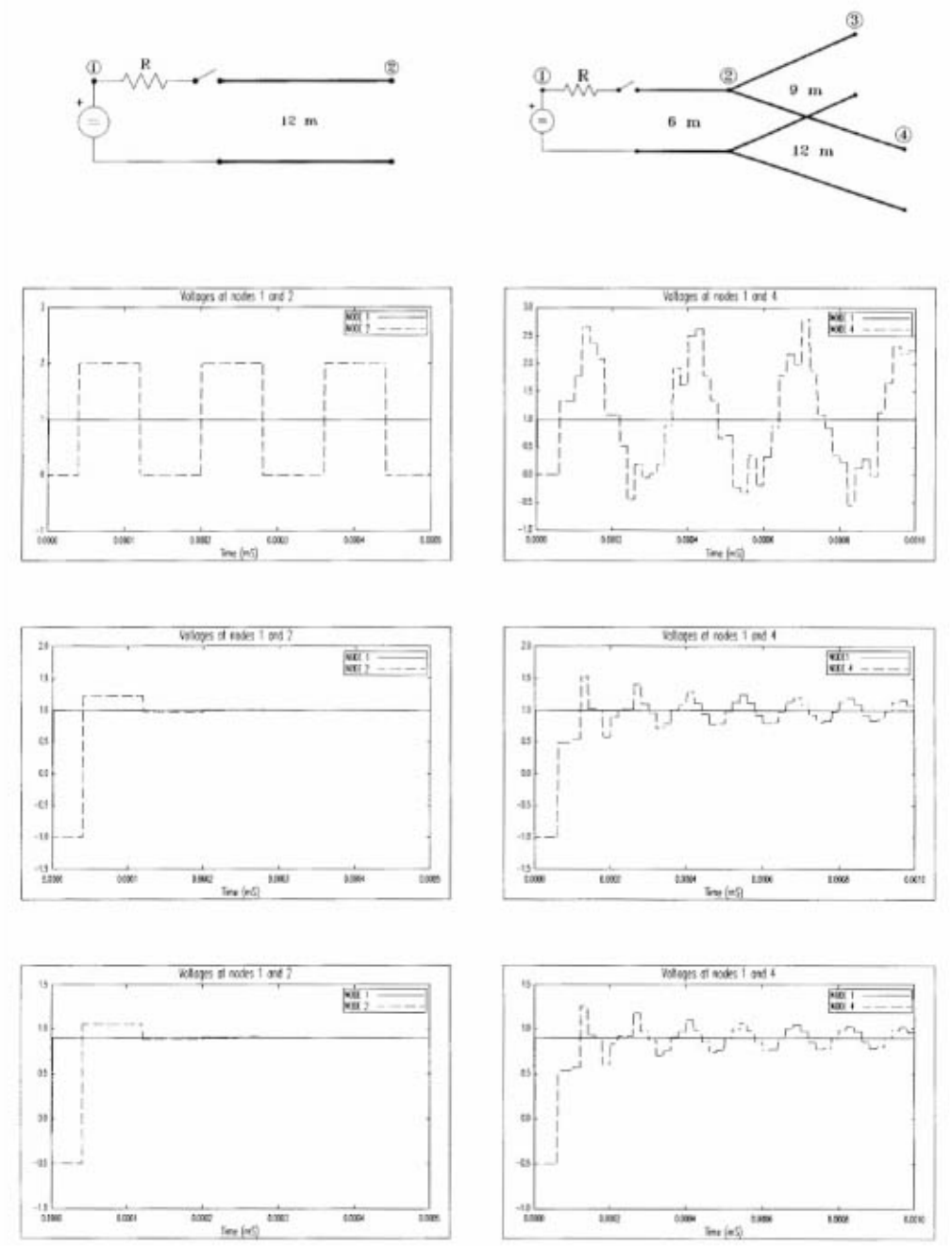

FIGURE 10.28 VFT overvoltages in GIS: (a) scheme of the network, (b) R = 0; V_1 = 1 pu; V_2 = 0, (c) R = 40 Ω; V_1 = 1 pu; V_2 = –1 pu, (d) R = 40 Ω; V_1 = 0.9 pu; V_2 = –0.5 pu.

transmission line, and a portion is coupled onto the GIS enclosure-to-ground transmission line. The wave that propagates along the enclosure-to-ground transmission line is the TEV. The usual location for these voltages is the transition GIS-overhead line at an air bushing, although they can also emerge at visual inspection ports, insulated spacers for CTs, or insulated flanges at GIS/cables interfaces.

TEV waveforms have at least two components; the first one has a short initial rise time and is followed by high-frequency oscillations, in the range of 5 to 10 MHz, determined by the lengths of various sections

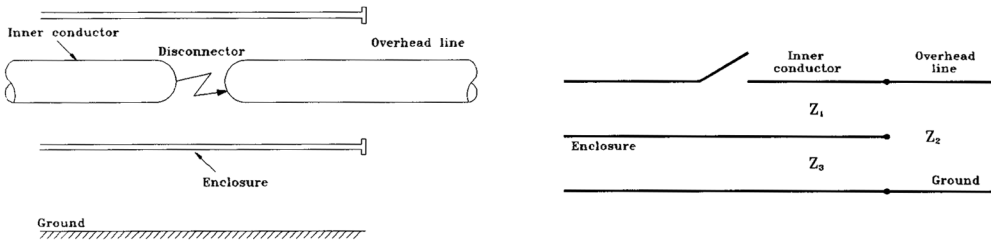

FIGURE 10.29 Generation of TEV: (a) GIS-air transition, (b) single-line diagram.

of the GIS. The second component is of lower frequency, hundreds of kHz, and is often associated with the discharge of capacitive devices with the earthing system. Both components are damped quickly as a result of the lossy nature of the enclosure-to-ground plane transmission mode. TEV generally persists for a few microseconds. The magnitude varies along the enclosure; it can be in the range of 0.1 to 0.3 pu of the system voltage, and reaches the highest magnitude near the GIS-air interface. Mitigation methods include short length leads, low impedance grounding, and the installation of metal-oxide arresters across insulating spacers.

Transients on Overhead Connections

A portion of the VFT traveling wave incident at a gas-air transition is coupled onto the overhead connection and propagates to other components. This propagation is lossy and results in some increase of the waveform rise time. In general, external waveforms have two different characteristics: the overall waveshape that is dictated by lumped circuit parameters, such as the capacitance of voltage transformers or line and earthing inductance, with a rise time in the range of a few hundred nanoseconds; and a fast front portion that is dictated by transmission line effects, with a rise time in the range of 20 ns. A fast rise time of the initial portion is possible as capacitive components, such as bushings, are physically long and distributed and cannot be treated as lumped elements; the magnitude is generally lower than that of internal VFT, it is usually reduced by discontinuities in the transmission path, with a voltage rate-of-rise in the range of 10-30 kV/μs.

Transient Electromagnetic Fields

These fields are radiated from the enclosure and can cause some stress on secondary equipment. Their frequency depends on the GIS arrangement, but are typically in the range of 10 to 20 MHz.

Modeling Guidelines and Simulation

Due to the origin and the traveling nature of VFT, modeling of GIS components makes use of electrical equivalent circuits composed of lumped elements and distributed parameter lines. At very high frequencies, the skin losses can produce an important attenuation; however, these losses are usually neglected, which produces conservative results. Only the dielectric losses in some components (e.g., capacitively graded bushing) need be taken into account. The calculation of internal transients may be performed using distributed parameter models for which only an internal mode (conductor-enclosure) is taken into account, and assuming that the external enclosure is perfectly grounded. If TEV is a concern, then a second mode (enclosure-ground) is to be considered.

The next two sections present modeling guidelines to represent GIS equipment in computation of internal and external transients (Fujimoto et al., 1986; Ogawa et al., 1986; Witzmann, 1987; CIGRE, 1988; Povh, 1996; Fujimoto et al., 1982; Dick et al., 1982). They make use of single-phase models and very simple representations. Depending on the substation layout and the study to be performed, three-phase models for inner conductors (Miri and Binder, 1995) or the outer enclosures (Dick et al., 1982) should be considered. More advanced guidelines have been analyzed and proposed in by Haznadar et al. (1992).

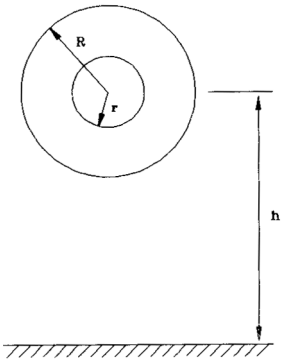

FIGURE 10.30 Coaxial bus duct cross section.

Computation of Internal Transients

A short explanation about the representation of the most important GIS components follows.

Bus Ducts

For frequencies lower than 100 MHz, a bus duct can be represented as a lossless transmission line. The surge impedance and the travel time are calculated from the physical dimensions of the duct. The inductance and the capacitance per unit length of a horizontal single-phase coaxial cylinder configuration, as that shown in Fig. 10.30, are given by the following expressions

$$L_1' = \frac{\mu_0}{2\pi} \ln \frac{R}{r} \tag{10.93}$$

$$C_1' = \frac{2\pi\varepsilon}{\ln \dfrac{R}{r}} \qquad \left(\varepsilon \approx \varepsilon_0\right) \tag{10.94}$$

from where the following form for the surge impedance is derived

$$Z_1 = \sqrt{\frac{L_1'}{C_1'}} = \frac{\sqrt{\mu_0 \varepsilon}}{2\pi} \ln \frac{R}{r} \approx 60 \ln \frac{R}{r} \tag{10.95}$$

A different approach should be used for vertically oriented bus sections (Miri and Binder, 1995). As for the propagation velocity, empirical corrections are usually needed to adjust its value. Experimental results show that the propagation velocity in GIS ducts is close to 0.95–0.96 of the speed of light (Fujimoto et al., 1986).

Other equipment, such as elbows, can also be modeled as lossless transmission lines.

Surge Arresters

Experimental results have shown that if switching operations in GIS do not produce voltages high enough to cause metal-oxide surge arrester to conduct, then the arrester can be modeled as a capacitance-to-ground. However, when the arrester conducts, the model should take into account the steep front wave effect, since the voltage developed across the arrester for a given discharge current increases as the time to crest of the current increases, but reaches crest prior to the crest of the current. A detailed model must represent each internal shield and block individually, and include the travel times along shield sections, as well as capacitances between these sections, capacitances between blocks and shields, and the blocks themselves.

Circuit Breakers

A closed breaker can be represented as a lossless transmission line whose electrical length is equal to the physical length, with the propagation velocity reduced to 0.95–0.96 of the speed of light. The representation of an open circuit breaker is more complicated due to internal irregularities. In addition, circuit breakers with several chambers contain grading capacitors, which are not arranged symmetrically. The electrical length must be increased above the physical length due to the effect of a longer path through the grading capacitors, while the speed of progression must be decreased due to the effects of the higher dielectric constant of these capacitors.

Gas-to-Air Bushings

A bushing gradually changes the surge impedance from that of the GIS to that of the line. A simplified model may consist of several transmission lines in series with a lumped resistor representing losses; the surge impedance of each line section increases as the location goes up the bushing. If the bushing is distant from the point of interest, the resistor can be neglected and a single line section can be used. A detailed model must consider the coupling between the conductor and shielding electrodes, and include the representation of the grounding system connected to the bushing (Fujimoto and Boggs, 1988; Ardito et al., 1992).

Power Transformers

At very high frequencies, a winding of a transformer behaves like a capacitive network consisting of series capacitances between turns and coils, and shunt capacitances between turns and coils to the grounded core and transformer tank; the saturation of the magnetic core can be neglected, as well as leakage impedances. When voltage transfer has to be calculated, interwinding capacitances and secondary capacitance-to-ground must also be represented. If voltage transfer is not a concern, an accurate representation can be obtained by developing a circuit that matches the frequency response of the transformer at its terminals. Details on the computation of equivalent capacitances have been covered by Chowdhuri (1996).

Spark Dynamics

The behavior of the spark in disconnector operations can be represented by a dynamically variable resistance with a controllable collapse time. In general, this representation does not affect the magnitude of the maximum VFT overvoltages, but it can introduce a significant damping on internal transients (Yanabu et al., 1990).

Computation of TEV

At very high frequencies, currents are constrained to flow along the surface of the conductors and do not penetrate through them. The inside and the outside of a GIS enclosure are distinct, so that transients generated within the substation do not appear on the outside surface of the enclosure until discontinuities in the sheath are encountered. These discontinuities occur at gas-to-air terminations, GIS-cable transitions, or external core current transformers. The modeling of the GIS for computation of TEV must include the effects of the enclosure, the representation of ground straps, and the earthing grid.

Enclosures

A GIS-air termination can be modeled as a junction of three transmission lines, each with its own surge impedance (Fig. 10.29). This equivalent network can be analyzed using lossless transmission line models to determine reflected and transmitted waves. The surge impedance of the enclosure-to-ground transmission line (Fig. 10.29) is derived from the following forms

$$L'_3 \approx \frac{\mu_0}{2\pi} \ln \frac{2h}{R} \tag{10.96}$$

$$C'_3 \approx \frac{2\pi\varepsilon_0}{\ln \dfrac{2h}{R}} \tag{10.97}$$

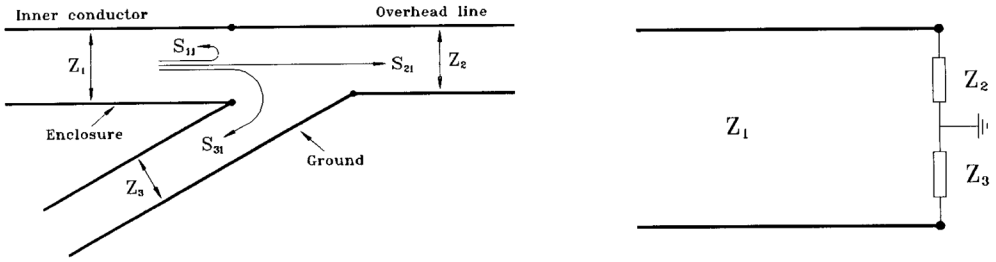

FIGURE 10.31 GIS–air transition. Scattering coefficients: (a) schematic diagram; (b) equivalent circuit.

$$Z_3 = \sqrt{\frac{L'_3}{C'_3}} = \frac{\sqrt{\mu_0 \varepsilon_0}}{2\pi} \ln \frac{2h}{R} \approx 60 \ln \frac{2h}{R} \tag{10.98}$$

The basic mechanism of TEV is defined by the refraction of waves from the internal coaxial bus duct to the enclosure sheath-to-ground system. Figure 10.31 shows the scattering coefficients involved in an air-SF6 transition, and the equivalent circuit to be used for calculating these coefficients. The coefficients S_{ji} represent the refraction of waves from line "i" into line "j".

The coefficient S_{11}, which is also the reflection coefficient at the transition, is given by

$$S_{11} = \frac{\left(Z_2 + Z_3\right) - Z_1}{Z_1 + Z_2 + Z_3} \tag{10.99}$$

The refraction coefficient at the transition is then

$$r_t = 1 + S_{11} = \frac{2\left(Z_2 + Z_3\right)}{Z_1 + Z_2 + Z_3} \tag{10.100}$$

The magnitude of the transmitted wave onto the outside of the enclosure sheath is given by following scattering coefficient

$$S_{31} = r_t \frac{-Z_3}{Z_2 + Z_3} = -\frac{2Z_3}{Z_1 + Z_2 + Z_3} \tag{10.101}$$

The negative sign means that there is an inversion of the waveform with respect to the internal transient.

Ground Straps

TEV propagates back from the gas-to-air termination into the substation on the transmission line defined by the enclosure and the ground plane. The first discontinuity in the propagation is generally a ground strap. For TEV rise times, most ground straps are too long and too inductive for effective grounding. Ground leads may have a significant effect on the magnitude and waveshape of TEV. This effect can be explained by considering two mechanisms (Fujimoto et al., 1982). First, the ground lead may be seen as a vertical transmission line whose surge impedance varies with height; when the transient reaches the ground strap, a reflected wave is originated that reduces the magnitude of the transmitted wave, with the reduction expressed by the coefficient

$$\frac{2Z_g}{2Z_g + Z_3} \tag{10.102}$$

where Z_g is the surge impedance of the ground strap. As Z_g is usually much larger than Z_3, the attenuation produced by the ground strap will usually be small. Second, when the portion of the wave that propagates down the ground strap meets the low impedance of the ground grid, a reflected wave is produced that propagates back to the enclosure where it will tend to reduce the original wave.

The representation of a ground lead as a constant surge impedance is not strictly correct. It has a continuously varying surge impedance, so that a continuous reflection occurs as a wave propagates down the lead. The ground strap can be divided into sections, each one represented by a surge impedance calculated from the following expression

$$Z_s = 60 \ln \frac{2\sqrt{2}\,h}{r} \tag{10.103}$$

where r is the lead radius and h is the average height of the section (Fujimoto et al., 1982). However, a constant inductor model may be adequate for straps with travel time less than the surge rise time, while a nonuniform impedance model may be necessary for very long straps.

Earthing Grid

The representation of the earthing grid at TEV frequencies is a very complex task. Furthermore, this grid may not be designed to carry very high frequency currents, as no standards for very high frequency earthing systems are currently available. A simplified modeling may be used by representing the earthing grid as a low value constant resistance.

Advanced models for GIS components in computation of TEV might consider a frequency-dependent impedance for ground straps, a frequency-dependent model for the enclosure-to-ground line (which could take into account earth losses), and the propagation of phase-to-phase modes on the three enclosures (Fujimoto et al., 1982).

Statistical Calculation

The largest VFT stresses under normal operating conditions originate from disconnector operations. The level reached by overvoltages is random by nature. The maximum overvoltage produced by a disconnector breakdown depends on the geometry of the GIS, the measuring point, the voltage prior to the transient at the load side (trapped charge), and the intercontact voltage at the time of the breakdown, as shown in the section on Internal Transients.

Several works have been performed to determine the statistical distribution of VFT overvoltages in a GIS (Boggs et al., 1982; Yanabu et al., 1990; Boggs et al., 1984; Fujimoto et al., 1988). A very simple expression can be used to calculate the transient overvoltages as a function of time t and position s (Boggs et al., 1984; Fujimoto et al., 1988)

$$V(t,s) = V_b * K(t,s) + V_q \tag{10.104}$$

where K(t,s) is the normalized response of the GIS, V_b is the intercontact spark voltage, and V_q the voltage prior to the transient at the point of interest. As V_b and V_q are random variables, V(t,s) is also random. This equation can be used to estimate worst-case values (Fujimoto et al., 1988).

The performance of a disconnector during an opening operation can be characterized by the pattern of arcing on a capacitive load (Fig. 10.26). A difference in breakdown voltages for the two polarities indicates a dielectric asymmetry. When the asymmetry is large compared to the statistical variance in breakdown voltage, a systematic pattern is originated near the end of the arcing sequence (Boggs et al., 1984). The final trapped charge voltage has a distribution which is very dependent on the asymmetry in the intercontact breakdown voltage.

The dielectric asymmetry of a disconnector is usually a function of contact separation. A disconnector may show a different performance at different operating voltages. A consequence of this performance is that very different stresses will be originated as a result of different operational characteristics.

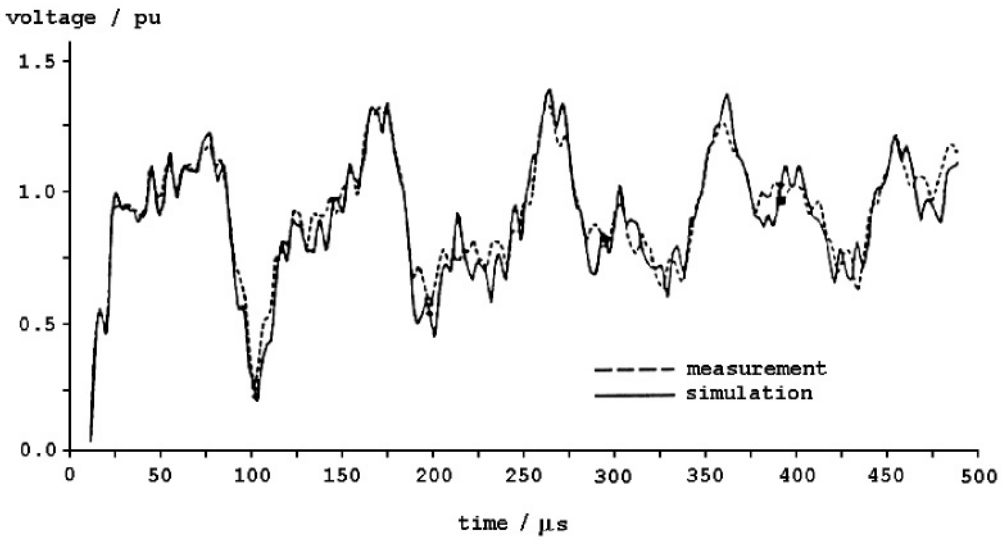

FIGURE 10.32 Comparison of simulation and measurement of disconnect switch induced overvoltages in a 420 kV GIS. (Copyright 1999 IEEE.)

From the results presented in the literature, the following conclusions may be derived (Boggs et al., 1982; Yanabu et al., 1990; Boggs et al., 1984; Fujimoto et al., 1988):

- The value of the trapped charge is mainly dependent on the disconnect switch characteristics: the faster the switch, the greater the mean value that the trapped charge voltage can reach.
- For slow switches, the probability of a re-/prestrike with the greatest breakdown voltage, in the range 1.8–2 pu, is very small; however, due to the great number of re-/prestrikes that are produced with one operation, this probability should not always be neglected.
- The asymmetry of the intercontact breakdown voltage can also affect the trapped charge distribution; in general, both the magnitude and the range of values are reduced if there is a difference in the breakdown voltage of the gap for positive and negative values.

Validation

The results presented in Figs. 10.32 and 10.33 illustrate the accuracy which can be obtained by means of a digital simulation. Figure 10.32 shows a good match between a direct measurement in an actual GIS and a computer result. The simulation was performed including the effects of spacers, flanges, elbows, and other hardware, but neglecting propagation losses (Witzmann, 1987). Figure 10.33 shows that important differences could occur when comparing a measurement and a digital simulation result, although a detailed representation of the GIS was considered. The differences were due to use of low damping equivalent circuits and to limitation of measuring instruments that did not capture very high frequencies (IEEE, 1996).

Effects of VFT on Equipment

The level reached by VFT overvoltages originated by disconnector switching or line-to-ground faults inside a GIS are below the BIL of substation and external equipment (Boersma, 1987). However, aging of the insulation of external equipment due to frequent VFT must be considered. TEV is a low energy phenomenon and it is not considered dangerous to humans; the main concern is in the danger of the surprise-shock effect. External transients can cause interference with or even damage to the substation control, protection, and other secondary equipment (Meppelink et al., 1989; Boersma, 1987). The main effects caused by VFT to equipment and the techniques that can be used to mitigate these effects are summarized below (CIGRE, 1988).

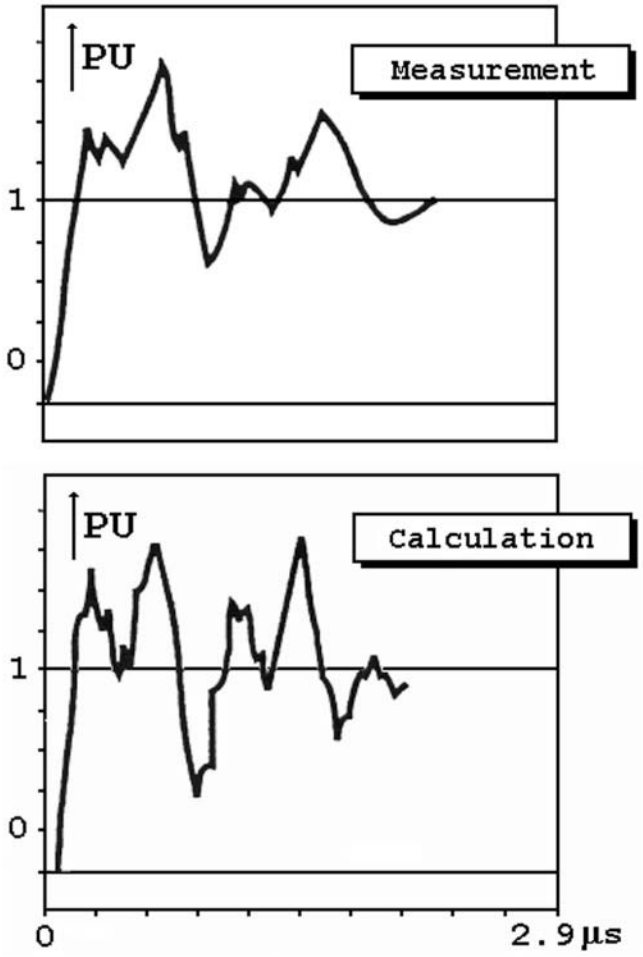

FIGURE 10.33 Measurement and simulation of overvoltages in a 420 kV GIS at closing a switch. (Copyright 1999 IEEE.)

SF6 insulation — Breakdown caused by VFT overvoltages is improbable in a well-designed GIS insulation system during normal operations. The breakdown probability increases with the frequency of the oscillations. In addition, breakdown values can be reduced by insulation irregularities like edges and fissures. However, at ultra high voltage systems, more than 1000 kV, for which the ratio of BIL to the system voltage is lower, breakdown is more likely to be caused. At these levels, VFT overvoltages can be reduced by using resistor-fitted disconnectors (Yamagata et al., 1996).

Transformers — Due to steep fronted wave impulses, direct connected transformers can experience an extremely nonlinear voltage distribution along the high-voltage winding, connected to the oil-SF6 bushings, and high resonance voltages due to transient oscillations generated within the GIS. Transformers can generally withstand these stresses; however, in critical cases, it may be necessary to install varistors to protect tap changers.

Disconnectors and breakers — The insulation system of breakers and switches is not endangered by VFT overvoltages generated in adjacent GIS equipment. Ground faults induced by VFT overvoltages have been observed in disconnectors operations, as residual leader branches can be activated by enhanced field gradient to ground. These faults can be avoided by a proper disconnector design.

Enclosure — TEV can cause sparking across insulated flanges and to insulated busbars of CTs, and can puncture insulation that is intended to limit the spread of circulating currents within the enclosure.

TEV can be minimized with a proper design and arrangement of substation masts, keeping ground leads as short and straight as possible in order to minimize the inductance, increasing the number of connections to ground, introducing shielding to prevent internally generated VFT from reaching the outside of the enclosure, and installing voltage limiting varistors where spacers must be employed.

Bushings — Very few problems have been reported with capacitively graded bushings. High impedances in the connection of the last graded layer to the enclosure should be avoided.

Secondary equipment — TEV may interfere with secondary equipment or damage sensitive circuits by raising the housing potential if they are directly connected, or via cable shields to GIS enclosure by emitting free radiation which may induce currents and voltages in adjacent equipment. Correct cable connection procedures may minimize interference. The coupling of radiated energy may be reduced by mounting control cables closely along the enclosure supports and other grounded structures, grounding cable shields at both ends by leads as short as possible, or using optical coupling services. Voltage limiting devices may have to be installed.

References

Ardito, A., Iorio, R., Santagostino, G., and Porrino, A., Accurate modeling of capacitively graded bushings for calculation of fast transient overvoltages in GIS, *IEEE Trans. on Power Delivery*, 7, 1316, 1992.

Boersma, R., Transient ground potential rises in gas-insulated substations with respect to earthing systems, *Electra*, 110, 47, 1987.

Boggs, S. A., Chu, F. Y., Fujimoto, N., Krenicky, A., Plessl, A., and Schlicht, D., Disconnect switch induced transients and trapped charge in gas-insulated substations, *IEEE Trans. on Power Appar. and Syst.*, 101, 3593, 1982.

Boggs, S.A, Fujimoto, N., Collod, M., and Thuries, E., The modeling of statistical operating parameters and the computation of operation-induced surge waveforms for GIS disconectors, *CIGRE*, Paper No. 13-15, Paris, 1984.

Chowdhuri, P., *Electromagnetic Transients in Power Systems*, RSP-John Wiley, 1996, Chap. 12.

CIGRE Working Group 33/13-09, Very fast transient phenomena associated with gas insulated substations, *CIGRE*, Paper 33-13, Paris, 1988.

CIGRE Joint WG 33/23-12, Insulation co-ordination of GIS: Return of experience, on site tests and diagnostic techniques, *Electra*, 176, 66, 1998.

CIGRE Working Group 33.02, *Guidelines for representation of networks elements when calculating transients*, CIGRE Brochure, 1990.

Dick, E. P., Fujimoto, N., Ford, G. L., and Harvey, S., Transient ground potential rise in gas-insulated substations — problem identification and mitigation, *IEEE Trans. on Power Appar. and Syst.*, 101, 3610, 1982.

Ecklin, A., Schlicht, D., and Plessl, A., Overvoltages in GIS caused by the operation of isolators, in *Surges in High-Voltage Networks*, Ragaller, K., Ed., Plenum Press, New York, 1980, chap. 6.

Fujimoto, N., and Boggs, S. A., Characteristics of GIS disconnector-induced short risetime transients incident on externally connected power system components, *IEEE Trans. on Power Delivery*, 3, 961, 1988.

Fujimoto, N., Chu, F. Y., Harvey, S. M., Ford, G. L., Boggs, S. A., Tahiliani, V. H., and Collod, M., Developments in improved reliability for gas-insulated substations, *CIGRE*, Paper No. 23-11, Paris, 1988.

Fujimoto, N., Dick, E. P., Boggs, S. A., and Ford, G. L., Transient ground potential rise in gas- insulated substations — experimental studies, *IEEE Trans. on Power Appar. and Syst.*, 101, 3603, 1982.

Fujimoto, N., Stuckless, H. A., and Boggs, S. A., Calculation of disconnector induced overvoltages in gas-insulated substations, in *Gaseous Dielectrics IV*, Pergamon Press, 1986, 473.

Haznadar, Z., Carsimamovic, S., and Mahmutcehajic, R., More accurate modeling of gas insulated substation components in digital simulations of very fast electromagnetic transients, *IEEE Trans. on Power Delivery*, 7, 434, 1992.

IEC 71-1, *Insulation Co-ordination — Part 1: Definitions, Principles and Rules*, 1993.

IEC 71-2, *Insulation Co-ordination — Part 2: Application Guide*, 1996.
IEEE TF on Very Fast Transients (Povh, D., Chairman), Modelling and analysis guidelines for very fast transients, *IEEE Trans. on Power Delivery*, 11, 2028, 1996.
Meppelink, J., Diederich, K., Feser, K., and Pfaff, W., Very fast transients in GIS, *IEEE Trans. on Power Delivery*, 4, 223, 1989.
Miri, A. M. and Binder, C., Investigation of transient phenomena in inner- and outer systems of GIS due to disconnector operation, in *Proc. Int. Conf. Power Systems Transients*, Lisbon, 1995, 71.
Ogawa, S., Haginomori, E., Nishiwaki, S., Yoshida, T., and Terasaka, K., Estimation of restriking transient overvoltage on disconnecting switch for GIS, *IEEE Trans. on Power Delivery* 1, 95, 1986.
Witzmann, R., Fast transients in gas insulated substations. Modelling of different GIS components, in *Proc. 5th Int. Symp. HV Engineering*, Braunschweig, 1987.
Yamagata, Y., Tanaka, K., Nishiwaki, S., Takahashi, N., Kokumai, T., Miwa, I., Komukai, T., and Imai, K., Suppression of VFT in 1100 kV GIS by adopting resistor-fitted disconnector, *IEEE Trans. on Power Delivery* 11, 872, 1996.
Yanabu, S., Murase, H., Aoyagi, H., Okubo, H., and Kawaguchi, Y., Estimation of fast transient overvoltage in gas-insulated substation, *IEEE Trans. on Power Delivery*, 5, 1875, 1990.

10.6 Transient Voltage Response of Coils and Windings

Robert C. Degeneff

Transient Voltage Concerns

Normal System Operation

Transformers are normally used in systems to change power from one voltage (or current) to another. This is often driven by a desire to optimize the overall system characteristics, e.g., economics, reliability, and/or performance. To achieve these system goals, a purchaser must specify and a designer must configure the transformer to meet a desired impedance, voltage and power rating, thermal characteristic, short circuit strength, sound level, physical size, and voltage withstand capability. Obviously, many of these goals will produce requirements that are in conflict and prudent compromise will be required. Failure to achieve an acceptable characteristic for any of these makes the overall transformer design unacceptable. Transformer characteristics and the concomitant design process is outlined in Blume et al., (1951); Bean et al., (1959); MIT, (1943); and Franklin, (1983).

Normally a transformer operates under steady voltage excitation. Occasionally a transformer (in fact, all electrical equipment) experiences dynamic and/or transient overvoltages. Often, it is these infrequent transient voltages that establish design constraints for the transformer's insulation system. These constraints often have far reaching effects on the overall equipment design. The transformer must be configured to withstand any abnormal voltages covered in the design specification and realistically expected in service. Often, these constraints have great impact on other design issues and, as such, have significant effect on the overall transformer cost, performance, and configuration. In recent years, engineers have explored the adverse effect of transient voltages on the reliability of transformers (Kogan et al., 1988; Working group 05, 1983; Kogan et al., 1990), and found it to be a major cause of transformer failure.

Sources and Types of Transient Voltage Excitation

The voltages subjected to a transformer's terminals can be broadly classed as steady state and "transient." Normally, the "transient" voltages a transformer experiences are commonly referred to as dynamic, transient, and very fast transients.

The majority of voltages a transformer experiences during its operational life are steady state, e.g., the voltage is within ±10% of nominal and the frequency is within 1% of rated. As power quality issues grow, the effect of harmonic voltages and currents on performance becoming more of an issue. These harmonics are effectively reduced magnitude, steady state voltages and currents at harmonic frequencies (say 2nd to

the 50th). These are addressed in great detail in reference IEEE Std. 519 (1999). Strictly speaking, all other voltage excitation are transients, e.g., dynamic, transient, and very fast transient voltages.

Dynamic voltages refer to relatively low frequency (60 to 1500 Hz), damped oscillatory voltage. Magnitudes routinely observed are from 1 to 3 times the systems peak nominal voltage. Transient voltage refers to the class of excitation caused by events like lightning surges, switching events, and line faults causing voltages of the chopped wave form (Degeneff et al., 1982). Normally, these are aperiodic waves. Occasionally, the current chopping of a vacuum breakers will produce transient periodic excitation in the 10 to 200 kHz range (Greenwood, 1994). The term *very fast transient* encompasses voltage excitation with rise times in the range of 50–100 ns and frequencies from 0.5 to 30 MHz. These types of voltages are encountered in gas-insulated stations. The voltages produced within the transformer winding structure by the system it is a part of, must be addressed and understood if a successful insulation design is to be achieved (Narang et al., 1998). Since transient voltages affect system reliability, and that, in turn, system safety and economics, a full understanding of the transient characteristic of a transformer is warranted.

Addressing Transient Voltages Performance

Addressing the issue of transient voltage performance can be divided into three activities: recognition, prediction, and mitigation. By 1950 over 1000 papers had been written to address these issues (Abetti, 1959; 1962; 1964). The first is to appreciate that transient voltage excitation can produce equipment responses different than one would anticipate at first glance. For example, the addition of more insulation around a conductor may in fact make the transient voltage distribution worse and the insulation integrity of the design weaker. Another example would be the internal voltage amplification a transformer experiences when excited near its resonant frequency. The transient voltage distribution is a function of the applied voltage excitation and the shape and material content of the winding being excited. The capability of the winding to withstand the transient voltage is a function of the specific winding shape, the materials voltage versus time characteristic, the past history of the structure, and the statistical nature of the structure's voltage withstand characteristic.

The second activity is to assess or predict the transient voltage within the coil or winding. Today this is generally accomplished using a lumped parameter model of the winding structure and some form of computer solution method that allows the internal transient response of the winding to be computed. Once this voltage distribution is known, its effect on the insulation structure can be computed with a two- or three-dimensional FEM. The resultant voltages, stresses, and creeps are examined in light of the known material and geometrical capability of the system in light of desired performance margins.

The third activity is to establish a transformer structure or configuration that, in light of the anticipated transient voltage excitation and material capability, variability, and statistics nature, will provide acceptable performance margins. Occasionally, nonlinear resistors are used as part of the insulation system to achieve a cost-effective, reliable insulation structure. Additionally, means of limiting the transient excitation include the use of nonlinear resistors, capacitors, and snubbers.

Complex Issue to Predict

The accurate prediction of the transient voltage response of coils and winding has been of interest for almost 100 years. The problem is complex for several reasons. The form of excitation varies greatly. Most large power transformers are unique designs, and as such, each transformer's transient response characteristic is unique. Each has its own impedance versus frequency characteristic. As such, the transient response characteristic of each transformer is different. Generally, the problem is addressed by building a large lumped parameter model of inductances, capacitances, and resistances. Constructing the lumped parameter model is challenging. The resultant mathematical model is ill-conditioned, e.g., the resultant differential equation is difficult to solve. The following sections outline how these challenges are currently addressed.

It should be emphasized that the voltage distribution within the winding is only the first component of the insulation design process. The spatial distribution of the voltages within the winding must be determined and finally the ability of the winding configuration in view of its voltage versus time characteristic must be assessed.

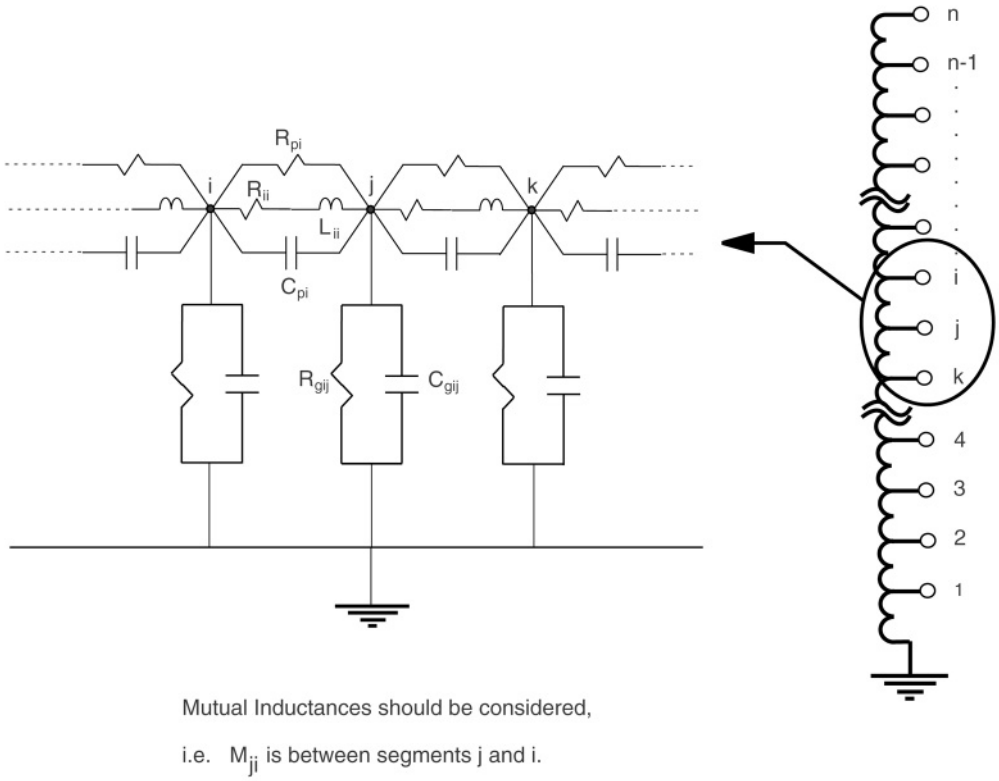

FIGURE 10.34 Sample of section used to model example coil

Surges in Windings

Response of a Simple Coil

Transformer windings are complex structures of wire and insulation. This is the result of many contradictory requirements levied during the design process. In an effort to introduce the basic concepts of transient response, a very simple disk coil was modeled and the internal transient response computed. The coil consisted of 100 identical continuous disk sections of 24 turns each. The inside radius of the coil is 12.55 in., the space between each disk coil is 0.220 in., and the coil was assumed to be in air with no iron core. Each turn was made of copper 0.305 in. in height, 0.1892 in. in the radial direction, with 0.0204 in. of insulation between the turns. For this example, the coil was subjected to a full wave with a 1.0 per-unit voltage. Figure 10.34 provides a sketch of the coil and the node numbers associated with the calculation. For this example, the coil has been subdivided into 50 equal subdivisions with each subdivision a section pair. Figure 10.35 contains the response of the winding as a function of time for the first 200 μsec. It should be clear that the response is complex and a function of both the applied excitation voltage and the characteristics of the coil itself.

Initial Voltage Distribution

If the voltage distribution along the helical shown in Fig. 10.35 is examined at times very close to time zero, it is observed that the voltage distribution is highly nonuniform. For the first few tenths of a microsecond, the distribution is dominated exclusively by the capacitive structure of the coil. This distribution is often referred to as the initial (or short-time) distribution and it is generally highly nonuniform. This initial distribution is shown in Fig. 10.36. For example, examining the voltage gradient over the first 10% of the winding, one sees that the voltage is 82% rather that the anticipated 10% or a rather large enhancement or gradient in some portions of the winding.

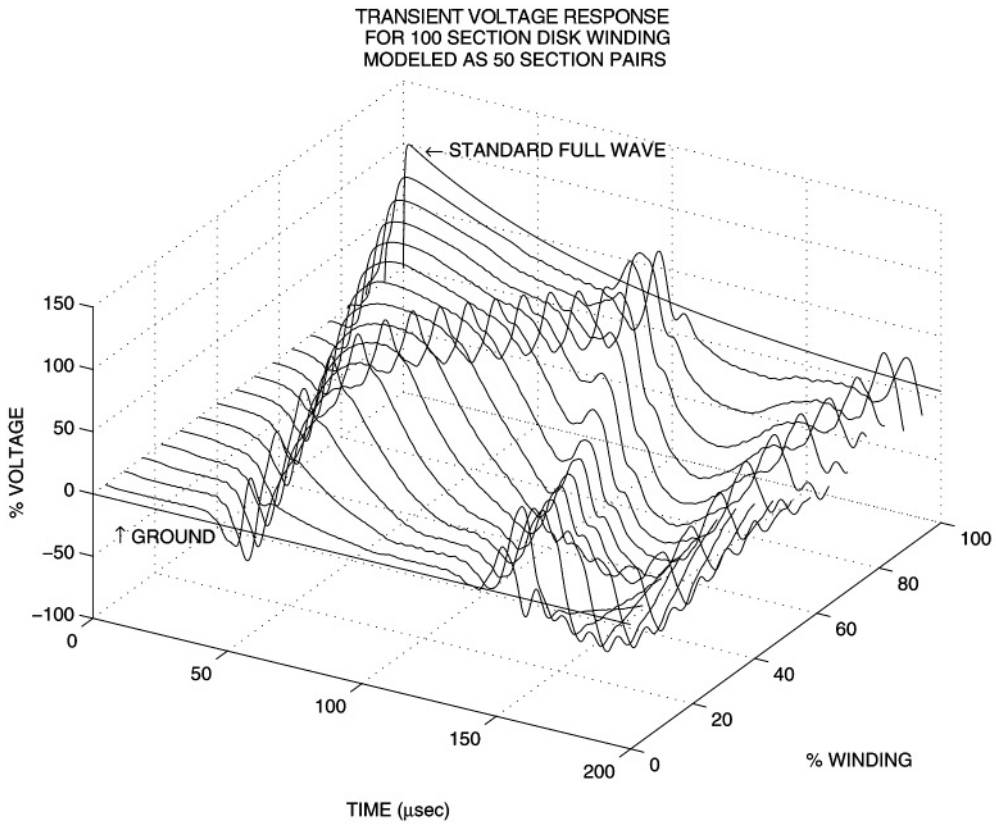

FIGURE 10.35 Voltage versus time for helical winding

The initial distribution shown in Fig. 10.36 is based on the assumption that the coil knows how it is connected, i.e., it requires some current to flow in the winding and this requires some few tens of a ηsecond. The initial distribution can be determined by evaluating the voltage distribution for the windings capacitive network and ignoring both the inductive and resistive components of the transformer. This discussion is applicable for times greater than approximately 0.25 μsec. This is the start of the transient response for the winding.

For times smaller than 0.25 μsec, the distribution is still dictated by capacitance, but the transformers capacitive network is unaware that it is connected. This is addressed in the chapter on very fast transients and in Narang et al. (1998).

Steady-State Voltage Distribution

The steady-state voltage distribution depends primarily on the inductance and losses of the winding's structure. This distribution, referred to by Abetti (1960) as the pseudo-final, is dominated primarily by the self and mutual inductance of the windings and the manner in which the winding is connected. This steady-state voltage distribution is very near (but not identical) to the turns ratio. For the simple winding shown in Fig. 10.34, the distribution is known by inspection and shown in Fig. 10.36, but for more complex windings it can be determined by finding the voltage distribution of the inductive network and ignoring the effect of winding capacitances.

Transient Voltage Distribution

Figure 10.35 shows the transient response for this simple coil. The transient response of the coil is the voltage the coil experiences as the coil transitions between the initial voltage distribution and the steady state distribution. It is the very same idea as pulling a rubber-band away from its stretched (but steady

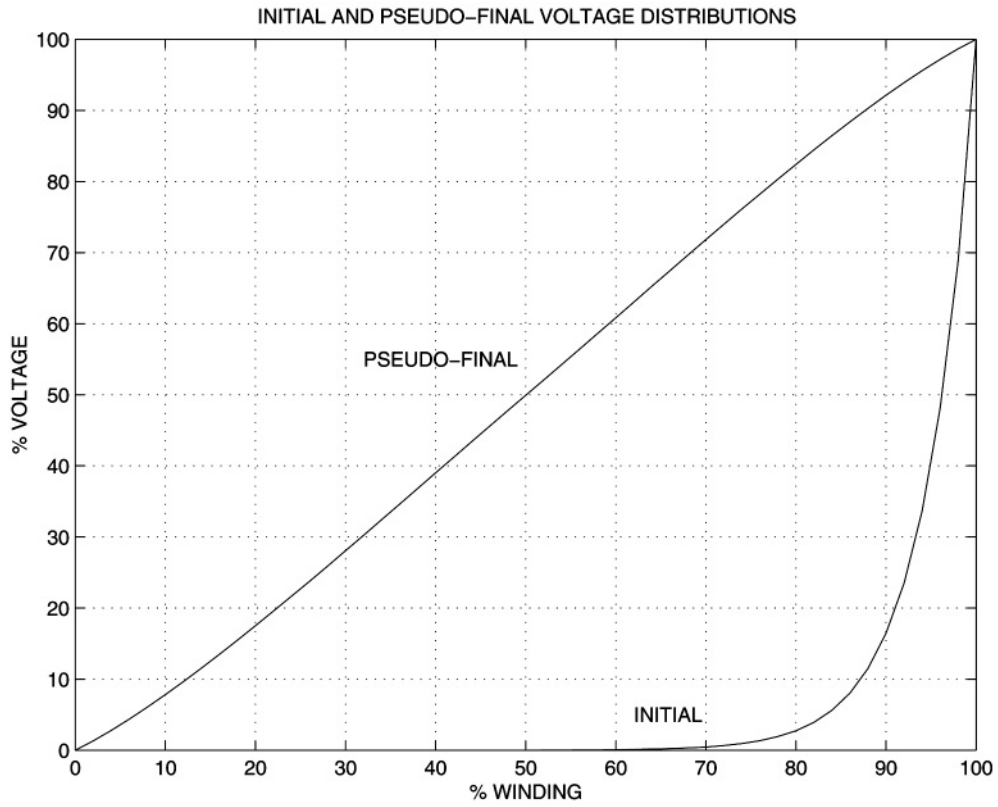

FIGURE 10.36 Initial and pseudo-final voltage distribution

state position) and then letting it go and monitoring its movement in space and time. What is of considerable importance is the magnitude and duration of these transient voltages and the ability of the transformer's insulation structure to consistently survive these voltages.

The coil shown in Fig. 10.34 is a very simple structure. The challenge facing transformer design engineers since the early 1900s has been to determine what this voltage distribution was for a complex winding structure of a commercial transformer design.

Determining Transient Response

History

Considerable research has been devoted to determining the transformer's internal transient voltage distribution. These attempts started at the beginning of the 1900s and have continued at a steady pace for almost 100 years (Abetti, 1959; 1962; 1964). The earliest attempts at using a lumped parameter network to model the transient response was in 1915. Until the early 1960s, these efforts were of limited success due to computational limitations encountered when solving large numbers of coupled stiff differential equations. During this period, the problem was attached in the time domain using either a standing wave approach or the traveling wave method. The problem was also explored in the frequency domain and the resultant individual results combined to form the needed response in the time domain. Abetti introduced the idea of a scale model, or analog for each new design. Then, in the 1960s, with the introduction of the high-speed digital computer, major improvements in computational algorithms, detail, accuracy, and speed were obtained.

In 1956, Rouxel and Waldvogel used an analog computer to calculate the internal voltages in the transformer by solving a system of linear differential equations with constant coefficients resulting from

a uniform, lossless, and linear lumped parameter model of the winding where mutual and self inductances were calculated assuming an air core. Later, McWhirter, Fahrnkopf, and Steel (1956) developed a method of determining impulse voltage stresses within the transformer windings through the use of the digital and analog computer applicable to some extent for nonuniform windings. But it was not until 1958 that Dent, Hartill, and Miles recognized the limitations of the analog models and developed a digital computer model in which any degree of nonuniformity in the windings could be introduced and any form of applied input voltage applied. During the mid-1970s, efforts at General Electric (White, 1977; Degeneff et al., 1980; White 1977) focused on building a program to compute transients for core form winding of completely general design. By the end of the 1970s, an adequate linear lossless model of the transformer was available to the industry. However, adequate representation of the effect of the nonlinear core and losses was not available. Additionally, the transformer models used in insulation design studies had little relationship with lumped parameter transformer models used for system studies.

Wilcox improved the transformer model by including core losses in a linear-frequency domain model where self and mutual impedance between winding sections were calculated considering a grain-oriented conductive core with permeability μ_r (1992). In this work, Wilcox modeled the skin effect, the losses associated with the magnetizing impedance, and a loss mechanism associated with the effect of the flux radial component on the transformer core during short circuit conditions. Wilcox applied this modified modal theory to model the internal voltage response on practical transformers. Vakilian and Degeneff (1993) modified White's inductance model (1977) to include the core's saturable characteristics and established a system of O.D.E.s for the linearized lumped parameter LRC network, then used Gear's method to solve for the internal voltage response in time. During the same year, Gutierrez and Degeneff (1993; 1994) presented a transformer model reduction technique as an effort to reduce the computational time required by linear and nonlinear detailed transformer models and to make these models small enough to fit into EMTP. In 1994, de Leon and Semlyen presented a nonlinear three phase transformer model including core and winding losses. This was the first attempt to combine frequency dependency and nonlinearity in a detailed transformer model. The authors used the principle of duality to extend their model to three phase transformers.

Lumped Parameter Model

A device's transient response is a result of the flow of energy between the distributed electrostatic and electromagnetic characteristics of the device. For all practical transformer winding structures, this interaction is quite complex and can only be realistically investigated by constructing a detailed lumped parameter model of the winding structure and then carrying out a numerical solution for the transient voltage response. The most common approach is to subdivide the winding into a number of segments (or groups of turns). The method of subdividing the winding can be complex and, if not addressed carefully, affects the accuracy of the resultant model. The resultant lumped parameter model is composed of inductances, capacitance, and losses. Starting with these inductances, capacitances, and resistive elements, equations reflecting the transformer's transient response can be written in numerous forms. Two of the most common are the basic admittance formulation of the differential equation and the state variable formulation. The admittance formulation is given by Degeneff, 1977:

$$\left[I(s)\right]=\left[\frac{1}{s}\left[\Gamma_n\right]+\left[G\right]+s\left[C\right]\right]\left[E(s)\right] \tag{10.105}$$

The general state-variable formulation is given by Vakilian (1993) describing the transformer's lumped parameter network at time t:

$$\begin{bmatrix}\left[L\right] & 0 & 0\\ 0 & \left[C\right] & 0\\ 0 & 0 & \left[U\right]\end{bmatrix}\begin{bmatrix}\left[di_e/dt\right]\\ \left[de_n/dt\right]\\ \left[df_e/dt\right]\end{bmatrix}=\begin{bmatrix}-\left[r\right] & \left[T\right]^t\\ -\left[T\right] & -\left[G\right]\\ -\left[r\right] & \left[T\right]^t\end{bmatrix}\begin{bmatrix}\left[i_e\right]\\ \left[e_n\right]\end{bmatrix}-\begin{bmatrix}0\\ \left[I_s\right]\\ 0\end{bmatrix} \tag{10.106}$$

where the variables in Eqs. (10.105) and (10.106)

$[i_e]$ = Vector of currents in the winding segments
$[e_n]$ = Model's nodal voltages vector
$[f_e]$ = Windings' flux-linkages vector
$[r]$ = Diagonal matrix of windings series resistance
$[T]$ = Windings connection matrix
$[T]^t$ = Transpose of [T]
$[C]$ = Nodal capacitance matrix
$[U]$ = Unity matrix
$[I(s)]$ = Laplace transform of current sources
$[E(s)]$ = Laplace transform of nodal voltages
$[\Gamma_n]$ = Inverse Nodal Inductance Matrix = $[T][L]^{-1}[T]^t$
$[L]$ = Matrix of self and mutual inductances
$[G]$ = Conductance matrix, for resistors connected between nodes
$[I_s]$ = Vector of current sources

In a liner representation of an iron core transformer, the permeability of the core is assumed constant regardless of the magnitude of the core flux. This assumption allows the inductance model to remain constant for the entire computation. Equations (10.105) and (10.106) are based on the assumption that the transformer core is linear and the various elements in the model are not frequency dependent. Work in the last decade has addressed both the nonlinear characteristics of the core and the frequency dependent properties of the materials. Much progress has been made, but their inclusion adds considerably to the model's complexity and the computational difficulty. If the core is nonlinear, the permeability changes as a function of the material properties, past history, and instantaneous flux magnitude. Therefore, the associate inductance model is time dependent. The basic strategy for solving the transient response of the nonlinear model in Eq. (10.105) or (10.106) is to linearize the transformer's nonlinear magnetic characteristics at an instant of time based on the flux in the core at that instant.

Two other model formulations should be mentioned. de Leon addressed the transient problem using a model based on the idea of duality (1994). The finite element method has found wide acceptance in solving for electrostatic and electromagnetic field distributions. In some instances it is a very useful in solving for the transient distribution in coils and windings of complex shape.

Frequency Domain Solution

A set of linear differential equations representing the transient response of the transformer can be solved either in the time domain or in the frequency domain. If the model is linear, the resultant solution will be the same for either method. The frequency domain solution requires that the components of the input waveform at each frequency be determined. These individual sinusoidal waves are then applied individually to the transformer and the resultant voltage response throughout the winding is determined. Finally, the total response in the time domain is determined by summing the component responses at each frequency applying superposition. An advantage of this method is that it allows the recognition of frequency-dependent losses to be addressed easily. Disadvantages of this method are that it does not allow the modeling of time-dependent switches, nonlinear resistors like ZnO, or the recognition of nonlinear magnetic core characteristics.

Solution in the Time Domain

The following briefly discusses the solution of Eqs. (10.105) and (10.106). There are numerous methods to solve Eq. (10.105) but it has been found that when solving the stiff differential equation model of a transformer, a generalization of Dommel's method (Dommel, 1969; Degeneff, 1977) works very well. A lossless lumped parameter transformer model containing n nodes has approximately $n(n+1)/2$ inductors and $3n$ capacitors. Since the total number of inductors far exceeds the number of capacitors in the network, this methodology reduces storage and computational time by representing each capacitor as an inductor in parallel with a current source. The following system of equations results:

$$\left[\hat{Y}\right]\left[F(t)\right]=\left[I(t)\right]-\left[H(t)\right] \tag{10.107}$$

where

$[F(t)]$ = nodal integral of the voltage vector
$[I(t)]$ = nodal injected current vector
$[H(t)]$ = Past History current vector

and

$$\left[\hat{Y}\right]=\frac{4}{\Delta t^2}\left[C\right]+\frac{2}{\Delta t}\left[G\right]+\left[\Gamma_n\right] \tag{10.108}$$

The lumped parameter model is composed of capacitances, inductances, and losses computed from the winding geometry, permittivity of the insulation, iron core permeability, and the total number of sections into which the winding is divided. Then the matrix $[\hat{Y}]$ is computed using the integration step size, Δt. At every time step, the above system of equations is solved for the unknowns in the integral of the voltage vector. The unknown nodal voltages, $[E(t)]$, are calculated by taking the derivative of $[F(t)]$. Δt is selected based on the detail of the model and the highest resonant frequency of interest. Normally, Δt is smaller that one-tenth the period of this frequency.

The state variable formulation shown as Eq. (10.106) can be solved using differential equation routines available in IMSL or others based on the work of Gear and Adams (1991). The advantage of these routines is that they are specifically written with the solution of stiff systems of equations in mind. The disadvantage of these routines is that they consume considerable time during the solution.

Accuracy vs. Complexity

Every model of a physical system is an approximation. Even the simplest transformer has a complex winding and core structure and as such possesses an infinite number of resonant frequencies. A lumped parameter model, or for that matter, any model is at best an approximation of the actual device of interest. A lumped parameter model containing a structure of inductances, capacitances, and resistances will produce a resonance frequency characteristic that contains the same number of resonant frequencies as nodes in the model. The transient behavior of a linear circuit (the lumped parameter model) is determined by the location of the poles and zeros of its terminal impedance characteristic. It follows then that a detailed transformer model must possess two independent characteristics to faithfully reproduce the transient behavior of the actual equipment. First, it must include accurate values of R, L, and C, reflecting the transformer geometry. This fact is well appreciated and documented. Second, the transformer must be modeled with sufficient detail to address the bandwidth of the applied waveshape. In a valid model, the highest frequency of interest would have a period at least ten times larger than the travel time of the largest winding segment in the model. If this second characteristic is overlooked, a model can produce results that appear valid, but may have little physical basis. A final issue is the manner in which the transformer structure is subdivided. If care is not taken, the manner in which the model is constructed will itself introduce significant errors and the computation will be mathematically robust but an inaccurate approximation of the physically reality.

Resonant Frequency Characteristic

Definitions

The steady state and transient behavior of any circuit, for any applied voltage, is established by the location of the poles and zeros of the impedance function of the lumped parameter model in the complex plane. The zeros of the terminal impedance function coincide with the natural frequencies of the model, by definition. McNutt (1974) defines terminal resonance as the terminal current maximum and a terminal

impedance minimum. In a physical system there are an infinite number of resonances. In a lumped parameter model of a system, there are as many resonances as nodes in the model (or the order of the system). Terminal resonance is also referred to as series resonance (Abetti, 1959; 1954). Terminal anti-resonance is defined as a terminal current minimum and a terminal impedance maximum (McNutt et al., 1974). This is also referred to as parallel resonance (Abetti, 1959; 1954). McNutt defines internal resonance as an internal voltage maximum and internal antiresonance as an internal voltage minimum.

Impedance vs. Frequency

The terminal resonances for a system can be determined by taking the square root of the eigenvalues of the system matrix, [A], shown in the state variable representation for the system shown as:

$$\begin{aligned}\left[\dot{q}\right] &= \left[A\right]\left[q\right] + \left[B\right]\left[u\right] \\ \left[y\right] &= \left[C\right]\left[q\right] + \left[D\right]\left[u\right]\end{aligned} \tag{10.109}$$

where

$[A]$ = State Matrix
$[B]$ = Input Matrix
$[C]$ = Output Matrix
$[D]$ = Direct Transmission Matrix
$[q]$ = Vector of state variables for system
$[\dot{q}]$ = First derivative of [q]
$[u]$ = Vector of input variables
$[y]$ = Vector of output variables

The impedance versus frequency characteristic requires a little more effort. In light of the previous definitions, terminal resonance may be defined as occurring when the reactive component of the terminal impedance is zero. Equivalently, terminal resonance occurs when the imaginary component of the quotient of the terminal voltage divided by the injected terminal current is zero. Recalling that in the Laplace domain, that s is equivalent to $j\omega$ with a system containing n nodes with the excited terminal code j, one can rewrite Eq. (10.105) to obtain:

$$\begin{bmatrix} e_1(s) \\ e_2(s) \\ - \\ e_j(s) \\ - \\ e_n(s) \end{bmatrix} = \begin{bmatrix} Z_{1j}(s) \\ Z_{2j}(s) \\ - \\ Z_{jj}(s) \\ - \\ Z_{nj}(s) \end{bmatrix} \left[i_j(s) \right] \tag{10.110}$$

The voltage at the primary (node j) is in operation form. Rearranging the terminal impedance is given by:

$$Z_t(\omega) = Z_{jj}(j\omega) = Z_{jj}(s) = \frac{e_j(s)}{i_j(s)} \tag{10.111}$$

In these equations the unknown quantities are the voltage vector and the frequency. It is a simple matter to assume a frequency and solve for the corresponding voltage vector. Solving Eq. (10.111) over a range of frequencies results in the well-known impedance versus frequency plot. Figure 10.37 contains the impedance versus frequency for the example used in Figs. 10.34 and 10.35.

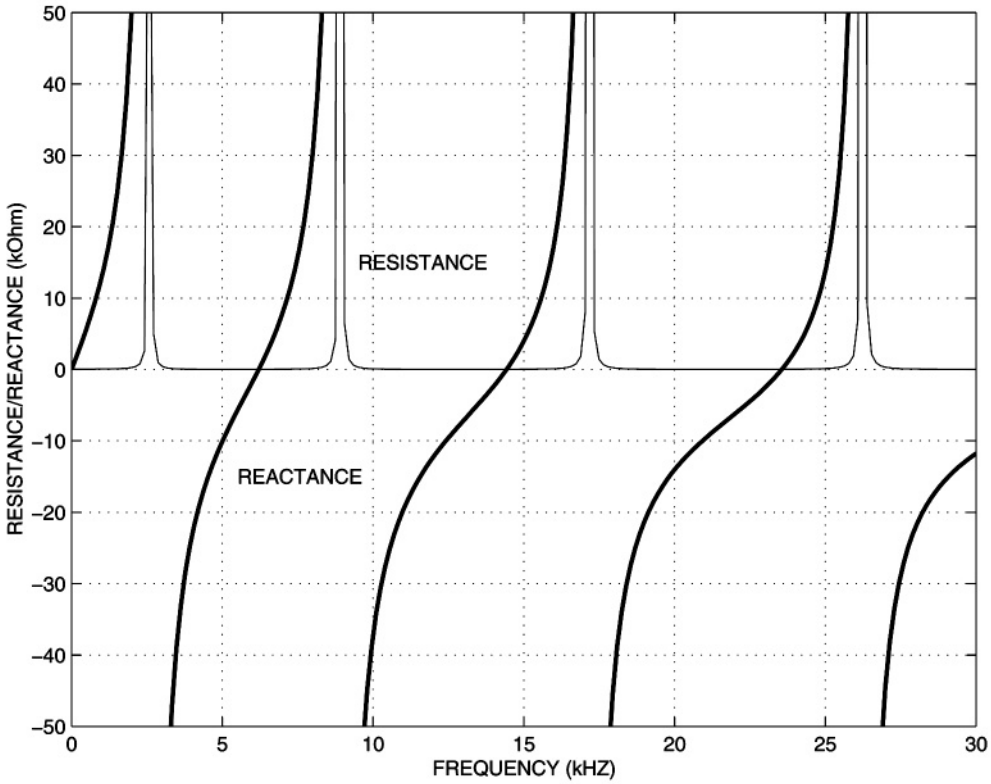

FIGURE 10.37 Terminal impedance for a helical winding

Amplification Factor

The amplification factor or gain function is defined as:

$$\left[N_{lm,j}\right] = \frac{\textit{Voltage between points } l \textit{ and } m \textit{ at frequency } \omega}{\textit{Voltage applied at input node } j \textit{ at frequency } \omega} \tag{10.112}$$

Degeneff (1977) shows that this results in:

$$N_{lm,j} = \frac{Z_{l1}(j\omega) - Z_{mj}(j\omega)}{Z_{jj}(j\omega)} \tag{10.113}$$

It is a simple matter to assume a frequency and solve for the corresponding voltage versus frequency vector. If one is interested in the voltage distribution within a coil at one of the resonant frequencies, this can be found from the eigenvector of the coil at the frequency of interest. If one is interested in the distribution at any other frequency, Eq. (10.113) can be utilized. This is shown in Fig. 10.38.

Inductance Model

Definition of Inductance

Inductance is defined as:

$$L = \frac{d\lambda}{dI} \tag{10.114}$$

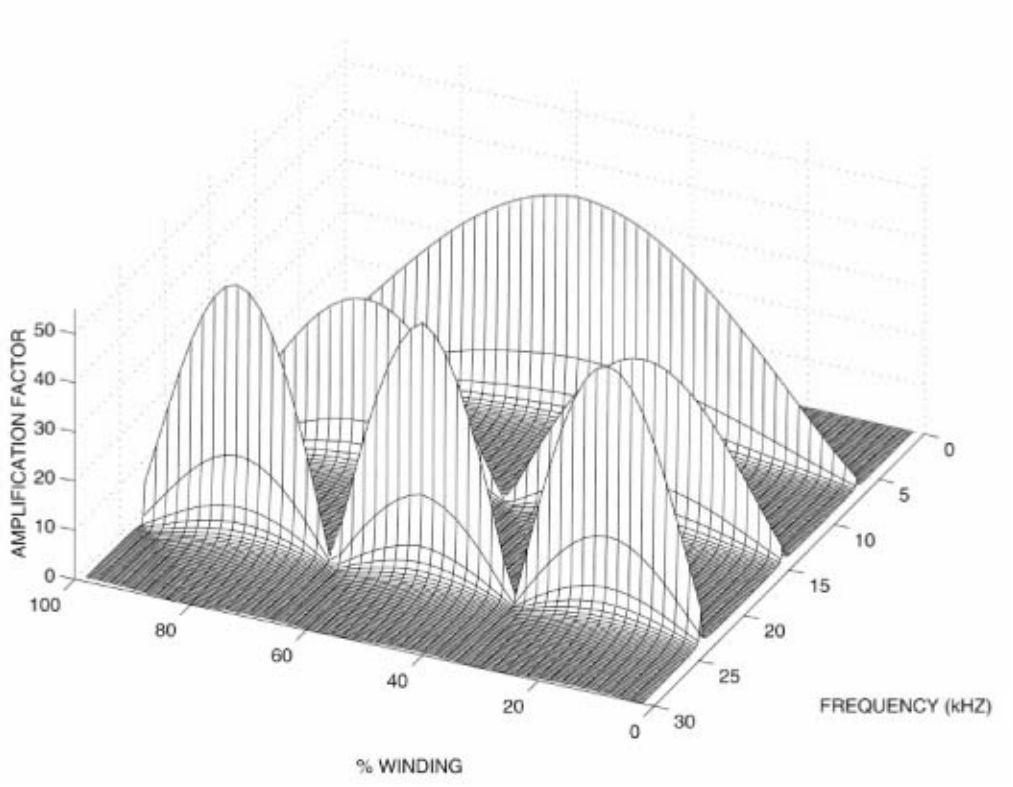

FIGURE 10.38 Amplification factor at 5 from 0 to 30kHz

and if the system is linear:

$$L = \frac{\lambda}{I} \tag{10.115}$$

where

L = inductance, Henrys
λ = flux linkage caused by current I, Weber turns
I = current producing flux linkages, Amperes
$d\lambda$ = first derivative of λ
dI = first derivative of I

L is referred to as self inductance if the current producing the flux is the same current being linked. L is referred to as mutual incidence if the current producing the flux is other than the current being linked (MIT, 1943). Grover (1962) published an extensive work providing expressions to compute the self and mutual inductance in air for a large number of practical conductor and winding shapes.

One of the most difficult phenomena to model is the magnetic flux interaction involving the different winding sections and the iron core. Historically this phenomenon has been modeled by dividing the flux in two components: the common and leakage flux. The common flux dominates when the transformer behavior is studied under open circuit conditions and the leakage flux dominates the transient response when the winding is shorted or loaded heavily. Developing a transformer model capable of representing the magnetic flux behavior for all conditions the transformer will see in factory test and in service requires the accurate calculation of the self and mutual inductances.

Transformer Inductance Model

Until the introduction of the computer there was a lack of practical analytical formulae to compute the self and mutual inductances of coils with an iron core. Rabins (1956) developed expressions to calculate self and mutual inductances for a coil on an iron core based on the assumption of a round core leg and infinite core yokes both of infinite permeability. Fergestad and Heriksen improved Rabins' inductance model in 1974 by assuming an infinite permeable core except for the core leg. In their approach, a set of state variable equations was derived from the classic lumped parameter model of the winding.

White (1977; 1978) derived an expression to calculate the self and mutual inductances in the presence of an iron core with finite permeability under the assumption of an infinitely long iron core. White's inductance model had the advantage that the open circuit inductance matrix could be inverted (White, 1978). White derived an expression for the self and mutual inductance between sections of a transformer winding by solving a two-dimensional problem in cylindrical coordinates for the magnetic vector potential assuming a nonconductive and infinitely-long open core. He assumed that the leakage inductance of an open-core configuration is the same as the closed core.

Starting from the definition of the magnetic vector potential $\vec{B} = \nabla \times \vec{A}$ and $\nabla \cdot \vec{A} = 0$ and using Ampere's law in differential form, $\vec{J}_f = \nabla \times \vec{H}$, White solved the following equation:

$$\nabla^2 \vec{A}(r,z) = -\mu_o \vec{J}(r,z) \tag{10.116}$$

The solution broke into two parts: the air core solution and the change in the solution due to the insertion of the iron core as shown in the following equations:

$$\vec{A}(r,z) = \begin{cases} \vec{A}_o(r,z) + \vec{A}_1(r,z), & 0 \le r \le R_c \\ \vec{A}_o(r,z) + \vec{A}_2(r,z), & r > R_c \end{cases}$$

$\vec{A}_0(r, z)$ is the solution when the core is present and $\vec{A}_1(r, z)$ and $\vec{A}_2(r, z)$ are the solutions when the iron core is added. Applying Fourier series to Eq. (10.116), the solution for $\vec{A}_0(r, z)$ was found first and then $\vec{A}_2(r, z)$.

Knowing the magnetic vector potential allows the flux linking a filamentary turn at (r, z) to be determined by recalling $\phi(r, z) = \oint \vec{A}(r, z) \cdot \vec{dl}$. The flux for the filamentary turn is given by:

$$\phi(r,z) = 2\pi r\left\{\vec{A}_o(r,z) + \vec{A}_2(r,z)\right\} = \phi_o(r,z) + 2\pi r \vec{A}_2(r,z) \tag{10.117}$$

The flux in air, $\phi_o(r, z)$, can be obtained from known formulae for filaments in air (Grover, 1962); therefore, it is only necessary to obtain the change in the flux linking the filamentary turn due to the iron core. If the mutual inductance, L_{ij} between two coil sections is going to be calculated, then the average flux linking section i needs to be calculated. This average flux is given by

$$\phi_{ave} = \frac{\int_{R_i}^{\bar{R}_i} \int_{Z_i}^{\bar{Z}_i} \phi(r,z)\, dz\, dr}{H_i\left(R_i - \bar{R}_i\right)} \tag{10.118}$$

Knowing the average flux, the mutual inductance can be calculated using the following expression:

$$L_{ij} = \frac{N_i N_{j\phi ave}}{I_j} \tag{10.119}$$

White's final expression for the mutual inductance between two coil segments is:

$$L_{ij} = L_{ijo} + 2N_i N_j \left(1-\nu_r\right)\mu_o R_c \int_0^{\infty} \frac{I_0\left(\omega R_c\right) I_1\left(\omega R_c\right) F\left(\omega\right)}{\nu_r + \left(1-\nu_r\right)\omega R_c I_1\left(\omega R_c\right) K_0\left(\omega R_c\right)} d\omega \tag{10.120}$$

where

$$F\left(\omega\right) = \frac{1}{\omega}\left[\frac{1}{\omega\left(\overline{R}_i - R_i\right)}\int_{\omega R_i}^{\omega \overline{R}_i} xK_1\left(x\right)dx\right]\frac{2}{\omega H_i}\sin\left(\frac{\omega H_i}{2}\right)$$
$$\left[\frac{1}{\omega\left(\overline{R}_j - R_j\right)}\int_{\omega R_j}^{\omega \overline{R}_j} xK_1\left(x\right)dx\right]\frac{2}{\omega H_j}\sin\left(\frac{\omega H_j}{2}\right)\cos\left(\omega d_{ij}\right) \tag{10.121}$$

L_{ijo} is the air core inductance. $\nu_r = \frac{1}{\mu_r}$ is the relative reluctivity. $I_0(\omega R_c)$, $I_1(\omega R_c)$, $K_0(\omega R_c)$, and $K_1(\omega R_c)$ are modified Bessel functions of first and second kind.

Inductance Model Validity

The ability of the inductance model to accurately represent the magnetic characteristic of the transformer can be assessed by the accuracy with which it reproduces the transformer electrical characteristics, e.g., the short circuit and open circuit inductance, and the pseudo-final (turns ratio) voltage distribution. The short circuit and open circuit inductance of a transformer can be determined by several methods, but the simplest is to obtain the inverse of the sum of all the elements in the inverse nodal inductance matrix, Γ_n. This has been verified (Degeneff, 1978; Degeneff and Kennedy, 1975). The pseudo-final voltage distribution is defined in (Abetti, 1960). It is very nearly the turns ratio distribution and must match what ever voltage distribution the winding arrangement and number of turns dictates. An example of this is contained in (Degeneff and Kennedy, 1975).

Capacitance Model

Definition of Capacitance

Capacitance is defined as:

$$C = \frac{Q}{V} \tag{10.122}$$

where

C = capacitance between the two plates, farads
Q = charge on one of the capacitor plates, coulombs
L = voltage between the capacitor plates, volts

Snow (1954) published an extensive work on computing the capacitance for unusually shaped conductors. Practically, however, most lumped parameter models of windings are created by subdividing the winding into segments with small radial and axial dimensions and large radiuses where a simple parallel plate formula can be used (1980) to compute both the series and shunt capacitance for a segment. For example:

$$C = \epsilon_o \epsilon_r \frac{RadCir}{nD} \tag{10.123}$$

where

ϵ_o = permittivity of freespace, 8.9×10^{-12} coulomb/meters
ϵ_r = relative permittivity between turns
Rad = radial build of the segments turns, meters
Cir = circumference of the mean turn within segment, meters
n = number of turns with the segment
D = separation between turns, meter

In computing these capacitances, the relative permittivity, ϵ_r, of the materials must be recognized. This is a function of the material, moisture content, temperature, and effective age of the material. Clark and Von Hippel (1962; 1964) provide a large database of this type of information. Since most lumped parameter models assume the topology has circular symmetry, if the geometry is unusually complex it may be appropriate to model the system with a three-dimensional FEM. It should be emphasized that all of the above is based on the assumption that the capacitive structure of the transformer is frequency invariant. If the transient model is required to be valid over a very large bandwidth, then the frequency characteristic of dielectric structure must be taken into account.

Series and Shunt Capacitance

In order to construct a lumped parameter model, the transformer is subdivided into segments (or groups of turns). Each of these segments contains a beginning node and an exit node. Between these two nodes there will generally be associated a capacitance, traditionally called the series capacitance. These are the intrasection capacitances. In most cases they are computed using the simple parallel plate capacitance given in Eq. (10.123). An exception to this is the series capacitance of disk winding segments. Expressions for their series capacitance is given in the next section.

Additionally, each segment will have associated with it, capacitances between adjacent sections of turns or to a shield or earth. These are the intersection capacitances. These capacitances are generally referred to as shunt capacitances and are normally divided in half and connected to each end of the appropriate segments. This is an approximation, but if the winding is subdivided into relatively small segments, the approximation is acceptable and the error introduced by the model is small.

Equivalent Capacitance for Disk Windings

This section presents simplified expressions to compute the series capacitance for disk winding section pairs. Since most lumped parameter models are not turn-to-turn models, an electrostatic equivalent of the disk section is used for the series capacitance. It is well known that as the series capacitance of disk winding sections becomes larger with respect to the capacitances to ground, the initial distribution becomes more linear (straight line) and the transient response in general more benign. Therefore, since it is possible to arrange the turns within a disk section in many ways without affecting the section's inductance characteristic or the space or material it requires, the industry has offered many arrangements in an effort to increase this effective series capacitance.

The effective series capacitance of a disk winding is a capacitance, which when connected between the input and output of the disk winding section pair would store the same electrostatic energy the disk section pair would store (between all turns) if the voltage were distributed linearly within the section. This modeling strategy is discussed in detail by Scheich (1965) and Degeneff and Kennedy (1975). Figure 10.39 illustrates the cross-section of three common disk winding configurations. The series capacitance of the continuous disk is given by:

$$C_{continuous} = \frac{2}{3} C_s + \left[\frac{n-2}{n^2}\right] C_t \tag{10.124}$$

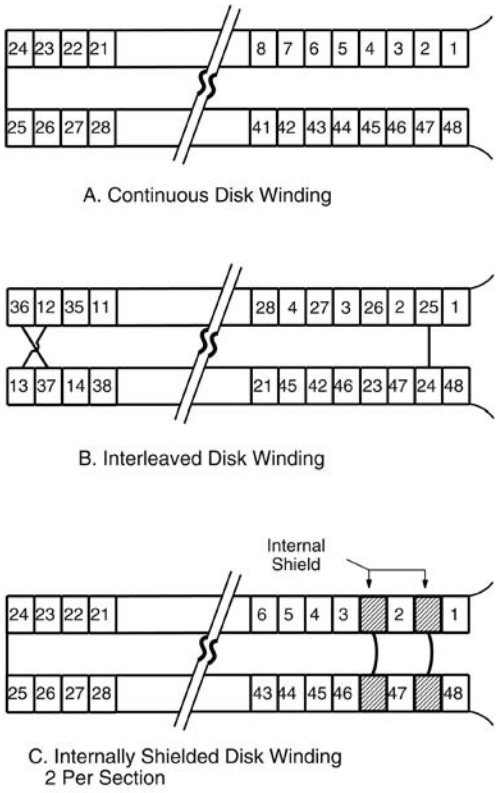

FIGURE 10.39 Common disk winding section pairs: A. Continuous; B. Interleaved; and C. Internal Shield.

The series capacitance of the interleaved disk section pair is given by:

$$C_{interleaved} = 1.128C_s + \left[\frac{n-4}{4}\right]C_t \tag{10.125}$$

The interleaved disk provides a greater series capacitance than the continuous disk but is more difficult to produce. A winding that has a larger series capacitance than the continuous disk but simpler to manufacture than the interleave is the internally shielded winding. Its series capacitance is given by:

$$C_{internal\ shield} = \frac{2}{3}C_s + \left[\frac{n-2-2n_s}{n^2}\right]C_t + 4C_{ts}\sum_{i=1}^{n_s}\left[\frac{n_i}{n}\right]^2 \tag{10.126}$$

where

C_s = Capacitance between sections
C_t = Capacitance between turns
C_{ts} = Capacitance between turn and internal shield
n = Turns in section pair
n_i = Location of shield within section
n_s = Internal shields within section pair

Selecting the disk winding section is often a compromise of electrical performance, economics, and manufacturing preference for a given firm.

Initial Voltage Distribution

The initial voltage distribution can be determined experimentally by applying a voltage wave with a fairly fast rise time (say 0.5 μsec) and measuring the normalized distribution within the winding structure an intermediate time (say 0.3 μsec). The initial distribution can be computed analytically by injecting a current into the excited node and determining the normalized voltage throughout the transformer winding structure. This computational method is outlined in detail by Degeneff and Kennedy (1975). If one is considering a single coil, it is common practice to determine the gradient of the transient voltage near the excited terminal (which is the most severe). This gradient is referred to as α and is found by (Greenwood, 1991):

$$\alpha = \sqrt{\frac{C_g}{C_s}} \tag{10.127}$$

where

α = winding gradient
C_g = capacitance to ground, farads
C_s = effective series capacitance, farads

For the coil shown in Fig. 10.36, the α is on the order of 12.

Loss Model

At steady state, losses are a costly and unwanted characteristic of physical systems. At high frequency, losses produce a beneficial effect in that they reduce the transient voltage response of the transformer by reducing the transient voltage oscillations. In general, the oscillations are underdamped. The effect of damping on the resonant frequency is to reduce the natural frequencies slightly. Losses within the transformer are a result of a number of sources, each source with a different characteristic.

Copper Losses

The losses caused by the current flowing in the winding conductors are referred to as series losses. Series losses are composed of three components: DC losses, skin effect, and proximity effect.

DC Resistance

The conductor's DC resistance is given by:

$$R_{dc} = \rho \frac{l}{A} \tag{10.128}$$

With:

ρ = conductor resistivity, ohm-m
l = length of conductor, m
A = conductor area, m^2

ρ is a function of the conductor material and its temperature.

Skin Effect

Lammeraner and Stafl (1966) give an expression for the skin effect in a rectangular conductor. The impedance per unit length of the conductor is given in by:

$$Z = \frac{k}{4h\sigma} \coth kb \quad \Omega/m \tag{10.129}$$

where

$$k = \frac{1+j}{a} \tag{10.130}$$

with

$$a = \sqrt{\frac{2}{\omega\sigma\mu}} \tag{10.131}$$

h = half the conductor height, m
b = half the conductor thickness, m
σ = conductivity of the conductor, S/m
μ = permeability of the material, H/m
ω = frequency, rad/s

Defining

$$\xi = b\sqrt{j\omega\sigma\mu} \tag{10.132}$$

and Eq. (10.129) is expressed as

$$Z_{skin} = R_{dc}\xi\coth\xi \quad \Omega/m \tag{10.133}$$

where R_{dc} is the DC resistance per unit length of the conductor. Equation (10.133) is used to calculate the impedance due to the skin effect as a function of frequency.

Proximity Effect

Proximity effect is the increase in losses in one conductor due to currents in other conductors produced by a redistribution of the current in the conductor of interest by the currents in the other conductors. A method of finding the proximity effect losses in the transformer winding consists of finding a mathematical expression for the impedance in terms of the flux cutting the conductors of an open winding section due to an external magnetic field. Since windings in large power transformers are mainly built using rectangular conductors, the problem reduces to the study of eddy current losses in a packet of laminations. Lammeraner and Stafl (1966) provide an expression for the flux as a function of frequency in a packet of laminations. It is given in the following equation:

$$\Phi = \frac{2al\mu}{1+j} H_o \tanh\left(1+j\right)\frac{b}{a} \tag{10.134}$$

where l is the conductor length, H_o is the rms value of the magnetic flux intensity, and the remaining variables are the same as defined in Eq. (10.131).

Assuming H_o in Eq. (10.134) represents the average value of the magnetic field intensity inside the conductive region represented by the winding section i and defining L_{ijo} as

$$L_{ijo} = N_i N_j \phi_{ijo} \tag{10.135}$$

where ϕ_{ijo} is the average flux cutting each conductor in section i due to the current I_j, and N is the number of turns in each section, the inductance L_{ij} as a function of frequency is:

$$L_{ij} = \frac{L_{ijo}}{\left(1+j\right)\frac{b}{a}} \tanh\left(1+j\right)\frac{b}{a} \quad \text{H} \tag{10.136}$$

The impedance Z_{proxij} is obtained by multiplying the inductance by the complex variable s. Using the same notation as in Eq. (10.133), the impedance of the conductor due to the proximity effect is given as

$$Z_{prox_{ij}} = s\frac{L_{ij_o}}{\xi} \tanh \xi \quad \Omega \tag{10.137}$$

Core Losses

The effect of eddy currents in the core have been represented in references (de Leon and Semlyen, 1994; Tarasiewicz et al., 1993; Avila-Rosales and Alvarado, 1982) by the well-tested formula:

$$Z = \frac{4N^2 A}{Id^2 \sigma} x \tanh x \tag{10.138}$$

where

$$x = \frac{d\sqrt{j\omega\mu\sigma}}{2} \tag{10.139}$$

and

l = Length of the core limb in meters (axial direction), m
d = Thickness of the lamination, m
μ = Permeability of the material, H/m
N = Number of turns in the coil
A = Total cross-sectional area of all laminations
ω = Frequency, rad/sec

This formula represents the equivalent impedance of a coil wound around a laminated iron core limb. The expression was derived by Avila-Rosales and Alvarado (1982) by solving Maxwell's equations assuming the electromagnetic field distribution is identical in all laminations and an axial component of the magnetic flux.

The total hysteresis loss in core volume, V, in which the flux density is uniform everywhere and varying cyclically at a frequency of ω, can be expressed as:

$$P_h = 2\pi\omega\eta V \beta_{max}^n \tag{10.140}$$

with

P_h = Total hysteresis loss in core
η = Constant a function of material
V = Core volume
β = Flux density
n = Exponent dependent upon material, 1.6–2.0
ω = Frequency, rad/sec

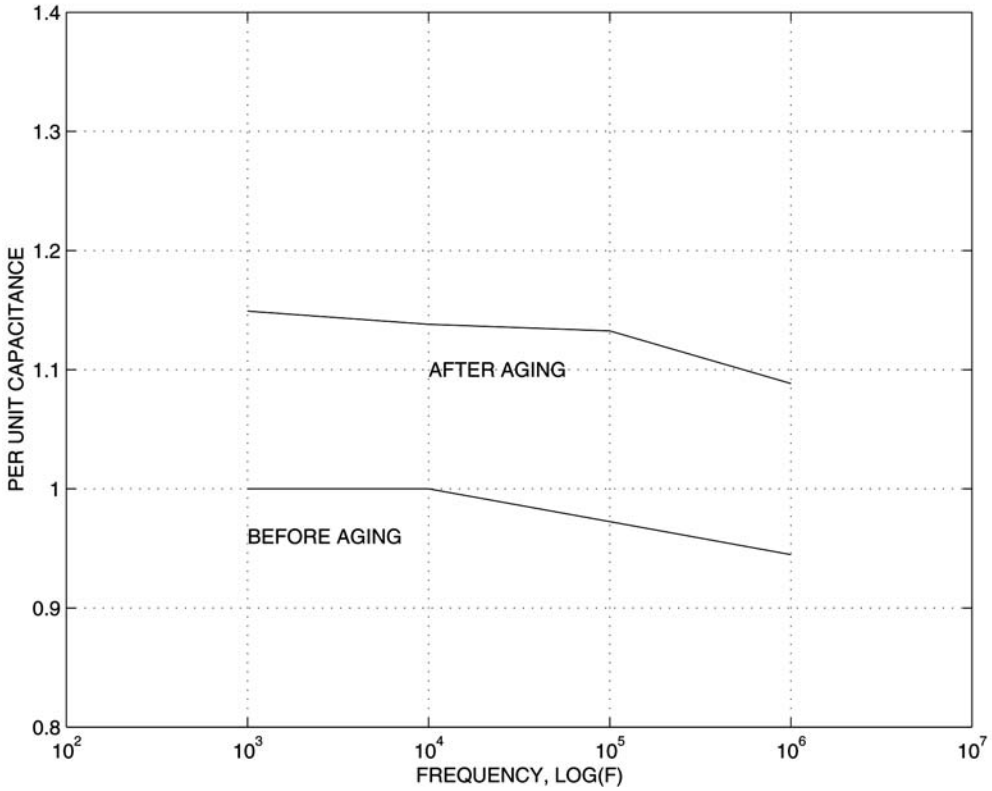

FIGURE 10.40 Oil-soaked paper capacitance and conductance as a function of frequency.

Dielectric Losses

The capacitive structure of a transformer has parallel losses associated with it. At low frequency, the effect of capacitance on the internal voltage distribution can be ignored. As such, the effect of the losses in the dielectric structure can be ignored. However, at higher frequencies the losses in the dielectric system can have a significant effect on the transient response. Batruni et al. (1996) explore the effect of dielectric losses on the impedance versus frequency characteristic of the materials in power transformers.

These losses are frequency dependent and are shown in Fig. 10.40.

Winding Construction Strategies

Design

The successful design of a commercial transformer requires the selection of a simple structure so that the core and coils are easy to manufacture. At the same time, the structure should be as compact as possible to reduce required materials, shipping concerns, and footprint. The form of construction should allow convenient removal of heat, sufficient mechanical strength to withstand forces generated during system faults, acceptable noise characteristics, and an electrical insulation system that meets the system steady state and transient requirements. There are two common transformer structures in use today. When the magnetic circuit is encircled by two or more windings of the primary and secondary, the transformer is referred to as a core-type transformer. When the primary and secondary windings are encircled by the magnetic material, the transformer is referred to as a shell-type transformer.

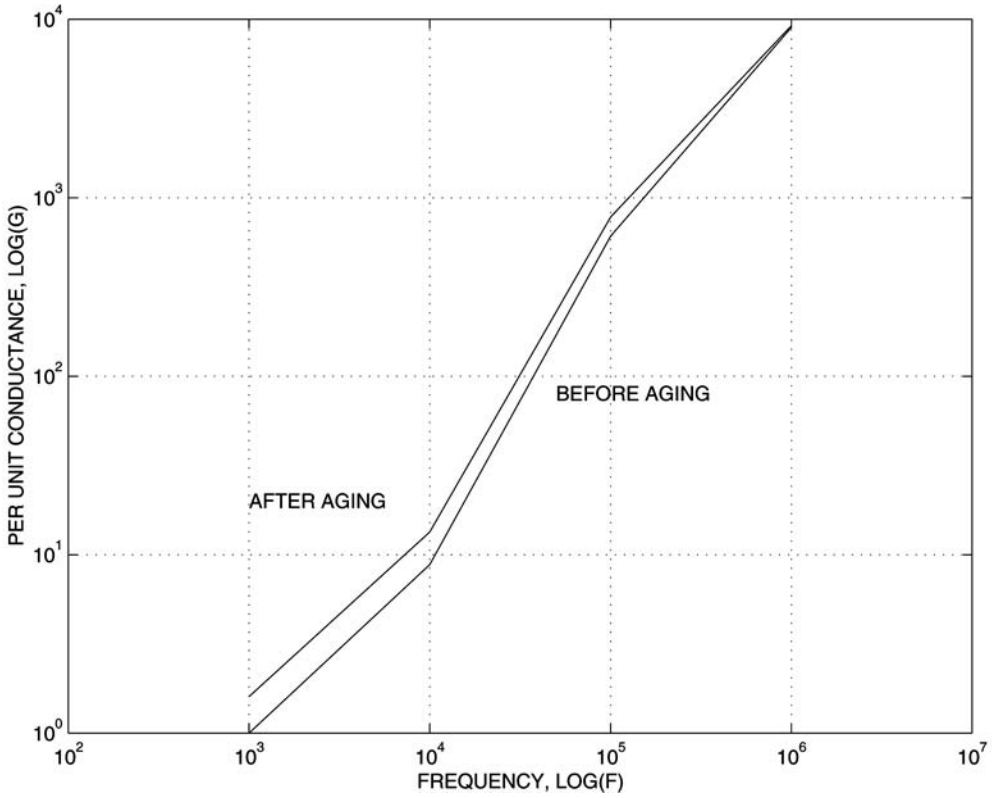

FIGURE 10.40 (continued)

Core-Form

Characteristics of the core-form transformer are a long magnetic path and a shorter mean length of turn. Commonly used core-form magnetic circuits are single phase transformers with a two-legged magnetic path with turns wound around each leg, a three-legged magnetic path with the center leg wound with conductor, and a legged magnetic path with the two interior legs wound with conductors (Bean et al., 1959; MIT, 1943). Three phase core-form designs are generally three legged magnetic cores with all three legs possessing windings and a five-legged core arrangement with the three center legs possessing windings. The simplest winding arrangement has the low voltage winding nearest the core and the high voltage winding wound on top of the low. Normally in the core form construction, the winding system is constructed from helical, layer, or disk type windings. Often the design requirements call for a winding arrangement that is a more complex arrangement, e.g., interleaving high and low voltage windings, interwound taps, windings that are bifurcated have and entry and exit points other than the top or bottom of the coil. All of these variations have, to one degree or another, an effect on the transformer's transient voltage response. To insure an adequate insulation structure, each possible variation must be explored during the design stage to evaluate its effect on the transient overvoltages.

Shell-Form

Shell-form transformer construction features a short magnetic path and a longer mean length of electrical turn. Fink and Beatty (1987) points out that this results in the shell-form transformer having a larger core area and a smaller number of winding turns than the core-form of the same output and performance. Additionally, the shell-form will generally have a larger ratio of steel to copper than an equivalently rated

core-form transformer. The most common winding structure for shell-form windings are the primary-secondary-primary (P-S-P) but it is not uncommon to encounter shell form windings of P-S-P-S-P. The winding structure for both the primary and secondary windings are normally of the pancake-type winding structure (Bean et al., 1959).

Proof of Design Concept

The desire of the purchaser is to obtain a transformer at a reasonable price that will achieve the required performance for an extended period of time. The desire of the manufacturer is to construct and sell a product, at a profit, that meets the customer's goals. The specification and purchase contract is the document that combines both the purchaser's requirements and the manufacturer's commitment in a legal format. The specification will typically address the transformer's service condition, rating, general construction, control and protection, design and performance review, testing requirements, and transportation and handling. Since it is impossible to address all issues in a specification, the industry uses standards that are acceptable to purchaser and supplier. In the case of power transformers, the applicable standards would include IEEE C57, IEC 76, and NEMA TR-1.

Standard Winding Tests

ANSI/IEEE C57.12.00 (1993) defines routine and optional tests and testing procedures for power transformers. The following are listed as routine tests for transformers larger than 501 kVA:

1. Winding resistance
2. Winding turns ratio
3. Phase-relationship tests: polarity, angular displacements, phase sequence
4. No-load loss and exciting current
5. Load loss and impedance voltage
6. Low frequency dielectric tests (applied voltage and induced voltage)
7. Leak test on transformer tank

The following are listed as tests to be performed on only one of a number of units of similar design for transformers 501 kVA and larger:

1. Temperature rise tests
2. Lightning-impulse tests (full and chopped wave)
3. Audible sound test
4. Mechanical test from lifting and moving of transformer
5. Pressure tests on tank

Other tests are listed in ANSI/IEEE C57.12.00 (1993) which include, for example, short circuit forces and switching surge impulse tests. Additionally, specific tests may be required by the purchaser based on their applications or field experience.

The variety of transient voltages a transformer may see in its normal useful life are virtually unlimited (Degeneff et al., 1982). It is impractical to proof test each transformer for all conceivable combinations of transient voltage. However, the electrical industry has found that it is possible, in most instances, to assess the integrity of the transformer's insulation systems to withstand transient voltages with the application of a few specific aperiodic voltage waveforms. Figure 10.41 illustrates the full, chopped, and switching surge waveforms. IEEE C57 contains the specific wave characteristics, relationships, and acceptable methods and connections required for these standard tests. Each of these test is designed to test the insulation structure for a different transient condition. The purpose of applying this variety of tests is to substantiate adequate performance of the total insulation system for all the various transient voltages it may see in service.

The insulation integrity for steady state and for dynamic voltages are also assessed by factory tests called out in ANSI/IEEE C57.12.00 (1993). One should not be lulled into thinking that a transformer that has passed all factory voltage tests (both impulse and low frequency) can withstand all transient

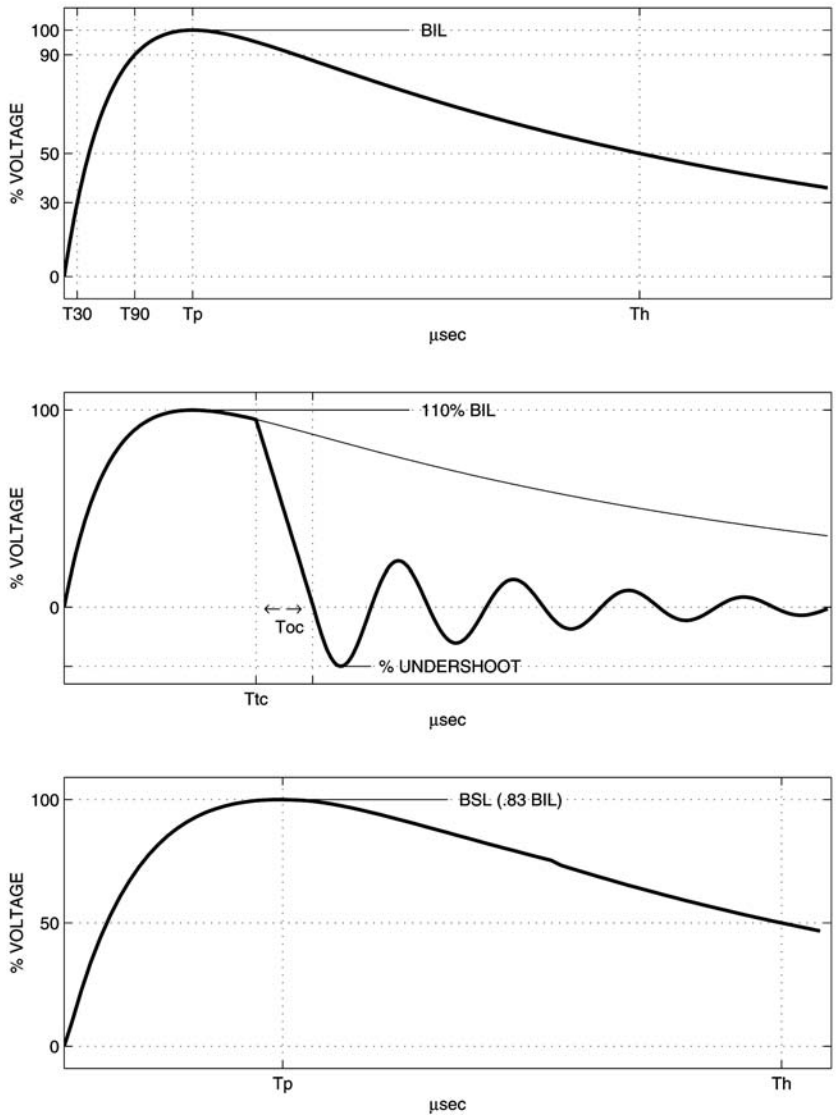

FIGURE 10.41 Standard voltage waveforms for impulse tests: full, chopped, switching surge.

voltages to which the system may subject it. One should always assess the environment the transformer is applied in and determine if there may be unusual transient voltage excitation present in an application that is not covered in the standards (see Degeneff et al., 1982; Greenwood, 1991; McNutt et al., 1974).

Design Margin

The actual level of insulation requested, e.g., BIL/BSL, is determined by recognizing the system within which the transformer will operate, and the arrester protective level. Normally, a minimum protective margin of 15 to 20% between the arrester peak voltage and the transformer capability at three (σ) is established. This is illustrated in Fig. 10.42 for a 230 kV transformer with a 750 kV BIL protected with a 180 kV rated arrester (Balma et al., 1996). The curve designated A in Fig. 10.42 is used to represent the transformer's insulation coordination characteristic (insulation capability) when subjected to aperiodic and oscillatory waveforms. The curve to be used to represent the transformer volt-time insulation

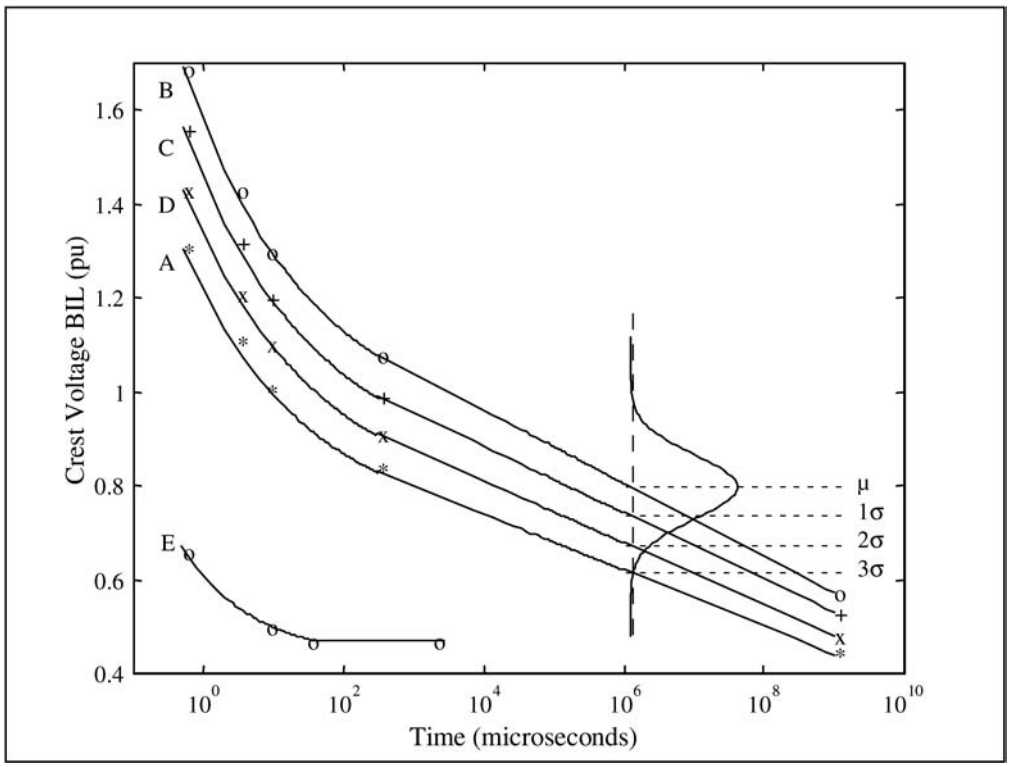

FIGURE 10.42 Voltage-time curve for insulation coordination

coordination characteristic when subjected to aperiodic wave forms with a time to failure between 0.1 and 2000 μsec is to be based on five points (IEEE C62.22-1991). The five points are:

1. Front of Wave Voltage plotted at its time of crest (about 0.5 μsec). If the front of wave voltage is not available, a value of 1.3 times the BIL should be plotted at 0.5 μsec.
2. Chopped Wave Voltage at its time of crest (about 3.0 μsec).
3. Full Wave Voltage (or BIL) plotted about 8 μsec.
4. Switching Surge Voltage (or BSL) plotted about 300 μsec.
5. A point at 2000 μsec where it magnitude is established with the following expression.:

$$logV_{2000} = \frac{logT_{BSL} - logT_{2000}}{m} + logV_{BSL} = \frac{log\dfrac{300}{2000}}{m} + logV_{BSL}$$

V_{2000} is the voltage at 2000 μsec, T_{2000}, V_{BSL} is the BSL voltage (or 0.83 the BIL), and T_{BSL} equal to 300 μsec. The value of m is established as the inverse of the slope of a straight line drawn on log-log paper from the BSL point to a point established by the peak of the one hour induced test voltage plotted at a time the induced voltage exceeds 90% of its peak value (this would be 28.7% of 3600 sec or 1033.2 sec).

The connection between all points is made with a smooth continuous curve. The first four points in the curve establish an approximate level of insulation voltage capability for which one would anticipate only one insulation failure out of 1000 applications of that voltage level, e.g., at 3 σ the probability of failure is 1.0 – 0.99865 or 0.001. Experience has shown that the standard deviation for transformer insulation structures is on the order of 10 to 15%. Figure 10.42 assumes that σ is 10%. Curve B, or the

50% failure rate curve, is established by increasing the voltage in Curve A by 30%. Therefore, for Curve B, on average the unit would be expected to fail one out of two times if it were subjected to this level of voltage. Curves C and D establish 1 and 2 σ curves, or 16% and 2.3% failure rate curves, respectively. The inserted normal distribution on the right of Fig. 10.42 illustrates this concept. All of this assumes the transformer is new.

Insulation Coordination

In a field installation, an arrester is normally placed directly in front of the transformer to afford it protection from transient voltages produced on the system. Curve E in Fig. 10.42 is a metal oxide arrester protective curve established in a manner similar to that described in IEEE standard C62.2. The curve is specified by three points:

1. The front of wave voltage held by the arrester plotted at 0.5 μs
2. The 8 × 20 μs voltage plotted at 8.0 μs
3. The switching surge voltage plotted in straight line from 30 to 2000 μs

The protective ratio is established by dividing the transformer insulation capability by the arrester protective level for the wave shape of interest. For example, in Fig. 10.42, the protective level for a switching surge is on the order of 177% or (0.83/0.47) × 100.

Additional System Considerations

The standards reflect the growing and learning within the industry and each year they expand in breadth, addressing issues that are of concern to the industry. However, at present the standards are silent with regard to the effects of system voltage on transient response, multi-phase surges, aging or mechanical movements of insulation structures, oscillatory voltage excitation, temperature variations, movement of oil, and loading history. A prudent user will seek similar users and explore their experience base.

Models for System Studies

Model Requirements

The behavior of large power transformers under transient conditions is of interest to both transformer designers and power engineers. The transformer designer employs detailed electrical models to establish a reliable and cost effective transformer insulation structure. The power engineer models not only the transformer, but the system, in order to investigate the effects of power system transients.

Considerable effort has been devoted to computing the transformer's internal transient response. Models of this type may contain several hundred nodes for each phase. This detail is necessary in order to compute the internal response in enough detail to establish an adequate transformer insulation design. The utility engineer usually is not interested in the internal response, but is concerned only with the transformer's terminal response. Even if the transformer's detailed models were available, their use would create system models too large to be effectively used in system studies. Normal practice has been to create a reduced order model of the transformer that represents the terminal response of the transformer. Experience has shown that great care must be taken to obtain a terminal model that provides a reasonable representation of the transformer over the frequency range of interest (Gutierrez et al., 1993; Degeneff, 1977).

The challenge in creating a high fidelity reduced model lies in the fact that as the size of the model is reduced, the number of valid eigenvalues must also decrease. In effect, any static reduction technique will produce a model which is intrinsically less accurate than the more detailed lumped parameters model (Morched et al., 1992; de Leon and Semlyen, 1992).

Reduced Order Model

McNutt (1974) suggested a method of obtaining a reduced order transformer model by starting with the detailed model and appropriately combining series and shunt capacitances. This suggestion was extended by de Leon (1992). This method is limited to linear models and cannot be used to eliminate large

proportions of the detailed models without affecting the resulting model's accuracy. Degeneff (1978) proposed a terminal model developed from information from the transformer's nameplate and capacitance measured among the terminals. This model is useful below the first resonant frequency but lacks the necessary accuracy at higher frequencies for system. Dommel (1982) proposed a reduced model for EMTP described by branch impedance or admittance matrix calculated from open and short circuit tests. TRELEG and BCTRAN matrix models for EMTP can be applied only for very low frequency studies. Morched (1992) proposed a terminal transformer model, composed of a synthesized LRC network, where the nodal admittance matrix approximates the nodal admittance matrix of the actual transformer over the frequency range of interest. This method is appropriate only for linear models.

Gutierrez et al. (1993) and Degeneff et al. (1994) present a method for reducing both a detailed linear and nonlinear lumped parameter model to a terminal model with no loss of accuracy. The work starts with Eq. (10.105), then progresses to Eq. (10.108), and then applies Kron reduction to obtain a terminal model of the transformer that retains all the frequency fidelity of the initial transformer lumped parameter model. Gutierrez et al., (1993) and Degeneff et al. (1994) present all the appropriate equations to apply this technique within EMTP.

References

Abetti, P.A., Correlation of forced and free oscillations of coils and windings, *IEEE PAS,* 986–996, December 1959.

Abetti, P.A., Survey and classification of published data on the surge performance of transformers and rotating machines, *AIEE Trans.,* 78, 1403–1414, 1959.

Abetti, P.A., First Supplement to Reference (12), *AIEE Trans.,* 81, 213, 1962.

Abetti, P.A., Second Supplement to Reference (12), *AIEE Trans.,* 83, 855, 1964.

Abetti, P.A., Pseudo-final voltage distribution in impulsed coils and windings, *Trans. AIEE,* 87–91, 1960.

Abetti, P.A., Maginniss, F.J., Fundamental oscillations of coils and windings, *IEEE PAS,* 1–10, February 1954.

Avila-Rosales, J. and Alvarado, L., Nonlinear frequency dependent transformer model for electromagnetic transient studies in power systems, *IEEE Trans. on PAS,* PAS-101, 11, Nov. 1982.

Balma, P.M., Degeneff, R.C., Moore, H.R., and Wagenaar, L.B., The Effects of Long Term Operation and System Conditions on the Dielectric Capability and Insulation Coordination of Large Power Transformers, Paper No. 96 SM 406-9 PWRD, presented at the *Summer Meetings of IEEE/PES,* Denver, CO, 1996.

Batruni, R., Degeneff R., Lebow, M., Determining the Effect of Thermal Loading on the Remaining Useful Life of a Power Transformer from Its Impedance Versus Frequency Characteristics, *IEEE Trans. on Power Delivery,* 11, 3, 1385–1390, July 1996.

Bean, R.L., Crackan, N., Moore, H.R., and Wentz, E., *Transformers for the Electric Power Industry,* Westinghouse Electric Corporation, McGraw-Hill, New York, 1959.

Blume, L.F., Boyajian, A., Camilli, G., Lennox, T.C., Minneci, S., and Montsinger, V.M., *Transformer Engineering,* 2nd ed., John Wiley & Sons, Inc., New York, 416–423, 1951.

Clark, F.M., *Insulating Materials for Design and Engineering Practice,* Wiley, New York, 1962.

Degeneff, R.C., A General Method For Determining Resonances in Transformer Windings, *IEEE Trans. on PAS,* 96, 2, 423–430, March/April 1977.

Degeneff, R.C., A Method for Constructing Terminal Models for Single-Phase n-Winding Transformers, IEEE Paper A78 539-9, Summer Power Meeting, Los Angeles, 1978.

Degeneff, R.C., Reducing Storage and Saving Computational Time with a Generalization of the Dommel (BPA) Solution Method, in *IEEE PICA Conference Proceedings,* Toronto, Canada, May 24–27, 1977, 307–313.

Degeneff, R.C., Simplified Formulas to Calculate Equivalent Series Capacitances for Groups of Disk Winding Sections, General Electric, TIS 75PTD017, August 16, 1976.

Degeneff, R.C., Blalock, T.J., and Weissbrod, C.C., *Transient Voltage Calculations in Transformer Windings,* General Electric Technical Information Series, No. 80PTD006, 1980.

Degeneff, R.C., Gutierrez, M., and Vakilian, M., Nonlinear, Lumped Parameter Transformer Model Reduction Technique, IEEE paper no. 94 SM 409-3 PWRD, 1994.
Degeneff, R.C. and Kennedy, W.N., Calculation of Initial, Pseudo-Final, and Final Voltage Distributions in Coils Using Matrix Techniques, Paper A75-416-8, Summer Power Meeting, San Francisco, CA,
Degeneff, R.C., Neugebaur, W., Panek, J., McCallum, M.E., and Honey, C.C., Transformer Response to System Switching Voltages, *IEEE Trans. on Power Appar. and Syst.,* Pas-101, 6, 1457–1465, June 1982.
Dent, B.M., Hartill, E.R., and Miles, J.G., A method of analysis of transformer impulse voltage distribution using a digital computer, *IEE Proceedings,* 105, Pt. A, 445–459, 1958.
Dommel, H.W., Digital computer solution of electromagnetic transients in single and multiphase networks, *IEEE Trans. on PAS,* 388–399, April 1969.
Dommel, H.W., Dommel, I.I., and Brandwajn, V., Matrix Representation of Three-Phase N-Winding Transformers for Steady State and Transient Studies, *IEEE PAS-1,* 6, June 1982.
Fergestad, P.I. and Henriksen, T., Transient Oscillations in Multiwinding Transformers, *IEEE Trans. on PAS,* 500–507, PAS-93, 1974.
Fink, D.G. and Beaty, H.W., *Standard Handbook for Electrical Engineers,* 12th Edition, McGraw-Hill Book Company, New York, 1987.
FORTRAN Subroutines for Mathematical Applications, Version 2.0, September 1991, MALB-USM-PER-FCT-EN9109-2.0.
Franklin, A.C., *The J & P Transformer Book,* 11th ed., chap. 15, 351–367, 1983.
Greenwood, A., *Electrical Transients in Power Systems,* John Wiley & Sons, Inc., New York, 1991.
Greenwood, A., *Vacuum Switchgear,* Institute of Electrical Engineers, Short Run Press Ltd., Exeter, 1994.
Grover, F.W., *Inductance Calculations — Working Formulas and Tables,* Dover Publications, New York, Inc., 1962.
Gutierrez, M., Degeneff, R.C., McKenny, P.J., and Schneider, J.M., Linear, Lumped Parameter Transformer Model Reduction Technique, IEEE paper no. 93 SM 394-7 PWRD, 1993.
IEEE C62.22-1991, *IEEE Guide for the Application of Metal-Oxide Surge Arrester for Alternating-Current Systems.*
IEEE Std. 519, *IEEE Recommended Practices and Requirements for Harmonic Control in Electrical Power Systems,* IEEE Industry Applications Society and Power Engineering Society, April 12, 1999.
C57, *IEEE Guide and Standards for Distribution, Power, and Regulating Transformers,* 1993.
Kogan, V.I., Fleeman, J.A., Provanzana, J.H., and Shih, C.H., Failure analysis of EHV transformers, *IEEE Trans. in Power Delivery,* 672–683, April 1988.
Kogan, V.I., Fleeman, J.A., Provanzana, J.H., Yanucci, D.A., and Kennedy, W.N., Rationale and implementation of a new 765kV generator step-up transformer specification, CIGRE Paper 12-202, August 1990.
Lammeraner, J. and Stafl, M., *Eddy Currents,* The Chemical Rubber Co. Press, Cleveland, 1966.
de Leon, F., and Semlyen, A., Complete transformer model for electromagnetic transients, *IEEE Transactions on Power Delivery,* 9, 1, 231–239, January 1994.
de Leon, F. and Semlyen, A., Reduced order model for transformer transients, *IEEE Trans. on PWRD,* 7, 1, 361–369, January 1992.
Massachusetts Institute of Technology, Department of Electrical Engineering, *Magnetic Circuits and Transformers,* John Wiley and Sons, 1943.
McNutt, W.J., Blalock, T.J., and Hinton, R.A., Response of Transformer Windings to System Transient Voltages, *IEEE PES Transactions,* 457–467, 1974.
McWhirter, J.H., Fahrnkopf, C.D., and Steele, J.H., Determination of impulse stresses within transformer windings by computers, *AIEE Transactions,* pt. III, 75, 1267–1273, 1956.
Morched, A., Marti, L., and Ottevangers, J., A High Frequency Transformer Model for EMTP, Paper No. 925M 359-0 IEEE 1992 Summer Meeting, Seattle, WA, July 12–16.
Narang, A., Wisenden, D., and Boland, M., *Characteristics of Stress on Transformer Insulation Subjected to Very Fast Transient Voltages,* CEA No. 253 T 784, Canadian Electricity Association, July 1998.
Rabins, Transformer Reactance Calculations with Digital Computers, *AIEE Trans.,* 75, 1, 261–267, July 1956.
Scheich, A., Behavior of Partially Interleave Transformer Windings Subject to Impulse Voltages, *Bulletin Oerlikon,* 389/390, 41–52, 1965.

Snow, C., *Formulas for Computing Capacitance and Inductances,* National Bureau of Standards, Circular 544, Sept. 10, 1954.
Tarasiewicz, E.J., Morched, A.S., Narang, A., and Dick, E.P., Frequency dependent eddy current models for the nonlinear iron cores, *IEEE Trans. on PAS,* 8, 2, 588–597, May 1993.
Vakilian, M., A Nonlinear Lumped Parameter Model for Transient Studies of Single Phase Core Form Transformers, Ph.D. Thesis, Rensselaer Polytechnic Institute, Troy, New York, 1993.
Vakilian, M., Degeneff, R., and Kupferschmid, M., Computing the internal transient voltage response of a transformer with a nonlinear core using Gear's method — Part 1: Theory, *IEEE Trans. on Power Delivery,* 10, 4, 1836–1841, October 1995.
Vakilian M., Degeneff, R., and Kupferschmid, M., Computing the internal transient voltage response of a transformer with a nonlinear core using Gear's method — Part 2: Verification, *IEEE Trans. on Power Delivery,* 10, 2, 702–708, May 1995.
Von Hippel, A., *Dielectric Materials and Applications,* Cambridge, MIT, 1954.
Waldvogel, P. and Rouxel, R., A new method of calculating the electric stresses in a winding subjected to a surge voltage, *Brown Boveri Rev.,* 43, 6, 206–213, June 1956.
White, W.N., *An Examination of Core Steel Eddy Current Reaction Effect on Transformer Transient Oscillatory Phenomena,* General Electric Technical Information Series, No. 77PTD012, April 1977.
White, W.N., *Inductance Models of Power Transformers,* General Electric Technical Information Series, No. 78PTD003, April 1978.
White, W.N., Numerical Transient Voltage Analysis of Transformers and LRC Networks Containing Nonlinear Resistive Elements, *1977 PICA Conference,* 288–294.
Wilcox, D.J., Hurley, W.G., McHale, T.P., and Conton, M., Application of modified modal theory in the modeling of practical transformers, *IEE Proceedings-C,* 139, 6, November 1992.
Wilcox, D.J., Conlon, M., and Hurley, W.G., Calculation of self and mutual impedances for coils on ferromagnetic cores, in *IEE Proceedings,* 135, A, 7, September 1988, pp. 470–476.
An international survey on failures in large power transformers in service, Final Report of Working Group 05 of Study Committee 12 (Transformers), *Electra,* 88, May 1983.

10.7 Transmission System Transients — Grounding

William Chisholm

General Concepts

Electric power systems are often grounded, that is to say "intentionally connected to earth through a ground connection or connections of sufficiently low impedance and having sufficient current-carrying capacity to prevent the buildup of voltages which may result in undue hazard to connected equipment or to persons" (IEEE Std. 100). Grounding affects the dynamic power-frequency voltages of unfaulted phases, and influences the choice of surge protection. Also, the tower-footing impedance is an important specification for estimating the severity of insulator-string transient voltage for a direct lightning strike.

Under AC fault conditions, systems can be grounded by any of three means (IEEE Std. 100) :

- **Inductance grounded,** such that the system zero-sequence reactance is much higher than the positive-sequence reactance, and is also greater than the zero-sequence resistance. The ground-fault current then becomes more than 25% of the three-phase fault current.
- **Resistance grounded,** either directly to ground, or indirectly through a transformer winding. The low-resistance-grounded system permits a higher ground-fault current (on the order of 25 A to several kA) for selective relay performance.
- **Resonant grounded,** through a reactance with a value of inductive current that balances the power-frequency capacitive component of the ground-fault current during a single line-to-ground fault. With resonant grounding of a system, the net current is limited so that the fault arc will extinguish itself.

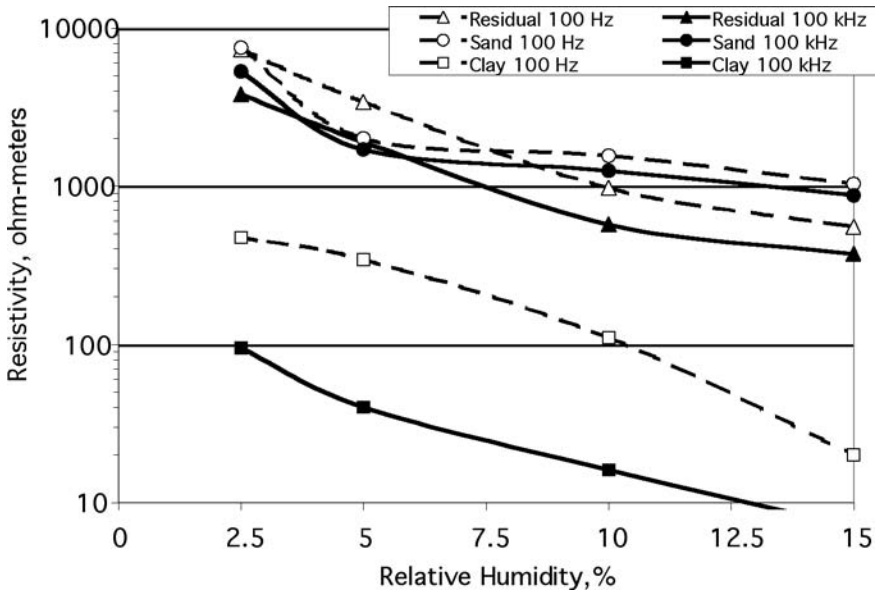

FIGURE 10.43 Change in resistivity with relative humidity and frequency for three typical surface materials. (Filho and Portela, 1987.)

Power system transients have a variety of waveshapes, with spectral energy ranging from the power frequency harmonics up to broadband content in the 300-kHz range, associated with 1-μs rise and fall times of lightning currents and insulator breakdown voltages. With the wide frequency content of transient waveshapes, resonant grounding techniques offer little benefit. Also, resistance grounds that may be effective for power frequency can have an additional inductive voltage rise (L dI/dt) that dominates the transient response. Both resistive and inductive aspects must be considered in the selection of an appropriate ground electrode.

Material Properties

The earth resistivity (ρ, units of Ω-m) dominates the potential rise on ground systems at low frequencies and currents. Near the surface, resistivity changes as a function of moisture, temperature, frequency, and electric field stress. Figure 10.43 shows that this variation can be quite large.

Reconnaissance of earth resistivity, from traditional four-terminal resistance measurements, is a classic tool in geological prospecting (Keller and Frischknecht, 1982). A current I is injected at the outer two locations of an equally spaced line of four probes. A potential difference U then appears between the inner two probes, which are separated by a distance a. The apparent resistivity ρ_a is then defined as:

$$\rho_a = 2\pi a \frac{U}{I}$$

At a given location, several measurements of ρ_a are taken at geometrically-spaced values of a, such as (a = 1, 2, 3, 5, 10, 20, 30,…1000 m). When ρ_a is constant with distance, the assumption of a uniform soil model is justified, and the effective resistivity ρ_e for any electrode size is simply ρ_a. However, in many cases, there are two or more layers of contrasting soil. The most difficult case tends to be a thin conducting top layer (clay, till, sand) over a thick, poorly conducting rock layer ($\rho_1 < \rho_2$). This case will have an increasing value of ρ_a with distance. A conservative interpretation in this case can be simplified: For flat electrodes, the effective resistivity, ρ_e, equals the value of ρ_a observed at a probe spacing of ($a = 2s$), where s is the maximum extent (for example, the radius of a ring electrode).

TABLE 10.3 Values of *A*, *s*, and *g* for Typical Ground Electrodes in Half-Plane

Geometry	*A*	*s*	*g*
Vertical Cylindrical Rod Length l and Radius r	$2\pi rl + \pi r^2 \approx 2\pi rl$	$\sqrt{l^2+r^2} \approx l$	$\sqrt{l^2+2r^2} \approx l$
Solid Conducting Cylinder Length l, Radius r	$2\pi rl + \pi r^2$	$\sqrt{l^2+r^2}$	$\sqrt{l^2+2r^2}$
Buried Circular Disk at Depth h with Radius r	$2\pi rh + \pi r^2$	$\sqrt{h^2+r^2}$	$\sqrt{h^2+2r^2}$
Buried Circular Ring at Depth h with Radius r	$2\pi rh + \pi r^2$	$\sqrt{h^2+r^2}$	$\sqrt{h^2+2r^2}$
Circular Disc on Surface Thickness t, Radius r	$2\pi rt + \pi r^2 \approx \pi r^2$	$\sqrt{t^2+r^2} \approx r$	$\sqrt{t^2+2r^2} \approx \sqrt{2}r$
Oblate (disc-like) Half Spheroid Radius a > thickness b $\varepsilon = SQRT(1 - b^2/a^2)$	$\pi a^2 + \pi b^2/(2\varepsilon) \ln((1+\varepsilon)/(1-\varepsilon))$	a	$\sqrt{2a^2+b^2}$
Hemisphere of radius r	$2\pi r^2$	r	$\sqrt{3}*r$
Prolate (tube-like) Half Spheroid Radius a < length b $\varepsilon = SQRT(1 - a^2/b^2)$	$\pi a^2 + \pi ab/\varepsilon \arcsin\varepsilon$	b	$\sqrt{2a^2+b^2}$
Rectangular Strip, l long, w wide and t thick	$wt + 2(t+w)l \approx 2lw$	$\sqrt{w^2/4+t^2/4+l^2}$	= *s*
Two or more Vertical Rods in a Straight Line, total length l, depth h, rod thickness w	$lw + 2(l+w)h \approx 2lh$	$\sqrt{w^2/4+l^2/4+h^2}$	= *s*
Buried Counterpoise at depth h, thickness w, total length l	$lw + 2(l+w)h \approx 2lh$	$\sqrt{w^2/4+l^2/4+h^2}$	= *s*
Conducting Box, l long by w wide by h deep	$lw + 2(l+w)h$	$\sqrt{l^2/4+w^2/4+h^2}$	= *s*
Buried Rectangular Plate, l long by w wide at Depth h	$lw + 2(l+w)h$	$\sqrt{l^2/4+w^2/4+h^2}$	= *s*
Buried Rectangular Grid l long by w wide at Depth h	$lw + 2(l+w)h$	$\sqrt{l^2/4+w^2/4+h^2}$	= *s*
Four Vertical Rods of length h on Corners of l by w Rectangle	$lw + 2(l+w)h$	$\sqrt{l^2/4+w^2/4+h^2}$	= *s*
Four Radial Wires, on Corners l by w at depth h	$lw + 2(l+w)h$	$\sqrt{l^2/4+w^2/4+h^2}$	= *s*
Surface Plate, l long by w wide by t thick	$lw + 2(l+w)t \approx lw$	$\sqrt{l^2/4+w^2/4+t^2}$	= *s*

Note: There are really only three equations in Table 10.3; one for a cylinder, one for a spheroid, and one for a box. Different dimensions dominate the *s*, *g*, and *A* terms, depending on the electrode shape.

Electrode Dimensions

Three dimensions are relevant for analysis of electrode response under steady-state and transient conditions. Electrodes with large surface area *A* in contact with soil will have lower resistance, lower impedance, and less susceptibility to unpredictable effects of soil ionization. For objects with concave features, the area of the smallest convex body that can envelop it is determined. With this model, a tube has the same area as a solid cylinder of the same dimensions. Disk electrodes have two sides. Buried horizontal wires expose area on both sides of the narrow trench. Table 10.3 provides further interpretations.

The second electrode dimension is the 3-dimensional distance from the center of the electrode to its outermost point. For a spheroid in a conducting half-plane, *s=MAX(a,b)* where *a* is the maximum cross-section radius and *b* is the length in the axis of symmetry. Table 10.3 shows that the 3-D extent *s* of cylinders and prisms are slightly larger than the *s* for a prolate spheroid of the same depth. The propagation time $\tau = s/c$, calculated from speed-of-light propagation at $c = 3.10^8$ m/s, is used to estimate transient electrode impedance.

The geometric radius of the electrode, $g = \sqrt{R_x^2 + R_y^2 + R_z^2}$ is the third important dimension of the electrode, since it is used to estimate self-capacitance. For long, thin, or rectangular shapes, $g = s$; for a disc, $g = \sqrt{2}\, s$; for a hemisphere, $g = \sqrt{3}\, s$.

Self-capacitance of Electrodes

Electrode capacitance is easily calculated (Chow, 1982; Chow, 1988) and offers an elegant description of grounding response to transients. Also, the self-capacitance C_{self} to infinity of an arbitrary conducting object in full space has a useful dual relation to its steady-state resistance R in a half-space of conducting medium, given by Weber (1950):

$$R = 2\,\varepsilon_o\,\rho / C_{self} \tag{10.141}$$

where ε_o is the permittivity constant, 8.854×10^{-12} F/m
ρ is the earth resistivity, in Ω-m

The transient impedance of the same arbitrary conducting object can be modeled using the time (τ) it takes to charge up its self-capacitance C_{self}. This time cannot be less than the maximum dimension of the electrode, s, divided by the speed of light. An average surge impedance Z, given by the ratio τ/C, can then be used to relate voltages and currents during any initial surge. The capacitance of an object is approximately (Chow, 1982):

$$C_{self} = \varepsilon_o\, c_f \sqrt{4\pi A} \tag{10.142}$$

where A is the total surface area of the object, including both sides of disk-like objects
c_f is a correction factor between the capacitance of the object and the capacitance of a sphere with the same surface area. For spheroids, $0.9 < c_f < 1.14$ for $0 < b/a < 8$ (Chow, 1988).

A good estimate for c_f is given by the following expression:

$$c_f = \frac{4\pi g}{\sqrt{4\pi A}\,\ln\dfrac{4\pi e^{\sqrt{3}} g^2}{3A}} \simeq \frac{3.54\,g}{\sqrt{A}\,\ln\dfrac{23.7\,g^2}{A}} \tag{10.143}$$

Equation (10.143) is exact for a sphere, and remains valid for a wide range of electrode shapes, from disc to rod.

Initial Transient Response from Capacitance

Once the capacitance of a conducting electrode has been estimated, its average transient impedance can be computed from the minimum charging time τ. The charging time τ would be the maximum three-dimensional extent s, divided by the speed of light c. The transient impedance of the ground electrode will be seen only during the charging time, and in general it will vary somewhat around the estimated average value.

Figure 10.44 gives the initial transient response of conducting spheroid electrodes.

TABLE 10.4 Transient Impedance of Conducting Electrodes

Shape	Surface Area	3-D Extent s	Capacitance	Travel Time	Transient Impedance
Circular Disc	$2\,\pi\,s^2$	s	$0.9\,\pi\,\varepsilon\,s\,\sqrt{8}$	s/c	47 Ω
Hemisphere	$3\,\pi\,s^2$	s	$1.0\,\pi\,\varepsilon\,s\,\sqrt{12}$	s/c	35 Ω
Long Cylinder	$2\pi r\,s$	s	$3.3\,\pi\,\varepsilon\,\sqrt{4rs}$	s/c	s/r = 100: 210 Ω
			$7.8\,\pi\,\varepsilon\,\sqrt{4rs}$		s/r = 1000: 270 Ω
			$20\,\pi\,\varepsilon\,\sqrt{4rs}$		s/r = 10000: 340 Ω

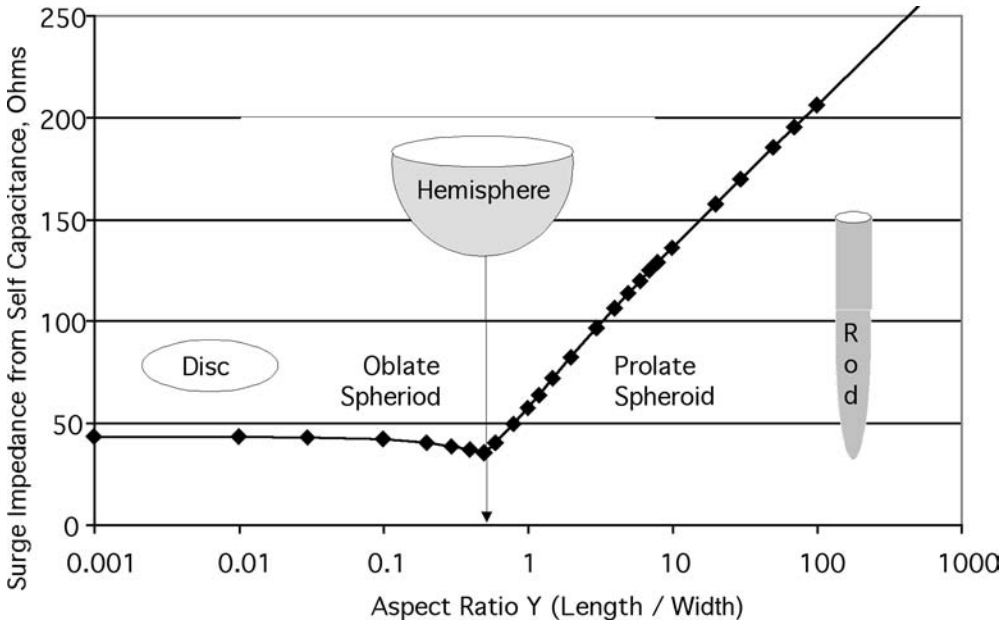

FIGURE 10.44 Relation between transient impedance and aspect ratio: spheroid electrodes in half space.

The main observation from Fig. 10.44 is that wide, flat electrodes will have inherently better transient response than long, thin electrodes. This includes electrodes in both horizontal and vertical planes, so long leads to remote ground electrodes are defective under transient conditions.

For compact electrodes, the response can be lumped into an inductance element ($L_{self} = \tau^2/C_{self}$) by ignoring electromagnetic considerations (lack of return path for inductance integrals). A potential rise on the earth electrode can then be estimated from the simple circuit model:

$$U_{electrode} = R\,I + \left(\tau^2/C_{self}\right) dI/dt \tag{10.144}$$

A numerical example for Eq. (10.144) is useful. For $\rho = 100\ \Omega$-m, and a disc electrode of 5 m radius, the resistance to remote ground will be 3.2 Ω and $\tau^2/C_{self} = 0.8\ \mu H$. For a typical (median) lightning stroke with I = 30 kA and dI/dt = 24 kA/μs at the peak, the two terms of the peak potential rise will be:

$$\left(30\ kA\right)\left(3.2\ \Omega\right) + \left(24\ kA/\mu s\right)\left(0.8\ \mu H\right) = 96\ kV + 19\ kV.$$

The inductive term is desirably low in the example, but it can dominate the response of long, thin electrodes in low-resistivity soil. For distributed electrodes, however, the circuit approximation in Eq. (10.144) eventually fails as rate of current rise (dI/dt) increases.

Ground Electrode Impedance over Perfect Ground

The per-unit inductance L of a distributed grounding connection over a conducting plane can be calculated from the surge impedance Z of the wire and its travel time τ:

$$L = Z\tau = \tau^2/C_{self} \tag{10.145}$$

where

$Z = 60 \ln (2h/r)$, the surge impedance (Ω) of a wire of radius r over a ground plane at a height h
$\tau = s/c$, the maximum length of the wire (m) divided by the speed of light (3.0×10^8 m/s).

Ground Electrode Impedance over Imperfect Ground

When the electrode is placed over imperfect ground, the effective return depth of current will increase. Bewley (1963) suggests that the plane for image currents, in his tests of buried horizontal wires, was 61 m (200′) below the earth surface. Some analytical indication of the increase in return depth is given by the normal skin depth, $\delta = 1/\sqrt{\pi f \mu_o / \rho}$, which decreases from 460 m (60 Hz) to 11 m (100 kHz) for 50 Ω-m soil. Deri (1981) proposes a more complete approach, with a frequency-dependent complex depth p, as follows:

$$Z = \frac{j\omega\mu_o}{2\pi} \ln\left(\frac{2(h+p)}{r}\right) \tag{10.146}$$

where

p is a complex depth, $1/\sqrt{j\omega\mu_o\sigma}$
ω is 2π times the frequency, Hz
μ_o is $4\pi \times 10^{-7}$ H/m
σ is the conductivity, Siemens/m ($1/\rho$)

For good soil with a resistivity of 50 Ω-m, the complex depth is 230 (1 – j) m at 60 Hz and 5.6 (1 – j) m at 100 kHz. The complex depth is related to the normal skin depth by the relation $1/p = (1 + j)\ 1/\delta$.

Analytical Treatment of Complex Electrode Shapes

Simple analytical expressions are documented for a variety of regular electrode shapes (see, e.g., Smythe, 1950; Weber, 1950; Keller and Frischknecht, 1982; Sunde, 1949). However, grounding of electrical systems often consists of several interconnected components, making estimation of footing resistance more difficult. The tower foundation can be a single or (more typically) four concrete cylinders, often reinforced with steel. In the preferred case, the steel is bonded electrically, and a grounding connection is brought out of the form before the concrete is poured. In areas with low soil resistivity, four concrete footings can often provide a low tower resistance without supplemental electrodes. In some cases on both transmission and distribution systems, a metal grillage (or pole butt-wrap) is installed at the base after excavation. This deep electrode is more effective than a surface electrode of the same area. Also, grillage and pole-wrap electrodes are protected from vandalism and frost damage.

Supplemental grounding electrodes are often installed during line construction or upgrade. The following approaches are used:

- Horizontal conductors are bonded to the tower, then buried at a practical depth.
- Vertical rods are driven into the soil at some distance from the tower, then bonded to the tower base, again using bare wires, buried at a practical depth.
- Supplemental guy wires are added to the tower (often for higher mechanical rating) and then grounded using rock or soil anchors at some distance away.

Supplemental grounding should be considered to have a finite lifetime of five to twenty years, especially in areas where the soil freezes in winter. Also, auxiliary electrodes such as rock anchors should be designed to carry their share of impulse current, and to withstand the associated traverse forces.

The resistance of an electrode that envelops all contacts can be used to obtain a good estimate of the combined resistance of a complex, interconnected electrode. The resistance of a solid electrode is:

$$R_{geometric} = \frac{\rho}{2\pi s} \ln \frac{2\pi e s^2}{A} \quad (10.147)$$

where

s is the three-dimensional distance from the center to the furthest point on the electrode
A is the convex surface area that would be exposed if the electrode were excavated
e is the exponential constant, 2.718 (noting $2\ \pi\ e \approx 17$)

The resistance can also be based on the geometric radius *g* rather than the maximum dimension *s*:

$$R_{geometric} = \frac{\rho}{2\pi g} \ln \frac{11.8 g^2}{A} \quad (10.48)$$

where

g = $\sqrt{R_x^2 + R_y^2 + R_z^2}$, the geometric radius of the electrode
$R_{x,\,y,\,z}$ = maximum x, y, and z dimensions
11.8 = $(2\ \pi\ e^{\sqrt{3}})/3$

If the electrode is a wire frame, rather than a solid, then a small correction should be added to the geometric resistance:

$$R_{wire\ frame} = R_{geometric} + \rho_1 / l \quad (10.149)$$

where

l is the total length of the wire frame
ρ_1 is the resistivity of the upper layer of soil (the layer next to the wire)

Numerical Treatment of Complex Electrode Shapes

The effectiveness of supplemental grounding can be conveniently evaluated and visualized using a numerical solution to Laplace's equation in two dimensions. This is readily accomplished using a spreadsheet (such as Excel™) and the following steps:

- Define a rectangular problem space, for example a 50×50 box with each cell representing 1×1 m.
- Calculate the resistance between nodes, $R_{ab} = \rho/(2\pi\Delta)$ where Δ is the spacing between nodes.
- Highlight the perimeter of the box and set all the values to 0 (the boundary condition).
- Disable iterative calculation (in Excel, at the *Tools…Options…Calculation* menu).
- Fill the interior of the box with the two-dimensional finite-difference operator (Sadiku, 1992). For the Laplace equation, this operator is simply the average of the four adjacent cells, for example cell G5, = *0.25*(G4 + G6 + F5 + H5)*. Ignore error messages about circular references.
- Calculate the resistances R_f of each individual electrode, using Eq. (10.147) or (10.148). Buried interconnection wire should use the resistance associated with the wire radius and the cell spacing Δ.
- Set the potentials at each electrode location to $(0.25*(G4 + G6 + F5 + H5)/R_{ab} + 1/R_f)/(4/R_{ab} + 1/R_f)$, again using cell G5 as an example.
- Enable iterative calculation (in Excel, at the *Tools…Options…Calculation* menu) and set convergence to a small value.
- Form the sum of all potentials just adjacent to the boundary of the problem space. Each term is proportional to the current density at that point, so the sum (integral), divided by Rab, gives the total current flowing 'out' of the problem space.
- Compute the input current at each electrode, which will be the unit potential minus the node potential, divided by the electrode resistance.

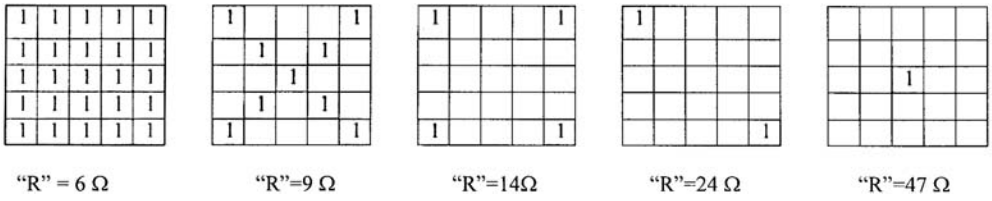

FIGURE 10.45 Numerical solutions of Laplace equation for 3-m rods at 1-m grid spacing.

- Form the sum of all input currents, which should agree with the current at the boundary after iteration.
- Iterate the solution manually (*F9 key*) or automatically until convergence is achieved to a tolerance of about 1 part in 10^5.
- Modify the electrode the shape, size, and configurations as desired and observe changes in resistance.
- Use the three-dimensional plot tool to observe areas of high step and touch potential differences.

There are many approximations and possible errors in the numerical procedure, based on cell size and soil resistivity. However, Fig. 10.45 illustrates the power of the visualization for driven rods:

The relative reduction in resistance is largest when the second electrode is added and additional nearby rods are seen to be less effective at the assumed spacing of $\Delta = 1$m.

Treatment of Multilayer Soil Effects

Generally, the treatment of footing resistance in lightning calculations considers a homogeneous soil with a finite conductivity. This treatment, however, seldom matches field observations, particularly in areas where grounding is difficult. Under these conditions, a thin layer of conducting clay, till, or gravel often rests on top of insulating rock. The distribution of resistivity values for a particular overburden material and condition can be narrow, with standard deviations usually less than 10%. However, the variation of overburden depth with distance can be large. Airborne electromagnetic survey techniques at multiple frequencies in the 10–100 kHz range offer an inexpensive new method of reconnaissance of the overburden parameters of resistivity and depth.

Once a resistivity survey has established an upper-layer resistivity ρ_1, a layer depth d and a lower-layer resistivity ρ_2, the equivalent resistivity ρ_e can be computed. For a disk-like electrode buried just below the surface. ρ_e is given approximately by the following three equations:

$$\rho_e = \rho_1 \frac{1 + C\dfrac{\rho_2}{\rho_1}\dfrac{r}{d}}{1 + C\dfrac{r}{d}}$$

Case 1: Upper Layer (ρ_1) > Lower Layer (ρ_2)

$$C = \frac{1}{1.4 + \left(\dfrac{\rho_2}{\rho_1}\right)^{0.8}}$$

Case 2: Upper Layer (ρ_1) < Lower Layer (ρ_2)

$$C = \frac{1}{1.4 + \left(\dfrac{\rho_2}{\rho_1}\right)^{0.8} + \left(\dfrac{\rho_2}{\rho_1}\dfrac{r}{d}\right)^{0.5}}$$

These equations provide an empirical fit to the solution of elliptic-integral potentials given by (Zaborsky, 1955).

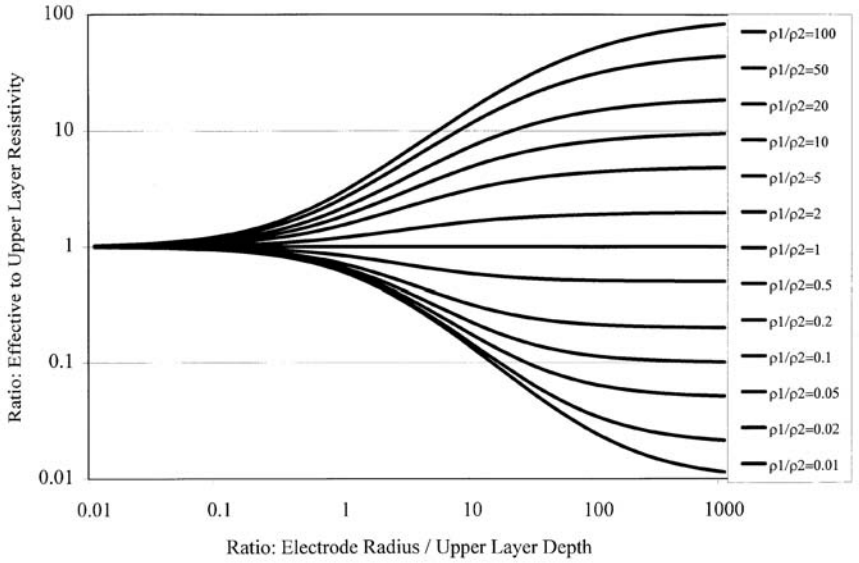

FIGURE 10.46 Relative effective resistivity versus ratio of electrode radius to upper layer depth, with resistivity ratio as a parameter.

Normally, electrode penetration through an upper layer would only be desirable in extreme examples of Case 1 ($\rho_1 \gg \rho_2$). Rather than recomputing the effective resistivity with revised image locations, the effects of the upper layer can be neglected, with the connection through ρ_1 providing only series self-inductance.

Layer of Finite Thickness over Insulator

A simpler two-layer soil treatment is appropriate for Case 2 when $\rho_2 \gg \rho_1$, e.g., (Loyka, 1999). Under these conditions, the following summation ($n = 1,2,3,\ldots\infty$) describes the resistance of a single sphere of radius s in a finitely conducting slab with resistivity ρ_1 and thickness d:

$$R = \rho_1 / \pi \left(1/s + 2\Sigma \left(1/\sqrt{s^2 + (2nd)^2} \right) \right)$$

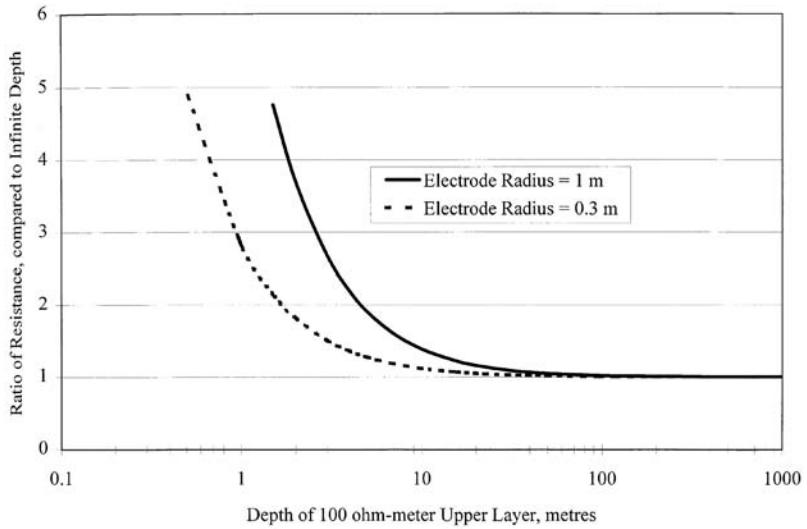

FIGURE 10.47 Asympotic behavior of spherical electrodes in conducting layer.

Treatment of Soil Ionization

Under high electric fields, the air will ionize and effectively become a conductor. The transient electric fields needed to ionize small volumes of soil, or to flashover across the soil surface are typically between 100 kV/m and 1000 kV/m (Korsuncev, 1958; Oettle, 1988). Considering that the potential rise on a small ground electrode can reach 1 MV, the origins of 10-m furrows around small (inadequate) ground electrodes after lightning strikes becomes clear. Surface arcing activity is unpredictable and may transfer lightning surge currents to unprotected facilities. Thus, power system ground electrodes for lightning protection should have sufficient area and multiplicity to limit ionization.

Korsuncev used similarity analysis to relate dimensionless ratios of s, ρ, resistance R, current I, and critical breakdown gradient Eo as follows:

$$\Pi_1^0 = \frac{1}{2\pi} \ln \frac{2\pi es^2}{A} \tag{10.150}$$

$$\Pi_2 = \rho I \Big/ \left(Eo\, s^2\right) \tag{10.151}$$

$$\Pi_1 = \text{MIN}\left(\Pi_1^0,\ 0.26\ \Pi_2^{-0.31}\right) \tag{10.152}$$

$$R = \rho \Pi_1 \Big/ s \tag{10.153}$$

where

s is the three-dimensional distance from the center to the furthest point on the electrode, m
I is the electrode current, A
ρ is the resistivity, Ω-m
Eo is the critical breakdown gradient of the soil, usually 300 to 1000 kV/m
R is the resistance of the ground electrode under ionized conditions

The calculation of ionzied electrode resistance proceeds as follows:

- A value of $\prod_1^0$ is calculated from Eq. (10.150). This un-ionized value will range from $\prod_1^0 = 0.159$ (for a hemisphere) to 1.07 for a 3-m long, 0.01-m radius cylinder.
- A value of $\prod_2$ is calculated from Eq. (10.151). For a 3-m rod at 100 kA in 100 Ω-m soil, with Eo of 300 kV/m, the value of $\prod_2 = 3.7$ is obtained.
- A value of $\prod_1$ is computed from $\prod_2$ using $0.26\ \prod_2^{-0.31}$. This value, from Eq. (10.152), represents the fully ionized sphere with the gradient of Eo at the injected current; for the rod example, $\prod_1 = 0.173$.
- If the ionized value of $\prod_1$ is not greater than $\prod_1^0$, then there is not enough current to ionize the footing, so the un-ionized resistance from $\prod_1^0$ will be seen for the calculation of resistance in Eq. (10.153). For the 3-m rod, ionization reduces the low-current resistance of 36 Ω to 6 Ω at 100 kA.

In two-layer soils with sparse electrodes, ionization effects will tend to reduce the contact resistance [from Eq. (10.149)] without altering the surface area A or characteristic dimension s. This will tend to reduce the influence of ionization.

Design Recommendations

The following advice is especially relevant for transmission towers or other tall structures, where a low-impedance ground is needed to limit lightning-transient overvoltages.

- Choose a wide, flat electrode shape rather than a long, thin shape. Four radial wires of 60 m will be two to eight times more effective than a single radial wire of 240 m under lightning surge conditions.
- Take advantage of natural elements in the structure grounding, such as foundations and guy anchors, by planning for electrical connections and by extending radial wires outwards from these points.
- In rocky areas, use modern airborne techniques to survey resistivity and layer depth using several frequencies up to 100 kHz. Place towers where conductive covering material is deep.
- Provide grounding staff with the tools and techniques to pre-estimate the amount of wire required for target footing impedance values, using simple interpretation of two-layer soil data.
- Near areas where transferred lightning potentials could be dangerous to adjacent objects or systems, use sufficient electrode dimensions to limit ionization, that is, to remain on the $\prod_1^0$ characteristic.

References

Bewley, L.V., *Travelling Waves on Transmission Systems*, Dover, New York, 1963.

Chisholm, W.A. and Janischewskyj, W., Lightning Surge Response of Ground Electrodes, *IEEE Trans. on Power Delivery,* 4(2), April 1989.

Chow, Y.L. and Srivastava, K.D., Non-Uniform Electric Field Induced Voltage Calculations, Final Report for Canadian Electrical Association Contract 117 T 317, February 1988.

Chow, Y.L. and Yovanovich, M.M., The shape factor of the capacitance of a conductor, *J. Appl. Physics,* 52, December 1982.

Deri, A., Tevan, G., Semlyen, A., and Castanheira, A., The Complex Ground Return Plane — A Simplified Model for Homogeneous and Multi-Layer Earth Return, *IEEE Transactions* PAS-100 8, August 1981.

Filho, S.V. and Portela, C.M., Soil Permittivity and Conductivity Behaviour on Frequency Range of Transient Phenomena in Electric Power Systems, Paper 93.06, Proceedings of 5th ISH, August 1987.

IEEE Standard 100, *Dictionary of Electrical and Electronics Terms,* 5th ed., IEEE, New York, 1992.

ANSI/IEEE Standard 80-1986, *IEEE Guide for Safety in AC Substation Grounding,* IEEE/Wiley, New York, 1986.

Keller, G.G. and Frischknecht, F.C., *Electrical Methods in Geophysical Prospecting,* Pergamon, New York, 1982.

Korsuncev, A.V., Application on the theory of similarity to calculation of impulse characteristics of concentrated electrodes, *Elektrichestvo* No. 5, 1958.

Liew, A. and Darveniza, M., Dynamic model of impulse characteristics of concentrated earths, *IEE Proceedings,* 121(2), Feb. 1974.

Loyka, S.L. A simple formula for the ground resistance calculation, *IEEE Transactions on EMC,* 41(2), 152-154, May 1999.

Oettle, E.E., A new general estimation curve for predicting the impulse impedance of concentrated earth electrodes, *IEEE Trans. on Power Delivery,* 3(4), October 1988.

Sadiku, M.N.O., Ed., *Numerical Techniques in Electromagnetics,* CRC Press, Boca Raton, FL, 1992.

Smythe, W.R., *Static and Dynamic Electricity,* McGraw-Hill, New York, 1950.

Sunde, E.D., *Earth Conduction Effects in Transmission Systems,* Van Nostrand, Toronto, 1949.

Tagg, G.F., *Earth Resistances,* George Newnes, London, 1964.

Weber, E., *Electromagnetic Fields Theory and Applications Volume 1 — Mapping of Fields,* Wiley, New York, 1950.

Zaborsky, J., Efficiency of grounding grids with nonuniform soil, *AIEE Transactions,* 1230-1233, December 1955.

Appendix A: Relevant IEEE Grounding Standards

ANSI/IEEE Std 80-1986: *IEEE Guide for Safety in AC Substation Grounding*

Presents essential guidelines for assuring safety through proper grounding at AC substations at all voltage levels. Provides design criteria to establish safe limits for potential differences within a station, under fault conditions, between possible points of contact. Uses a step-by-step format to describe test methods, design and testing of grounding systems. Also provides English translations of three fundamental papers on grounding by Rudenberg, Laurent, and Zeitschrift.

IEEE Std. 81-1983: *IEEE Guide for Measuring Earth Resistivity, Ground Impedance, and Earth Surface Potentials of a Ground System*

The present state of the technique of measuring ground resistance and impedance, earth resistivity, and potential gradients from currents in the earth, and the prediction of the magnitude of ground resistance and potential gradients from scale-model tests are described and discussed. Factors influencing the choice of instruments and the techniques for various types of measurements are covered. These include the purpose of the measurement, the accuracy required, the type of instruments available, possible sources of error, and the nature of the ground or grounding system under test. The intent is to assist the engineer or technician in obtaining and interpreting accurate, reliable data. The test procedures described promote the safety of personnel and property and prevent interference with the operation of neighboring facilities.

IEEE Std. 81.2-1991: *IEEE Guide for Measurement of Impedance and Safety Characteristics of Large, Extended or Interconnected Grounding Systems*

Practical instrumentation methods are presented for measuring the AC characteristics of large, extended, or interconnected grounding systems. Measurements of impedance to remote earth, step and touch potentials, and current distributions are covered for grounding systems ranging in complexity from small grids (less than 900 m^2) with only a few connected overhead or direct-burial bare concentric neutrals, to large grids (greater than 20,000 m^2) with many connected neutrals, overhead ground wires (sky wires), counterpoises, grid tie conductors, cable shields, and metallic pipes. This standard addresses measurement safety; earth-return mutual errors; low-current measurements; power-system staged faults; communication and control cable transfer impedance; current distribution (current splits) in the grounding system; step, touch, mesh, and profile measurements; the foot-equivalent electrode earth resistance; and instrumentation characteristics and limitations.

IEEE Std. 367-1996: *IEEE Recommended Practice for Determining the Electric Power Station Ground Potential Rise and Induced Voltage from a Power Fault*

Information for the determination of the appropriate values of fault-produced power station ground potential rise (GPR) and induction for use in the design of protection systems is provided. Included are the determination of the appropriate value of fault current to be used in the GPR calculation, taking into account the waveform, probability, and duration of the fault current; the determination of inducing currents, the mutual impedance between power and telephone facilities, and shield factors; the vectorial summation of GPR and induction; considerations regarding the power station GPR zone of influence; and communications channel time requirements for noninterruptible services. Guidance for the calculation of power station ground potential rise (GPR) and longitudinal induction (LI) voltages is provided, as well as guidance for their appropriate reduction from worst-case values, for use in metallic telecommunication protection design.

IEEE Std. 524a-1993: *IEEE Guide to Grounding During the Installation of Overhead Transmission Line Conductors—Supplement to IEEE Guide to the Installation of Overhead Transmission Line Conductors*

General recommendations for the selection of methods and equipment found to be effective and practical for grounding during the stringing of overhead transmission line conductors and overhead ground wires

are provided. The guide is directed to transmission voltages only. The aim is to present in one document, sufficient details of present day grounding practices and equipment used in effective grounding and to provide electrical theory and considerations necessary to safeguard personnel during the stringing operations of transmission lines.

IEEE Std. 789-1988 (R1994): *IEEE Standard Performance Requirements for Communications and Control Cables for Application in High Voltage Environments*

Requirements are set forth for wires and cables used principally for power system communications and control purposes that are located within electric power stations, installed within the zone of influence of the power station ground potential rise (GPR), or buried adjacent to electric power transmission and distribution lines. The cables can be subjected to high voltages either by conduction or induction coupling, or both. Cable specifications that ensure overall reliability in high-voltage environments are provided. Environmental considerations, operating service conditions, installation practices, and cable design requirements are covered. Design tests, routine production tests, and physical and electrical tests are included.

IEEE Std. 837-1989 (R1996): *IEEE Standard for Qualifying Permanent Connections Used in Substation Grounding*

Directions and methods for qualifying permanent connections used for substation grounding are provided. Particular attention is given to the connectors used within the grid system, connectors used to join ground leads to the grid system, and connectors used to join the ground leads to equipment and structures. The purpose is to give assurance to the user that connectors meeting the requirements of this standard will perform in a satisfactory manner over the lifetime of the installation provided, that the proper connectors are selected for the application, and that they are installed correctly. Parameters for testing grounding connections on aluminum, copper, steel, copper-clad steel, galvanized steel, stainless steel, and stainless-clad steel are addressed. Performance criteria are established, test procedures are provided, and mechanical, current-temperature cycling, freeze-thaw, corrosion, and fault-current tests are specified.

IEEE Std. 1048-1990: *IEEE Guide for Protective Grounding of Power Lines*

Guidelines are provided for safe protective grounding methods for persons engaged in deenergized overhead transmission and distribution line maintenance. They comprise state-of-the-art information on protective grounding as currently practiced by power utilities in North America. The principles of protective grounding are discussed. Grounding practices and equipment, power-line construction, and ground electrodes are covered.

IEEE Std. 1050-1996: *IEEE Guide for Instrumentation and Control Equipment Grounding in Generating Stations*

Information about grounding methods for generating station instrumentation and control (I & C) equipment is provided. The identification of I & C equipment grounding methods to achieve both a suitable level of protection for personnel and equipment is included, as well as suitable noise immunity for signal ground references in generating stations. Both ideal theoretical methods and accepted practices in the electric utility industry are presented.

IEEE Std. 1243-1997: *IEEE Guide for Improving the Lightning Performance of Transmission Lines*

Procedures for evaluating the lightning outage rate of overhead transmission lines at voltage levels of 69 kV or higher are described. Effects of improved insulation, shielding, coupling and grounding on backflashover, and shielding failure rates are then discussed.

IEEE Std. 1313.1-1996: *IEEE Standard for Insulation Coordination—Definitions, Principles, and Rules*

The procedure for selection of the withstand voltages for equipment phase-to-ground and phase-to-phase insulation systems is specified. A list of standard insulation levels, based on the voltage stress to which the equipment is being exposed, is also identified. This standard applies to three-phase AC systems above 1 kV.

IEEE Std. 1410-1997: *IEEE Guide for Improving the Lightning Performance of Distribution Lines*

Procedures for evaluating the lightning outage rate of overhead distribution lines at voltage levels below 69 kV are described. Effects of improved insulation, shielding, coupling, and grounding for direct strokes and induced over-voltage are then discussed.

10.8 Insulation Coordination

Stephen R. Lambert

Insulation coordination is the art of correlating equipment electrical insulation strengths with expected overvoltage stresses so as to result in an acceptable risk of failure while considering economics and operating criteria (McNutt and Lambert, 1992).

Insulation properties can be characterized as self-restoring and non-self-restoring. Self-restoring insulation has the ability to "heal" itself following a flashover, and such insulation media are usually associated with a gas — air, SF_6, etc. Examples include overhead line insulators, station buswork, external bushing surfaces, SF_6 buswork, and even switchgear insulation. With self-restoring insulation, some flashovers are often acceptable while in operation. An EHV transmission line, for example, is allowed to experience occasional line insulator flashovers during switching operations such as energizing or reclosing, or as a result of a lightning flash striking the tower, shield wires, or phase conductors.

Non-self-restoring insulation is assumed to have permanently failed following a flashover, and repairs must be made before the equipment can be put back into service. Insulation such as oil, oil/paper, and solid dielectrics such as pressboard, cross-link polyethylene, butyl rubbers, etc. are included in this insulation class. Any flashover of non-self-restoring insulation, say within a transformer or a cable, is unacceptable as such events usually result in lengthy outages and costly repairs.

The performance level of self-restoring insulation is usually addressed and defined in terms of the probability of a flashover. Thus, for a specific voltage stress, a given piece of insulation has an expected probability of flashover — e.g., a 1 meter conductor-to-conductor gap exposed to a 490 kV switching surge, would be expected to have a 50% chance of flashover; with a 453 kV surge, the gap would be expected to have a 10% chance of flashover, etc. Consequently, when self-restoring insulation is applied, the procedure is to select a gap length that will give the overall desired performance (probability of flashover) as a function of the stress (overvoltages) being applied.

For non-self-restoring insulation, however, any flashover is undesirable and unacceptable, and consequently for application of non-self-restoring insulation, a capability is selected such that the "100%" withstand level (effectively a zero percent chance of flashover) of the insulation exceeds the highest expected stress by a suitable margin.

Insulation Characteristics

Self-restoring (as well as non-self-restoring) insulation has, when exposed to a voltage, a probability of flashover that is dependent on:

- the dielectric material (air, SF_6, oil…)
- the waveshape of the stress (voltage)
- the electrode or gap configuration (rod-rod, conductor to structure…)
- the gap spacing
- atmospheric conditions (for gases)

Probability of Flashover (pfo)

Assuming the flashover characteristics of insulation follow a Gaussian distribution, and this is a good assumption for most insulation media (air, SF_6, oil, oil/paper), the statistical flashover characteristics of

insulation can be described by the $V_{50\%}$ or mean value of flashover, and a standard deviation. The $V_{50\%}$ is a function of the rise time of the applied voltage, and when at a minimum, it is usually known as the V_{CFO} or critical flashover voltage.

Consequently, for a given surge level and insulation characteristic, the pfo of a single gap can be described by "p," and can be determined by first calculating the number of standard deviations the stress level is above or below the mean:

$$\#\delta = \frac{V_{stress} - V_{50\%}}{1 \text{ standard deviation}} \tag{10.154}$$

For air insulation, one standard deviation is either 3% of the $V_{50\%}$ for fundamental frequency (50–60 Hz) voltages and for lightning impulses or 6% of the $V_{50\%}$ for switching surge impulses. That the standard deviation is a fixed percentage of the $V_{50\%}$ and is not a function of gap length is very fortuitous and simplifies the calculations. Once the number of standard deviations away from the mean has been found, then by calculation or by entering a table, the probability of occurrence associated with that number of standard deviations is found.

Example:

Assume an insulator has a $V_{50\%}$ of 1100 kV with a standard deviation of 6%, and a switching overvoltage of 980 kV is applied to the insulation. The stress is 1.82 standard deviations below the mean:

$$\#\delta = \frac{980 - 1100}{0.06 \times 1100} \tag{10.155}$$

$$= -1.82 \text{ standard deviations below the mean}$$

By calculation or table, the probability associated with –1.82 standard deviations below the mean (for a normal distribution) is 3.4%. Thus, there is a 3.4% chance of insulation flashover every time the insulation is exposed to a 980 kV surge.

The physics of the flashover mechanism precludes a breakdown or flashover below some stress level, and this is generally assumed to occur at 3.5–4 standard deviations below the mean.

Multiple Gaps per Phase

The probability of flashover, P_n, for n gaps in parallel (assuming the gaps have the same characteristics and are exposed to the same voltage) can be described by the following equation where p is the probability of flashover of one gap. This mathematical expression defines the probability of one or more gaps flashing over, but practically only one gap of the group will flashover as the first gap to flashover reduces the voltage stress on the other gaps.

$$P_n = 1 - \left(1 - p\right)^n \tag{10.156}$$

Multiple Gaps and Multiple Phases

Analysis of some applications may not only require consideration of multiple gaps in a given phase but also of multiple phases. Consider the pfo analysis of a transmission line; during a switching operation, for example, multiple towers are exposed to surges and at each tower, each of the three phases is stressed (typically by different surge magnitudes). Thus it is important to consider not only the multiple gaps associated with the multiple towers, but also all three phases often need to be considered to determine the overall line probability of flashover. The overall probability of flashover for a given surge, PFO, can be expressed as:

$$\mathrm{PFO} = 1 - \left(1 - \mathrm{pfo}_{n,a}\right)^{g} \left(1 - \mathrm{pfo}_{n,b}\right)^{g} \left(1 - \mathrm{pfo}_{n,c}\right)^{g} \tag{10.157}$$

where $\mathrm{pfo}_{n,x}$ is the pfo of the x phase for the given surge, n
g is the number of towers (gaps in parallel)

The simultaneous analysis of all three phases can be important especially when various techniques are used to substantially suppress the surges (Lambert, 1988).

Flashover Characteristics of Air Insulation

Voltage Waveshape

Waveshapes used for testing and for determining the flashover response of insulation have been standardized by various groups and while there is not 100% agreement, the waveshapes used generally conform to the following:

- Fundamental frequency 50 or 60 Hz sine wave (8000 μs rise time)
- Switching impulse 200–250 μs by 2000 μs
- Lightning impulse 1.2 μs by 50 μs

The impulse waveshapes are usually formed by a double exponential having the time to crest indicated by the first number and the time to 50% of the crest on the tail of the wave indicated by the second number. Thus, a lightning impulse would crest at 1.2 μs and following the crest, would fall off to 50% of the crest at 50 μs.

Fundamental frequency characteristics have been published, and typical values are indicated in Fig. 10.48 (Aleksandrov et al., 1962; EPRI, 1982).

Equations have also been published which define the typical responses to positive polarity switching and lightning impulses (Fig. 10.49). Insulation usually has a lower withstand capability when exposed to positive polarity impulses than when exposed to negative impulses; thus, designs are usually based on positive magnitude impulses.

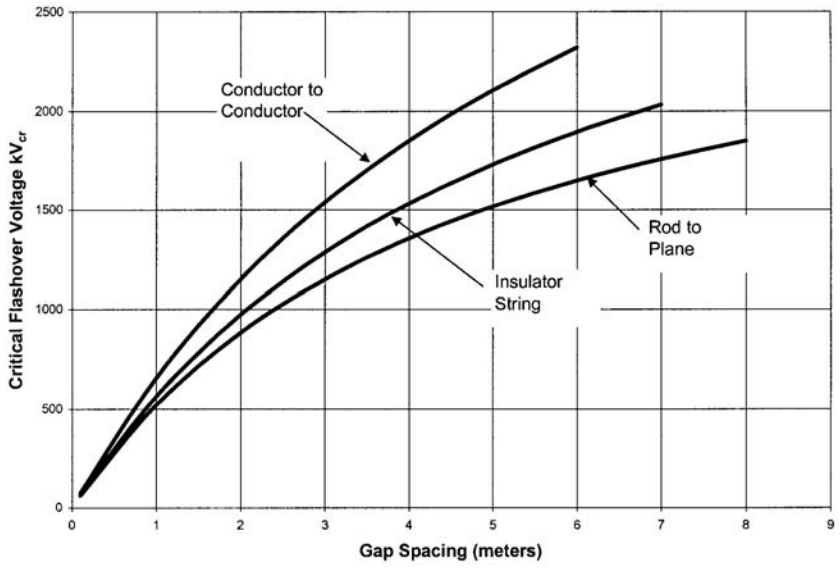

FIGURE 10.48 $V_{50\%}$ for fundamental frequency waveshapes.

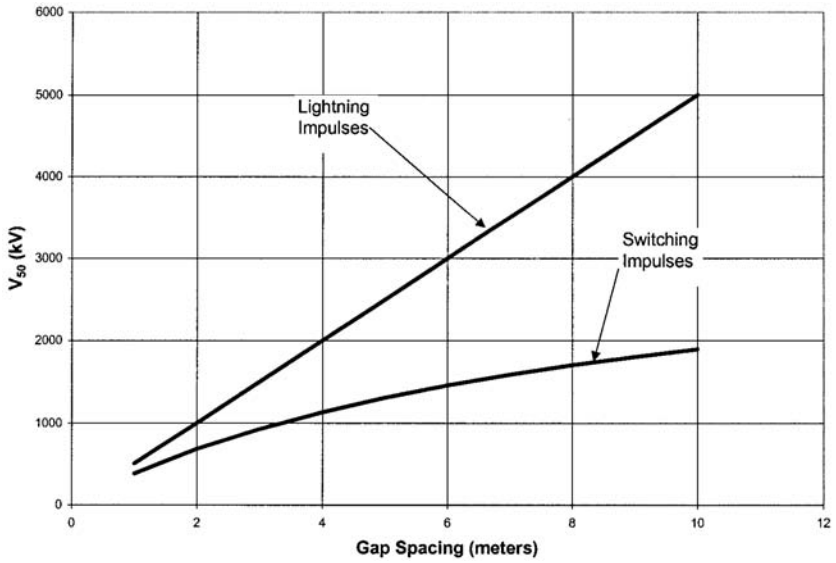

FIGURE 10.49 $V_{50\%}$ for impulses.

For switching surge impulses (Gallet et al., 1976):

$$V_{50\%} = k\frac{3400}{1+\frac{8}{d}} \text{ kV} \tag{10.158}$$

For lightning impulses:

$$V_{50\%} = k * 500 * d \text{ kV} \tag{10.159}$$

where k is an electrode factor reflecting the shape of the electrodes (Paris, 1967)
d is the electrode gap spacing in meters

Electrode Configuration

Electrode configuration has a pronounced effect on the $V_{50\%}$ characteristics, and this is reflected as a gap or electrode factor, k (Paris, 1967). Examples of k are:

rod — plane	1.00
conductor — structure	1.30
rod — rod	1.30
conductor — conductor	1.40
conductor — rod	1.65

Effect of Insulator

The presence of an insulator in a gap tends to reduce the gap factor from those given above, mainly due to the terminal electrode configuration (and intermediate flanges for multi-unit column bus support insulators). The reduction increases with increased gap factor and typical correction values may be found in Fig. 10.50. Note that these corrections are subject to variations (Thione, 1984).

Rain has little effect on a gap without an insulator, however, rain does reduce the gap factor when an insulator is present. Reductions as high as 20% have been noted, but in general, a reduction of 4–5% is typical (Thione, 1984).

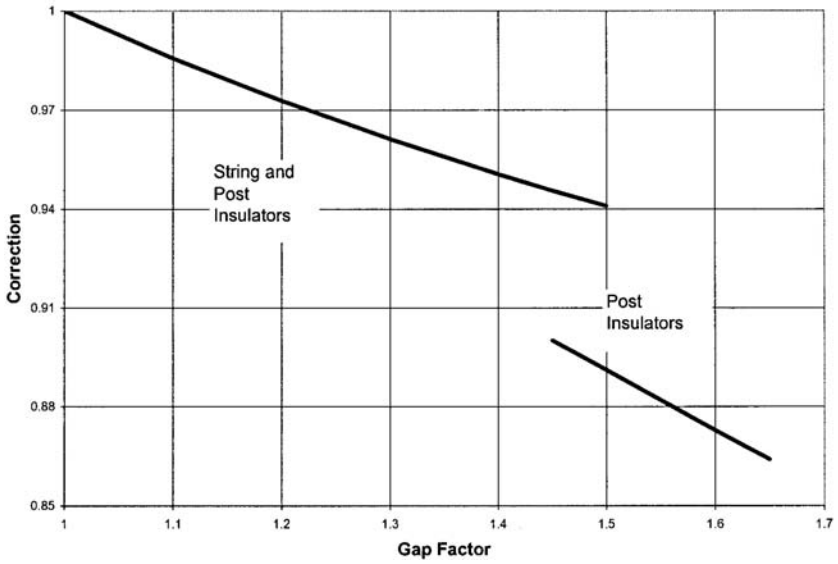

FIGURE 10.50 Gap factor correction for presence of insulator.

Effect of Atmospheric Conditions on Air Insulation

$V_{50\%}$ for gases is affected by temperature, atmospheric pressure, and humidity, and for air the correction can be expressed as:

$$V_{50\%,\ \text{ambient}} = V_{50\%,\ \text{STP}} \left(\frac{H_o}{\delta} \right)^n \tag{10.160}$$

where H_o is the humidity correction factor
n is a gap length correction factor
δ is the relative air density correction factor

The correction for temperature and pressure, δ, is known as the RAD (relative air density) correction factor and is expressed by:

$$\delta = \frac{0.386\ H_{\text{mm of Hg}}}{273.33 + T_{o_C}} \tag{10.161}$$

where $H_{\text{mm of Hg}}$ is the atmospheric pressure in mm of Hg
$T_{°C}$ is the temperature in °C

The humidity correction factor, H_o, is given in IEEE 4 (1978) and can be expressed approximately by:

$$\begin{aligned} H_o &\cong 1.1 - 0.00820 * H_{AB} \\ &\cong 1.1 - 0.008071 * VP \end{aligned} \tag{10.162}$$

where H_{AB} is the absolute humidity in g/m^3
VP is the vapor pressure in mm of Hg

For switching impulses (and fundamental frequency), the effect of the RAD and humidity on $V_{50\%}$ is, however, a function of the gap length and has less effect on longer gap than on shorter gap lengths. For lengths of 0–1 m, the "n" correction factor is 1.0; from 1–6 m, the correction decreases linearly from

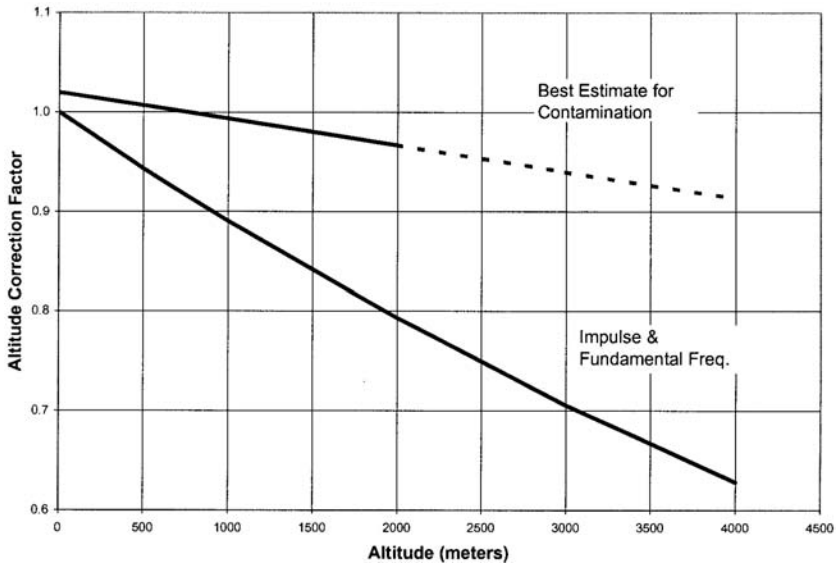

FIGURE 10.51 Altitude correction factors.

1.0 to 0.4; and for lengths greater than 6 m, the factor is 0.4. There is no gap length correction for positive lightning impulses (EPRI, 1982; EPRI, 1975; EEI, 1968). Other approaches for humidity corrections can be found in Menemenlis et al. (1988); Thione (1984); Feser and Pigini (1987).

Altitude

Corrections for altitude are also important as the insulation capability drops off about 10% per 1000 m as shown in Fig. 10.51. There are various equations for the altitude correction factor (ACF), and the following expression is representative of most in use (IEEE 1312, 1999):

$$\mathrm{ACF} = e^{-\frac{\mathrm{Ht}}{8600}}$$

where Ht is the altitude in meters

Insulator Contamination

Insulator contamination is an important issue for fundamental frequency voltage considerations, and the equivalent salt density, ESDD, approach is extensively used as a design tool. The contamination severity is defined by the ESDD in mg/cm^2, and an insulator creepage distance, in terms of mm/kV$_{\text{rms, phase to phase}}$, can then be selected (IEC 815, 1986). Note that insulator/bushing shed/skirt design has a significant impact on the performance, and some past designs performed poorly due to skirt configuration even though they had large creepage distances. With the ESDD approach, insulators are tested to define their expected performance. Table 10.5 shows the relationship between contamination level, ESDD, and recommended creepage distances.

Altitude also has an effect on the performance of contaminated insulation, and the degradation of capability as a function of altitude may be found in Fig. 10.51 (Mizuno et al., 1997).

Example:

Assume ten identical substation bus support insulators in parallel located in a 500 kV substation located at sea level; this configuration can be described as an air gap, conductor to rod configuration at standard atmospheric conditions. Assume that an overall probability of flashover for the ten gaps of 0.5% is desired when the configuration is exposed to a switching surge of 939 kV (2.3 pu on a 500 kV system). What is the required gap clearance in meters?

TABLE 10.5 Relationship Between Contamination Level, ESDD, and Recommended Creepage Distances

Contamination Level	Example	ESDD (mg/cm²)	Minimum Recommended Creepage Distance ($mm/kV_{rms,\ phase\ to\ phase}$)
Light	Low industrial activity	0.03–0.06	16
Medium	Industrial activity — some exposure to wind from the sea	0.1–0.2	20
Heavy	Industrial area and areas close to the sea	0.3–0.6	25
Very Heavy	Heavy industrial or sea coast area	>0.6	31

The desired pfo of one gap, p, then should be:

$$\text{pfo}_{10\ \text{gaps}} = 0.005 = 1 - \left(1 - \text{p}\right)^{10}$$

and

$$\text{p} = 1 - \left(1 - 0.005\right)^{1/10}$$

$$= 0.0005011$$

From tables or calculations for a normal or Gaussian distribution, a probability of 0.0005011 corresponds to 3.29 standard deviations below the mean ($V_{50\%}$). Therefore, the desired $V_{50\%}$ value is:

$$939\ \text{kV} = V_{50\%}\left(1 - 3.29 * 0.06\right)$$

and

$$V_{50\%} = 1170\ \text{kV}$$

A standard deviation of 6% is often used for the air gap for switching surge stresses.

With the $V_{50\%}$ of 1170 kV and noting that a conductor to rod gap has a k factor of 1.65 assumed to be reduced to 1.42 due to the presence of the insulator, the desired gap spacing value can be calculated by:

$$1170\ \text{kV} = 1.42\frac{3400}{1 + \frac{8}{\text{d}}}$$

and

$$\text{d} = 2.56\ \text{meters}$$

Application of Surge Arresters

Surge arresters are used to limit overvoltages and as a result, allow reductions in the clearances required for self-restoring gaps (e.g., transmission line towers) as well as the capability required for non-self-restoring insulation such as transformer windings. In most applications the proper approach is to determine the minimum arrester rating that can be applied without resulting in damage to the arrester, and then to define the insulation level required so as to result in an acceptable probability of flashover or risk of failure.

For a transmission line application, for example, although the arrester reduces higher magnitude surges to lower levels, the line is still allowed to have a finite, albeit low, probability of flashover for a specific switching operation. Thus, the arrester, by limiting the higher magnitude surges, allows smaller conductor-to-tower clearances.

However, when arresters are used to protect a transformer for example, an insulation level is selected that has a significantly higher capability than the maximum surge allowed by the arrester. This margin between the arrester protective level (lightning or switching surge) is a function of various considerations as well as the conservatism of the person applying the arrester/insulation system.

Today, for new applications, only metal oxide (ZnO) arresters are being applied. Although there are certainly many of the gapped, silicon carbide type arresters still in service and which still perform effectively, in what follows, only metal oxide arresters will be considered to protect insulation. Successful application requires that the arrester survive the electrical environment in which it is placed, and the following arrester capabilities must be carefully considered:

MCOV — maximum fundamental frequency continuous operating voltage applied to the arrester
TOV — temporary fundamental frequency overvoltages to which the arrester may be exposed
Energy — the energy which must be absorbed by the arrester when limiting switching surges

MCOV — The highest system voltage which can be continuously applied to the arrester needs to be determined and the arrester capability, its MCOV rating, should at least be equal to and should usually exceed the highest continuous system voltage by some small margin. For example, if a nominal 345 kV system is never operated above 352 kV, then the maximum continuous voltage that would be expected to be applied to a line to ground arrester would be $352\text{kV}/\sqrt{3} = 203.2$ kV. With today's typical arresters, the next highest available MCOV capability would be 209 kV and is associated with an arrester rated 258 kV.

TOV — On occasion, the fundamental frequency voltage applied to an arrester will exceed the expected MCOV. Examples include fault conditions during which line-to-ground voltages on unfaulted phases can rise significantly (as high as phase-to-phase voltage for ungrounded systems); rise in line voltage when energizing a transmission line (ferranti effect); and voltages that occur during load rejection events — these are usually associated with voltages experienced on a radial transmission line emanating from a generating plant when the load terminal of the line opens unexpectedly.

Energy — When an arrester limits switching surges on a transmission line, it can absorb a significant amount of energy, and it can be important to examine events and determine the energy that could be absorbed. Exceeding the arrester's capability could result in immediate damage to the arrester and failure. It is also important to the arrester's TOV capability as absorbing energy heats the arrester material, and application of a significant temporary overvoltage immediately following absorption of a significant amount of energy could result in thermal runaway and arrester failure.

Following selection of an arrester that would be expected to survive the electrical environment (i.e., the minimum rated arrester), the protective levels of the arrester must be correlated with the insulation capability and acceptable margins between the protective levels and the insulation capability achieved.

The protective level or discharge voltage of an arrester is the voltage magnitude to which the arrester will limit the voltage while discharging a surge, and these levels are a function of the waveshape and rise time of the surge as well as the current magnitude of the discharge. In general, the discharge or protective levels considered for coordination with insulation capability are:

- a 10 kA, 8×20 μs discharge for coordination with the insulation full wave or lightning impulse (BIL) capability, and
- a 0.5–2.0 kA, 36×90 μs discharge for coordination with the switching impulse capability.

There should always be margin between the protective level of the arrester and the insulation capability to allow for uncertainties in arrester protective levels due to surge rise times, discharge currents, and arrester separation distance (faster rise times, higher currents, and longer separation distance or lead lengths generate higher protective levels). Uncertainties in insulation capability include reduced insulation

strength due to aging (especially for paper insulation in transformers for example) and limitations of the ability of laboratory dielectric testing to accurately relate to field conditions.

In the author's opinion, a margin of at least 40% is appropriate unless all the uncertainties and the risks are carefully evaluated.

Examples of Surge Arrester Application (Non-Self-restoring Insulation)

34.5 kV System Application

Surge arresters are to be applied line-to-ground at the terminals of a circuit breaker (38 kV rating, 150 kV BIL) used on a solidly grounded 34.5 kV system. The highest expected continuous system voltage is 37 kV, and during fault conditions, the phase-to-ground voltage can rise to 1.4 pu or 27.9 kV. Faults can persist for 20 cycles.

The maximum line-to-ground voltage is $37/\sqrt{3} = 21.4$ kV, and the MCOV of the arrester must meet or exceed this value. An arrester rated 27 kV would be acceptable as it has an MCOV of 22.0 kV. The 1 second TOV capability of the arrester is 31.7 kV, and as this exceeds the 27. 9 kV phase-to-ground voltage expected during faults, the 27 kV arrester meets the TOV criteria as well.

A 27 kV arrester has a 10 kA discharge level of 67.7 kV, and thus the margin between the discharge or protective level and the insulation BIL is $(150/67.7 \times 100 - 100)$ or 121%. This margin is obviously more than adequate, and selection of an arrester rated 27 kV would be appropriate.

500 kV System Application

A 500 kV shunt reactor (solidly grounded neutral) is being applied at the end of a 300 km, 500 kV transmission line, and arresters are to be applied line-to-ground on the terminals of the reactor to limit surges to reasonable levels. The reactor is solidly connected to the line and is switched with the line, and the substation at which the reactor resides is at an altitude of 1800 m. The highest expected continuous system voltage is 550 kV. During line switching operations, the circuit breaker at the reactor terminal may not be closed for some period following energizing of the line/reactor from the other terminal, and the phase-to-ground voltage at the reactor can be as high as 1.15 pu for as long as five minutes. Arrester energy requirements were determined (by EMTP or TNA simulations of switching operations) to be well within the capability of an arrester rated 396 kV.

The minimum required MCOV is $550/\sqrt{3} = 317.5$ kV. The minimum required TOV is $1.15 \times 500/\sqrt{3} = 332$ kV for 300 seconds, and for most arresters, such a requirement would correlate with a 1 second TOV rating of 451 kV. An arrester rated 396 kV has a 318 kV MCOV and a 1 second TOV rating of 451 kV; thus, a 396 kV arrester would be the minimum rating that could be used. Of course any arrester rated higher than 396 kV could also be used. The 10 kA lightning (8×20 μs waveform) and switching surge (2 kA, 36×90 μs) discharge levels for a 396 kV and a 420 kV arrester are:

	Discharge Levels	
Rating	10 kA	Switching Surge
396 kV	872 kV	758 kV
420 kV	924 kV	830 kV

BIL values of 1300 kV and 1425 kV for the reactor's *internal insulation* (i.e., insulation not affected by altitude) could be considered as reasonable candidates for a specification. The corresponding switching impulse levels (SIL) would be 1080 kV and 1180 kV, respectively, and the following table indicates the margin between the arrester protective levels and the insulation level.

	1300 kV BIL		1425 kV BIL	
Arrester	396 kV	420 kV	396 kV	420 kV
SIL	42%	30%	56%	42%
BIL	49%	41%	63%	54%

Application of a 420 kV arrester for a 1300 kV BIL insulation level results in margins below 40%, and unless the application is very carefully considered from the point of view of arrester separation distance and lead length, expected maximum discharge current level, wave rise time, etc., a 396 kV arrester would be a better choice. For a 1425 kV BIL, either the 396 kV or the 420 kV arrester would result in sufficient margins.

For *external insulation*, i.e., the reactor bushings, the effect of altitude on the insulation capability needs to be considered. At 1800 m the insulation has only 81% of the withstand capability demonstrated at sea level or 0 m. For example, the SIL of a 1425 kV bushing (1180 kV at sea level) would be reduced to 956 kV at 1800 m ($1108 \times 0.81 = 956$ kV), and application of even a 396 kV arrester would result in a margin of 26% — hardly acceptable.

Assume that a 420 kV arrester was selected to protect the reactor (the arrester itself is rated for application to 3000 m). The switching surge and 10 kA protective levels are 830 kV and 924 kV, respectively. With a desired minimum margin of 40% , and correcting for altitude, the minimum SIL and BIL at sea level (0 m) should be:

$$\text{Minimum SIL} = \frac{830 \times 1.4}{0.81} = 1435 \text{ kV}$$

$$\text{Minimum BIL} = \frac{924 \times 1.4}{0.81} = 1597 \text{ kV}$$

A 1550 kV BIL bushing would have a 1290 kV SIL, and even if one would accept the slightly less than a 36% margin for the BIL, the SIL margin would only be 26%. A 1675 kV BIL bushing would be expected to have a 1390 kV SIL capability, and so the SIL margin would be 36% with a BIL margin of 47%. The next higher rated bushing (1800 kV BIL) would mean applying 800 kV system class bushings, and their increased size and cost would likely not make for a reasonable design. Consequently, specifying a 1675 kV BIL bushing and accepting the slightly reduced SIL margin would be a reasonable compromise.

Effect of Surge Reduction Techniques on Overall PFO

Application of surge arresters to significantly reduce switching surge levels on transmission line and substation insulators can be effective; however, the designer should be aware that the overall pfo of all three phases needs to be considered as it will usually be higher than that found for a single phase by a factor often approaching three. Also for long transmission lines, application of arresters at the line terminals will certainly limit the surges at the terminals but will not limit the surges at other points on the line to the same level. Consequently, the surge distribution along the line may need to be considered (Lambert, 1988; Ribiero et al., 1991).

References

Aleksandrov, G. N., Kizvetter, V. Y., Rudakova, V. M. Tushnov, A. N., The AC flashover voltages of long air gaps and strings of insulators, *Elektrichestvo*, 6, 27, 1962.

EHV Transmission Line Reference Book, Edison Electric Institute, 1968.

Feser, K., Pigini, A., Influence of atmospheric conditions on the dielectric strength of external insulation, *ELECTRA*, No. 112, 83, 1987.

Gallet, G., Bettler, M., Leroy, G., Switching impulse results obtained on the outdoor testing area at Renardieres, *IEEE Trans. on Power Appar. and Syst.*, PAS-95, 2, 580, 1976.

Guide for the Selection of Insulators in Respect of Polluted Conditions, IEC Publication 815, 1986.

IEEE Standard for Insulation Coordination — Part 2, Application Guide, IEEE 1312-1999, Institute of Electrical and Electronic Engineers.

IEEE Standard Techniques for High-Voltage Testing, IEEE 4 — 1978, Institute of Electrical and Electronic Engineers.

Lambert, S. R., Effectiveness of zinc oxide surge arresters on substation equipment probabilities of flashover, *IEEE Transactions on Power Delivery*, 3(4), 1928, 1988.

McNutt, W. J., Lambert, S. R., *Transformer Concepts and Applications Course,* Power Technologies, Inc., Schenectady, NY, 1992.

Menemenlis, C., Carrara, G., Lambeth, P. J., Application of insulators to withstand switching surges in substations, part I: Switching impulse insulation strength, 88 WM 077-0, IEEE/PES Winter Meeting, New York, New York, January 31–February 5, 1988.

Mizuno, Y., Kusada, H., Naito, K., Effect of climatic conditions on contamination flashover voltage of insulators, *IEEE Trans. on Dielectrics and Electrical Insulation*, 4(3), 286, 1997.

Paris, L., Influence of air gap characteristics on line-to-ground switching surge strength, *IEEE Trans. on Power Appar. and Syst.*, PAS-86, 8, 936, 1967.

Ribeiro, J. R., Lambert, S. R., Wilson, D. D., Protection of compact transmission lines with metal oxide arresters, in *CIGRE Leningrad Symposium 1991,* 400–6, S33–91.

Thione, L., Evaluation of the switching impulse strength of external insulation, *Electra*, No. 94, 77, 1984.

Transmission Line Reference Book, 345 kV and Above, 1st ed., Electric Power Research Institute, 1975.

Transmission Line Reference Book, 345 kV and Above/Second Edition, Electric Power Research Institute, 1982.